Aus dem Institut für Kardiovaskuläre Physiologie und Pathophysiologie
(im Walter-Brendel-Zentrum für Experimentelle Medizin, WBex)
der Ludwig-Maximilians-Universität München
Kommissarischer Direktor: Prof. Dr. med. dent. Reinhard Hickel
Ehemaliger Direktor: Prof. Dr. med. Ulrich Pohl

Myosin 1f plays a fundamental role for neutrophil migration in 3D environments during acute inflammation

Dissertation

zum Erwerb des Doktorgrades der Naturwissenschaften

an der Medizinischen Fakultät der

Ludwig-Maximilians-Universität München

vorgelegt von

Melanie Salvermoser

aus München

Jahr

2018

Mit Genehmigung der Medizinischen Fakultät
der Universität München

Betreuer: Prof. Dr. rer. nat. Barbara Walzog

…………………………………………………..

Zweitgutachter: Priv. Doz. Dr. Reinhard Obst

Dekan: Prof. Dr. med. dent. Reinhard Hickel

Tag der mündlichen Prüfung: 18.10.2018

In Erinnerung an meinen Opa

Table of Contents

Abstract

During the acute inflammatory response, polymorphonuclear neutrophils migrate from the blood into the inflamed tissue following a multi-step cascade of consecutive adhesion and activation events. The efficient recruitment of neutrophils is fundamentally important for an adequate immune response against pathogenic microorganisms. Hereby, neutrophil migration within 3D environments, i.e. transmigration and interstitial migration, depends on the dynamic deformation of the nucleus to pass restrictive sites. The unconventional class I Myosin 1f (Myo1f) protein has been previously reported to be involved in neutrophil trafficking by controlling neutrophil adhesion under static conditions and accumulation at sites of inflammation[1]. Nonetheless, the functional importance of Myo1f during neutrophil recruitment under physiological shear stress conditions as well as the precise function of Myo1f remained largely unresolved so far. Thus, the aim of this thesis was to study the role of Myo1f for neutrophil trafficking during the acute inflammatory response on the cellular and molecular level in detail.

Analysis of *in vitro* flow chamber experiments revealed that neutrophil rolling and adhesion as well as spreading, polarization and migration in two-dimensional (2D) environments, i.e. mechanotactic crawling, under physiological flow conditions were not affected in the genetic absence of Myo1f. This was further confirmed by intravital microscopy of inflamed mouse cremaster muscle venules which revealed no differences of neutrophil rolling and adhesion between wild-type (Myo1f$^{+/+}$) and Myo1f knock out (Myo1f$^{-/-}$) mice. Spinning disk confocal microscopy of Myo1f$^{+/+}$ and Myo1f$^{-/-}$ neutrophils deciphered Myo1f as an indispensable molecular key player in the process of nuclear deformation during neutrophil migration in three-dimensional (3D) environments. Accordingly, neutrophil extravasation was severely compromised in the TNFα-stimulated mouse cremaster muscle model, in the CXCL1 induced peritonitis model and in the LPS-triggered acute lung injury model.

Taken together, these findings provide evidence that Myo1f plays a fundamental role in the acute inflammatory response by specifically regulating neutrophil migration in 3D environments but not in 2D environments. During neutrophil migration in 3D environments, Myo1f coordinates the dynamic deformation of the nucleus during neutrophil migration through physical barriers and is therefore indispensable for neutrophil trafficking in innate immunity.

Zusammenfassung

Während der akuten Entzündungsreaktion migrieren polymorphkernige neutrophile Granulozyten in einem mehrstufigen Prozess bestehend aus aufeinander folgenden Adhäsions- und Aktivierungsereignissen aus dem Blut in das entzündete Gewebe. Im Verlauf dieses Prozesses migrieren Neutrophile im dreidimensionalen (3D) Raum durch Engstellen im Gewebe. Hierbei ist die dynamische Verformung des Zellkerns von essentieller Bedeutung und stellt somit einen wesentlichen Schritt in der gezielten Immunantwort gegen pathogene Mikroorganismen dar. Es wurde bereits gezeigt, dass das zur Klasse I der unkonventionellen Myosine gehörende Protein Myosin 1f (Myo1f) bedeutsam für die Rekrutierung von Neutrophilen ist, da es die Adhäsion von Neutrophilen unter statischen Bedingungen und die Anreicherung von Neutrophilen am Entzündungsort kontrolliert[1]. Hierbei ist die genaue Funktion von Myo1f für die Rekrutierung von Neutrophilen unter physiologischen Bedingungen weitgehend ungeklärt. Daher war das Ziel der vorliegenden Arbeit, die Bedeutung von Myo1f für die Rekrutierung von Neutrophilen im Rahmen der akuten Entzündungsreaktion auf zellulärer und molekularer Ebene im Detail zu untersuchen.

In vitro Flusskammerexperimente zeigten, dass das Rollen und die Adhäsion von Neutrophilen, sowie das Ausbreiten, die Polarisierung und die Migration in der 2D Umgebung, d.h. das sogenannte „*intraluminal crawling*", bei genetischer Abwesenheit von Myo1f nicht beeinträchtigt waren. Dies wurde intravitalmikroskopisch in den entzündeten Venolen des *M. cremaster* der Maus bestätigt. Hier trat keine Veränderung im Rollverhalten, sowie der Adhäsion von Neutrophilen zwischen Wildtyp- (Myo1f$^{+/+}$) und Myo1f Knock-out- (Myo1f$^{-/-}$) Mäusen auf. Durch Spinning-Disk-Konfokalmikroskopie-Analysen an Neutrophilen aus Myo1f$^{+/+}$- und Myo1f$^{-/-}$-Mäusen, konnte Myo1f als unverzichtbarer molekularer Faktor während der Deformierung des Zellkerns in der 3D-Migration identifiziert werden. Dementsprechend war die Neutrophilenextravasation in dem Modell der TNFα-induzierten venulären Entzündung am *M. cremaster,* in der CXCL1-induzierten Peritonitis und in der LPS-induzierten Lungenentzündung stark beeinträchtigt.

Insgesamt zeigen diese Ergebnisse, dass Myo1f essenziell für die Migration von Neutrophilen in dreidimensionalen Gewebestrukturen ist und somit eine bedeutsame Rolle in der akuten Entzündungsantwort spielt. Hierbei koordiniert Myo1f während der Migration von Neutrophilen die dynamische Deformation des Zellkerns und ist daher unabdingbar für die effiziente Rekrutierung von Neutrophilen an den Entzündungsort im Rahmen der angeborenen Immunantwort.

Table of Figures and Tables

Abbreviations

2D	2-dimensional		EDTA	ethylenediamine-tetraacetic acid
3D	3-dimensional		ESL-1	E-selectin ligand-1
ADM	adhesion medium		FACS	fluorescence-activated cell sorting
ALI	acute lung injury		FITC	fluorescein isothiocyanate
ARDS	acute respiratory distress syndrome		FOV	field of view
ANOVA	analysis of variance		fMLP	N-formyl-L-methionyl-L-leucyl-phenylalanine
BAL	bronchoalveolar lavage		GPCR	G-protein coupled receptor
BM	basement membrane		GTPase	guanosine triphosphatase
bp	base pair		HEPES	4-(2-hydroxyethyl)-1-piperazineethanesulfonic acid
BSA	bovine serum albumin			
CD	cluster of differentiation		HPK-1	hematopoietic progenitor kinase-1
CXCL1	C-X-C motif chemokine ligand 1		ICAM-1	intercellular adhesion molecule-1
Dap12	DNAX activation protein 12		IgG	immunoglobulin G
DAMPs	damage-associated molecular patterns		IL-1β	interleukin-1β
DC	dendritic cell		i.p.	intraperitoneal
(d)HL-60	(differentiate) human promyelocytic leukemia cells		ITAM	immunoreceptor tyrosine-based activation motif
DFP	diisopropyl phosphofluoridate		LAD	leukocyte adhesion deficiency
DMEM	Dulbecco's Modified Eagle's Medium		LBR	lamin B receptor
DMSO	dimethyl sulfoxid		LER	low-expression region
DNA	deoxyribonucleic acid		LFA-1	lymphocyte function-associated antigen-1
EC	endothelial cell			
ECM	extracellular matrix		LINC	linkers of nucleocytoskeleton to cytoskeleton
EGFP	enhanced green fluorescent			

LPS	lipopolysaccharide		ROCK	Rho-associated protein kinase
LTB_4	leukotriene B4		ROS	reactive oxygen species
Mac-1	macrophage-1 antigen		RPMI	Roswell Park Memorial Institute 1640
mAbp1	mammalian actin binding protein		SEM	standard error of the mean
MHC	major histocompatibility complex		SFK	Src family kinase
MLL	mixed lineage leukemia		SH3 domain	Src homology 3 domain
Myo	myosin		Syk	spleen tyrosine kinase
NADPH	nicotinamide adenine dinucleotide phosphate		TAE	tris base, acetic acid and EDTA
NE	neutrophil elastase		TBS	tris buffered saline
NETs	neutrophil extracellular traps		TBST	tris buffered saline with Tween®20
PAMP	pathogen associated molecular pattern		TEM	transendothelial migration
PBS	phosphate buffered saline		TH domain	tail homology domain
PCR	polymerase chain reaction		TLR4	toll-like receptor 4
PE	phycoerythrin		TNF-α	tumor necrosis factors-α
PECAM-1	platelet/endothelial adhesion molecule-1		VCAM-1	vascular cell adhesion molecule-1
PFA	paraformaldehydePI3K phosphatidylinositol 3-kinase		WB	western blot
PIP_3	phosphatidylinositol (3,4,5)-triphosphate			
PMA	phorbol myristate acetate			
PSGL-1	P-selectin glycoprotein ligand-1			
RhoG	Ras homology growth-related			
rm	recombinant murine			

1. INTRODUCTION

Polymorphonuclear neutrophils are the predominant leukocyte subset in the circulation of most mammals[2]. After their generation and maturation in the bone marrow, neutrophils circulate in the blood stream with a half-live of 6 h up to 4.5 day[3]. During the acute inflammatory response which is initiated by physical (e.g. radiation), biological (e.g. bacteria), or chemical (e.g. acid burn) insults or ischemia[4], neutrophils are the first immune cells arriving at the site of lesion. Generally, neutrophils fight pathogens and control local infections via different defense mechanisms, including phagocytosis and production of reactive oxygen species (ROS), as well as release of antimicrobial peptides and neutrophil extracellular traps (NETs)[5-9]. The segmented nuclei as well as granule and secretory vesicle containing cytoplasm represent typical characteristics of neutrophils[10]. Besides their pro-inflammatory nature, neutrophils exhibit anti-inflammatory functions, play a critical role in e.g. wound healing and angiogenesis, and they interact with dendritic cells (DCs), B and T cells and therefore are capable to modulate the adaptive immune response[5,11-13].

1.1 The neutrophil recruitment cascade

During the acute inflammatory response neutrophils are recruited from the blood stream into the inflamed tissue following a well-defined multi-step recruitment cascade which is a fundamental process in the innate immune response[5,14] (Figure 1). The initial steps, including leukocyte capturing, rolling, slow rolling, induction of adhesion, adhesion strengthening, as well as intraluminal crawling and transendothelial migration (TEM) are regulated by specific interactions between adhesion molecules on leukocytes and their ligands on endothelial cells (ECs)[15,16]. Neutrophil capturing and rolling are mediated by engagement of selectins and their receptors[17] followed by neutrophil adhesion, adhesion strengthening, intraluminal crawling, transmigration, and abluminal crawling which all depend on β_2 integrins[18]. Extravasated neutrophils enter the interstitial space and are guided to the site of inflammation or infection by heparan sulfate immobilized chemokine gradients[19]. At the site of lesion, neutrophils fight invading pathogens and microorganisms via different defense mechanisms. During phagocytosis, neutrophils engulf and trap antibody- or complement protein fragment C3bi-opsonized bacteria into a phagosome. Primary and secondary granules fuse with the phagosome and form the so called phagolysosome. The nicotinamide adenine dinucleotide phosphate (NADPH)-oxidase becomes activated and the

ingested material is eliminated by e.g. the production of reactive oxygen species (ROS) and antimicrobial peptides[9,20-22]. An additional killing mechanism is the formation of NETs which are extracellular fibers consisting of granule and nuclear components that kill bacteria[6].
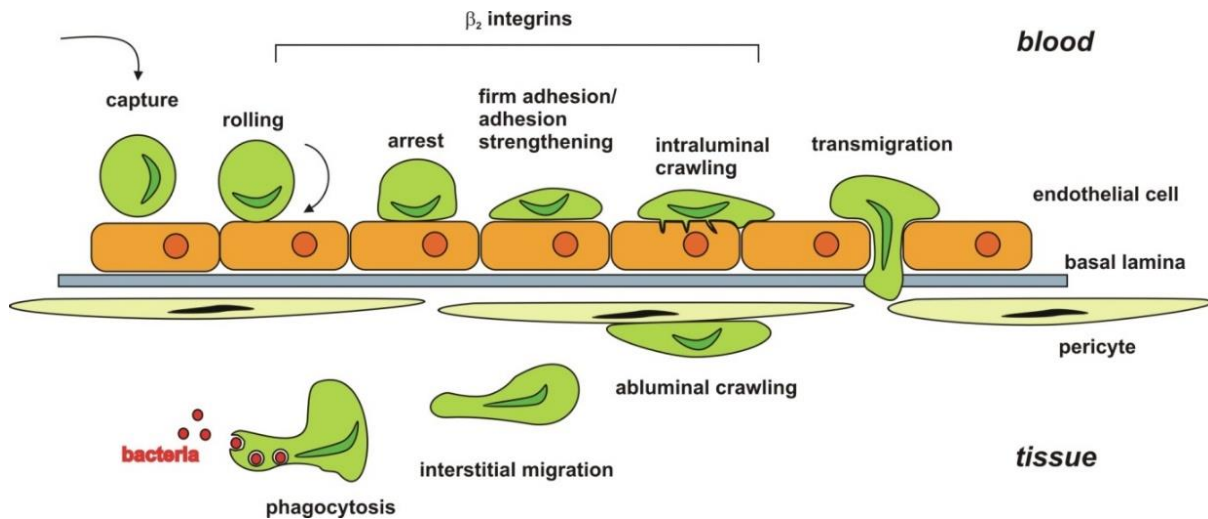
Figure 1. The neutrophil recruitment cascade. Schematic representation of the defined steps neutrophils undergo during acute inflammation to migrate from the blood stream to the site of infection/injury. The individual steps are classified into capturing, rolling, arrest, firm adhesion/adhesion strengthening, intraluminal crawling, transmigration, abluminal crawling and interstitial migration. At the site of infection, neutrophils eliminate pathogens (e.g. bacteria) by various defense mechanisms including phagocytosis of C3bi-opsonized bacteria. Neutrophil slow rolling, adhesion, intraluminal crawling, transmigration, and abluminal crawling depend on β_2 integrins, whereas interstitial migration is mainly β_2 integrins independent (modified from Schymeinsky et al., 2011[23]).

Upon infection, tissue resident macrophages or DCs recognize pathogen-associated molecular patterns (PAMPs). Similarly, inflammation by tissue damage is recognized by damage-associated molecular patterns (DAMPs)[24]. The recognition of these factors leads to the secretion of pro-inflammatory mediators like tumor necrosis factor (TNF) or interleukin-1β (IL-1β)[25]. These cytokines activate ECs resulting in an upregulation of proinflammatory mediators and adhesion molecule expression on the surface of the endothelium initiating the neutrophil recruitment cascade[26,27].

Selectins are a family of Ca^{2+}-dependent transmembrane lectins with three different family members: P-selectin (CD62P) expressed on platelets and ECs, E-selectin (CD62E) expressed on ECs, and L-selectin (CD62L) expressed on leukocytes[28,29]. The different adhesion molecules differ in their amino acid sequence as well as in their interaction partners. P-selectin is stored in α-granules of platelets and in Weibel-Palade bodies of ECs. Upon activation of these cells, P-selectin is redistributed onto the plasma membrane where it interacts with P-selectin glycoprotein ligand-1 (PSGL-1, CD162) on leukocytes[30,31]. E-selectin is *de novo* synthesized by inflamed ECs. E-selectin on the surface of ECs interacts with ligands expressed on leukocytes including PSGL-1, CD44 and E-selectin ligand 1 (ESL-1)[32]. L-selectin is constitutively expressed on leukocytes and is essential for lymphocyte homing[33] and further triggers homozygous leukocyte-leukocyte interactions, resulting in enhanced leukocyte recruitment to the inflamed endothelium, a process called secondary tethering[34]. The interactions of selectins with their specific ligands initiate capturing and rolling of circulating neutrophils. Selectin-selectin ligand interactions are characterized by rapid catch bond formation at the front and bond breakage at the trailing edge of the cell. Catch bonds are interactions which are strengthened by increasing pulling forces leading to a tighter bond between selectins and their ligands[35]. In addition, the formation of subcellular structures like tethers and slings further promotes neutrophil rolling and arrest[17,36,37].

Subsequent slow leukocyte rolling and adhesion are mainly mediated by the adhesion molecules of the β_2 integrin family. β_2 integrins are a family of αβ heterodimers consisting of four members with different α-subunits (CD11) and the conserved CD18 β-subunit: the lymphocyte function-associated antigen 1 (LFA-1, $\alpha L\beta_2$, CD11a/CD18) the macrophage-1 antigen (Mac-1, $\alpha M\beta_2$, CD11b/CD18), p150,95 (CR4, $\alpha x\beta_2$, CD11c/CD18), and $\alpha d\beta_2$ (CD11d/CD18)[38]. Circulating neutrophils present these β_2 integrins in an inactive, bent E(-)H(-) conformation with a closed headpiece. Activation leads to conformational changes of β_2 integrins into the extended intermediate ligand affinity E(+) H(-) conformation with a closed headpiece and further into the extended high ligand affinity E(+) H(+) conformation with an open headpiece[39] (Figure 2). Recently, a fourth β_2 integrin E(-) H(+) conformation has been discovered which interacts with neutrophil intercellular adhesion molecule 1 (ICAM-1) in cis resulting in the inhibition of leukocyte adhesion and aggregation[40].

Interaction of PSGL-1 on neutrophils with selectins on the inflamed endothelium initiates intracellular integrin inside-out signaling events. This activation of LFA-1 and its conformational switch into the intermediate E(+) H(-) conformation with a closed headpiece leads to an increased binding of LFA-1 to ICAM-1 on the endothelium which mediates slow neutrophil rolling[41,42]. For

the induction of the intermediate E(+) H(-) conformation, binding of the adaptor molecule talin-1 to the CD18 cytoplasmic tail is essential[41,43]. Further activation by e.g. exposure to chemokines on the endothelium like CXCL8 (IL-8) in humans or CXCL1, CXCL2 and CXCL5 in mice leads to the conformational switch of LFA-1 into the high E(+) H(+) conformation with an open headpiece resulting in firm adhesion. In addition, binding of kindlin-3 to the CD18 cytoplasmic tail of LFA-1 is required to induce full activation of β_2 integrins[44,45]. It has been previously shown that the mammalian actin binding protein (mAbp1) as well as the hematopoietic progenitor kinase 1 (HPK1) are critically involved in the process of firm neutrophil adhesion by regulating the high affinity E(+) H(+)conformation of LFA-1[46,47].
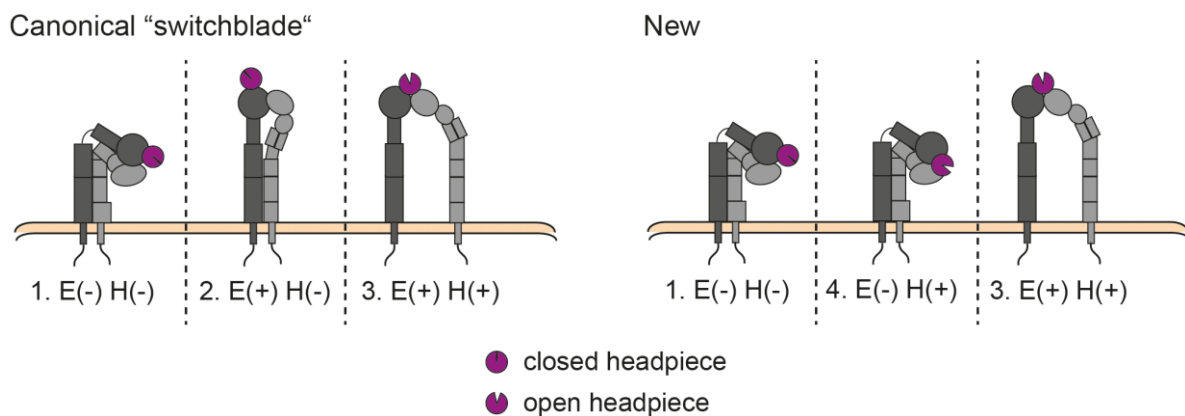
Figure 2. Four conformational states of the β_2 integrins. Left panel: The canonical "switchblade" activation pathway leads to the conformational switch from the inactive, bent E(-) H(-) conformation with a closed headpiece to the intermediate affinity E(+) H(-) conformation with a closed headpiece and to the full activated E(+) H(+) conformation with an open headpiece. Right panel: A new proposed E(-) H(+) conformation state of β_2 integrin (modified from Fan et al., 2016[40]).

In the high affinity E(+) H(+) conformation, β_2 integrins bind their extracellular ligands leading to outside-in signaling events and the redistribution and clustering of the integrins resulting in adhesion strengthening as well as actin cytoskeleton remodeling which is important for the following post-adhesion events like spreading, intraluminal crawling, and TEM[18].

Before neutrophils transmigrate through the wall of postcapillary venules (transmigration) into the inflamed tissue towards the site of inflammation (interstitial migration), they crawl inside the vessels along the inflamed endothelium (intraluminal crawling) to search for exit sites (Figure 3).
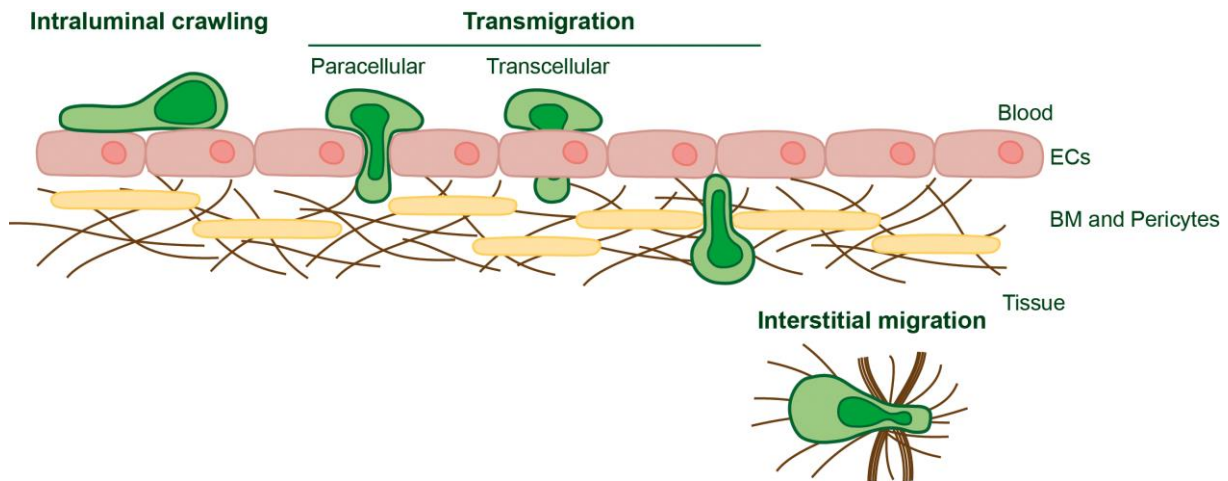
Figure 3. Migration of neutrophils through venular walls into the inflamed tissue. Adherent neutrophils crawl within the circulation on the inflamed endothelium of postcapillary venules to search exit sites (Intraluminal crawling). Neutrophil transmigration from the blood into the inflamed tissue involves passing the ECs by the paracellular or transcellular pathway and the associated BM and the embedded pericytes (Transmigration). Within the inflamed tissue, neutrophils migrate towards the site of inflammation/injury (Interstitial migration).

The processes of intraluminal crawling and TEM are tightly controlled by the interaction of neutrophils and ECs. It has been shown, that intraluminal crawling is mainly dependent on the interaction between Mac-1 and ICAM-1[48,49]. Once arrived at potential exit sites, neutrophils have to pass three distinct barriers, the endothelial layer, the basement membrane (BM) and the pericytes. The perivascular BM is a heterogeneous network of extracellular matrix proteins mainly consisting of laminins (isoform 411 and 511), collagen type IV, heparan sulfate proteoglycans and nidogens[50-55]. Embedded pericytes are long vascular mural cells forming a discontinuous layer with cellular protrusions around the vessel associated with the endothelium[56,57].

Neutrophils migrate through the endothelial layer via the paracellular (through EC junctions) or to a lesser extend via the transcellular route within 2-5 min[5,58]. The interaction of neutrophil integrins and the EC ligands ICAM-1 and vascular cell adhesion molecule 1 (VCAM-1) may activate the Ras homology growth-related (RhoG) signaling downstream of ICAM-1 in ECs[59]. This induces the formation of ICAM-1- and VCAM-1-rich membrane structure so called 'docking structures'[60] or 'transmigratory cup'[61] which surround emigrating leukocytes and may initiate TEM through the paracellular or transcellular route.

After successful penetration of the EC barrier, leukocytes pass the underlying BM and the pericytes. This process takes place within 5-15 min. To date, the mechanism how neutrophils breach the BM is not fully understood. Degradation of the BM by the serine protease neutrophil

elastase (NE) presents one potential mechanism. It has been shown that after TEM, neutrophils crawl towards regions in the BM with low expression of laminins and collagen IV so called low-expression regions (LER)[62,63]. The LERs are highly associated with gaps between the pericytes and are favored by neutrophils as exit spots for penetrating the BM[15,62]. Neutrophils additionally enlarge these LER by transient remodeling the BM possibly facilitated by the binding of the neutrophil receptors VLA-3 ($\alpha 3\beta 1$) and VLA-6 ($\alpha 6\beta 1$) to laminins in the BM[64,65], or by the surface expression of NE[62]. Neutrophils migrate along pericytes in an ICAM-1- (expressed by pericytes), LFA-1- and Mac-1- (expressed by neutrophils) dependent manner[66]. Once emigrated into the tissue, neutrophils crawl within fibrillary networks in the interstitial space towards the site of inflammation[67]. In contrast to intraluminal crawling on ECs and abluminal crawling on pericytes, interstitial migration is low-adhesive and largely β_2 integrin-independent[68,69].

In general, the clinical relevance for efficient neutrophil recruitment during the acute inflammatory response, becomes evident in patients with leukocyte adhesion deficiency (LAD) which is characterized by defective leukocyte recruitment leading to insufficient immune response to injury or infection. To date, there are four types of LAD described (LAD I-IV) characterized by recurrent bacterial and fungal infections[70-75]. LAD type I is caused by mutations in the β subunit (CD18) of β_2 integrins[70,71], whereas LAD type II shows a defect in the function of selectin ligands[72,73] both leading to impaired neutrophil adhesion and recruitment. A mutation within kindlin-3 prevents the conformational shift of the β_2 integrins into their high-affinity E(+) H(+) conformation and is the reason for LAD type III syndrome[45,74]. LAD type IV is caused by a dominant negative mutation in the Rac2 gene which is involved in the regulation of the actin cytoskeleton[75-78].

1.2 The different migration modes of neutrophils and their requirements

In general, cell migration is fundamental for different cellular functions, including embryogenesis, angiogenesis, wound healing, and elimination of invading pathogens[79-81]. There are two basic types of cell migration, the mesenchymal migration mode and the amoeboid migration mode occurring in either 2D or 3D environments. Fibroblasts, smooth muscle cells, pericytes and many dedifferentiated cancer cells migrate using the mesenchymal migration mode which is characterized by a spindle-shaped morphology, low migration speed (0.1-1 μm/min) and proteolytic remodeling of the surrounding extracellular matrix[82-85]. In contrast, leukocyte migration occurs in the amoeboid migration mode and is characterized by cell polarization, 10 to

40 fold higher migration speed and the lack of proteolytic degradation of the extracellular matrix[86,87].

Leukocytes are very flexible in changing their cell morphology and adopt their mode of migration rapidly to the environmental requirements. They detect environmental signals, e.g. from cytokines or chemokines, and translate them into intracellular signals leading to the establishment of a polarized cell shape. Cell polarization into an actin-rich lamellipodium and a contractile uropod precedes cell movement. Leukocytes can either perform directed migration towards a gradient of an extracellular chemoattractant in a process called chemotaxis or they migrate in a nondirected fashion in a homogenous field of soluble chemokines, a process called chemokinesis. Also chemoattractans bound to surfaces initiate leukocyte directed (haptotaxis) or random (haptokinesis) migration along surfaces[69] (Figure 4).
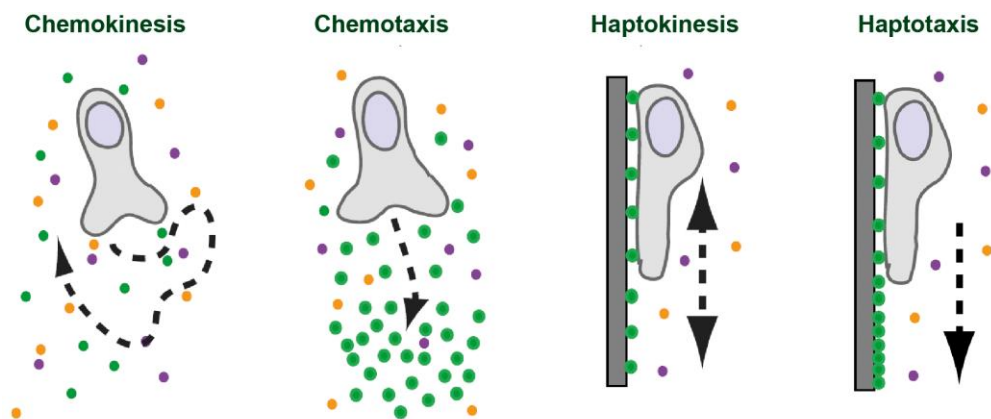
Figure 4. Leukocyte migration initiated by soluble or surface-bound chemoattractans. Homogenous fields of soluble chemokines induce self-polarization and random migration, a process called chemokinesis. Leukocytes perform directed migration towards a chemoattractant gradient in a process called chemotaxis. Surface-bound chemoattractans induce migration in a nondirected manner (haptokinesis) or directed manner (haptotaxis) towards a (modified from Lämmermann et al., 2014[69]).

Chemoattractans induce cell polarization via binding to the respective G-protein-coupled receptor (GPCRs). These receptors are seven-transmembrane domain receptors interacting with heterotrimeric G-proteins. Heterotrimeric G-proteins consist of three subunits, the α-subunit, β-subunit and γ-subunit[88,89]. Activation of GPCRs leads to the dissociation of the subunits Gα and Gβγ regulating activity of different enzymes including ion channels, adenylyl cyclases and phosphatidylinositol 3-kinase (PI3K). Direct activation of PI3K by the Gβγ subunit in the front of

the cell leads to the accumulation of phosphatidylinositol (3,4,5)-triphosphate (PIP₃) and the recruitment of the Rho family of small guanosine triphosphatases (GTPases) Rac and Cdc42. Rac and Cdc42 are crucial for actin polymerization as well as formation and stabilization of the leading edge[90,91]. The PI3K antagonist (PIP₃ 5-phosphatase PTEN) is simultaneously recruited to the rear of the cell in a RhoA/ROCK-dependent manner resulting in locally restricted production of PIP₃ and the localization of RhoA to the rear of the cell[92]. Here, RhoA controls contraction and retraction of the uropod by phosphorylating and thereby activating MyosinII (MyoII, Figure 5)[93-95].
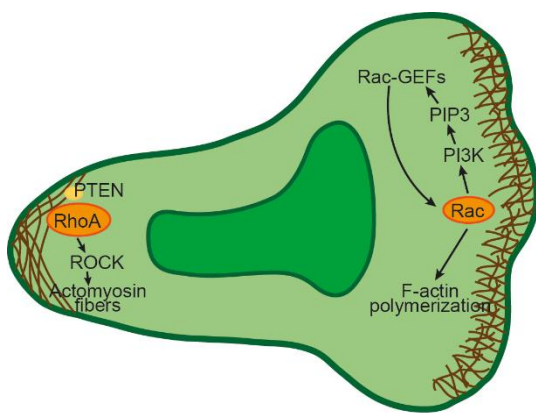
Figure 5. Signaling during neutrophil polarization. Signaling molecules such as PI3K and its product PIP₃ as well as Rac are enriched in the leading edge of polarized neutrophils. The production of PIP₃ activates Rac-GEFs which stimulate Rac resulting in F-actin polymerization and the formation of a lamellipodium. Active RhoA/ROCK signaling and inhibited Rac activity at the rear of the polarized cell leads to the presence of actomyosin fibers which are formed by MyoII light chains (adapted from Mocsai et al., 2015[18]).

Due to this rapid change of cell morphology, leukocyte migration is defined by the following steps occurring in a cyclic manner, pseudopod formation by actin polymerization at the cell front, contraction of the cell body and detachment of the cell back executed by actomyosin-driven forces. These intracellular forces of actin polymerization and actomyosin contraction are transduced to the surrounding environment to fulfill efficient cell migration[96-98].

1.2.1 Resistance to shear stress of neutrophils during migration

In vivo, neutrophil recruitment from the blood stream into the inflamed tissue occurs under vascular flow conditions. Neutrophils have the ability to crawl along the inflamed endothelium against and perpendicular to the blood flow in a mechanotactic manner to reach optimal junctional extravasation sites[48]. Specific molecular players have been shown to be involved in neutrophil migration under wall shear stress conditions[99]. The Rho-specific guanine exchange

factor (GEF) Vav1 is indispensable during mechanotactic migration[100]. In the genetic absence of Vav1, neutrophils migrate exclusively with the direction of blood flow and fail to crawl against or perpendicular to the flow. Under static conditions, the migration behavior of wild-type and Vav1$^{-/-}$ neutrophils is similar highlighting the critical role of Vav1 for shear-induced perpendicular migration. In line with these findings, Hepper et al. showed that mAbp1 is critically involved in post-adhesive events under flow conditions, but was indispensable for migration under static conditions[101]. The same was true for the mAbp1 interacting protein HPK1 indicating that HPK1 was additionally required for intraluminal crawling against the direction of blood flow[47]. The RhoA-specific GEF-H1 has been identified as another molecular player in stress-induced neutrophil migration[102]. This molecule regulates the function of RhoA, which is localized at the uropod and involved in the establishment of cell polarization as mentioned above[91]. GEF-H1$^{-/-}$ neutrophils displayed impaired spreading and migration behavior exclusively under flow conditions compared to control neutrophils[102,103].

1.2.2   The role of integrins during neutrophil migration

In 2D environments, effective neutrophil migration, e.g. intraluminal crawling relies on β_2 integrin-mediated adhesion to the endothelial surface (Figure 6, left panel). Using Mac-1$^{-/-}$ mice, it has been shown that Mac-1 is the major adhesion molecule involved in intraluminal crawling, as Mac-1-deficient neutrophils failed to crawl towards potential exit sites[48]. Several studies demonstrated that integrin blocking or depletion in diverse cell types, including neutrophils, DCs and T cells resulted in abolished migration in 2D environments[68,93,104,105]. However, migration of integrin-deficient ($\beta_2$$^{-/-}$ $\beta_7$$^{-/-}$ $\beta_1$$^{-/-}$ $\alpha_V$$^{-/-}$) neutrophils in 3D environments was intact compared to control cells[68,106,107]. This was also true for talin-deficient neutrophils suggesting that the high affinity conformation of LFA-1 is dispensable for successful 3D migration of neutrophils[68]. These data indicate that leukocyte migration in the interstitial space occurs in the absence of β_2 integrin-mediated adhesion showing that traction forces can be transmitted to the environment without anchoring the cell to the surface via integrins. Thus, forces necessary for interstitial cell movement can be obviously generated by the physical interactions between the cell and the extracellular matrix[68,108] (Figure 6, right panel).
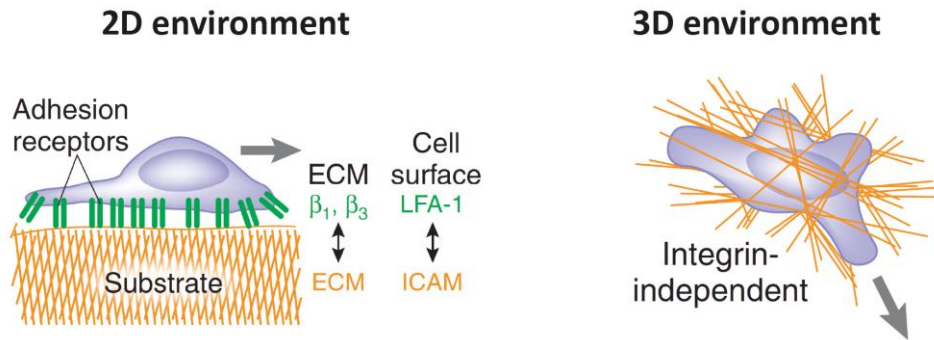
Figure 6. Schematics of β₂ integrin involvement during migration in 2D and 3D environment. Left panel: Migration in 2D environment requires adhesion to the extracellular matrix (ECM) via β₁, β₃ integrins or via binding of the β₂ integrin LFA-1 to ICAM-1 presented on the endothelial surface. Right panel: In contrast, migration in 3D environment is largely β₂ integrin independent (modified from Friedl et al., 2008[97]).

Within the interstitial space neutrophils rapidly migrate towards the site of injury or infection, where they accumulate and form clusters to isolate infected tissue from healthy tissue. This migration behavior was recently described as neutrophil swarming[106,109,110]. Studies in inflamed mouse skin using 2-photon microscopy indicated that neutrophil recruitment, accumulation and cluster formation was caused by neutrophil-derived leukotriene B4 (LTB4). Accumulated neutrophils were found to remodel the collagen fibers resulting in a collagen-free area at the wound. Talin- and integrin-deficient neutrophils were not able to migrate into this remodeled zone suggesting that high-affinity integrins are essential for neutrophil accumulation at the wound[106]. These data clearly demonstrate that the neutrophil migration mode and the involvement of β₂ integrins are dependent on the environment.

Infiltrated neutrophils are removed from sites of injury or inflammation by different mechanisms, including NETosis, apoptosis or necrosis followed by phagocytosis of macrophages[111-113]. Previous data have shown that neutrophil clearing from sites of infection can occur by active reverse interstitial and transendothelial migration away from sites of inflammation[114,115]. These processes were observed in zebrafish[114,116], mice[117], and in human neutrophils *in vitro[118]*, however the underlying migration mode, the involvement of β₂ integrins and the (patho-) physiological role of this process for the control of the inflammatory response remain elusive so far.

1.2.3   Deformation of the nucleus during neutrophil migration

During migration within 3D environments, i.e. transmigration and interstitial migration, cells have to squeeze through restriction sites generated by the surrounding extracellular matrix[119]. In general, there are two mechanisms cells undergo to successfully migrate through these constraints namely proteolytic degradation of the surrounding matrix and deformation of the cell body[120,121]. Since the nucleus is the largest cellular organelle, its deformation is indispensable and rate-limiting for migration without proteolytic degradation through constriction sites[122]. Cell nuclei consist of the nuclear envelope and the nuclear interior. The nuclear envelope is composed of the inner and outer nuclear membrane connected at the nuclear pore complexes and the underlying nuclear lamina. The nuclear lamin network of Lamin A/C at the inner nucelar membrane is involved in the structural determination of the nuclear shape and stiffness[123]. Friedl et al. described four phases the nucleus undergoes while migrating through narrow pores[121]. First the nuclear envelope pushes against the constraints generating intracellular forces leading to the formation of a small nuclear lobe which initiates the deformation of the nucleus. This phenomenon was also observed in T cells during TEM[124]. Subsequently, the nucleus adopts an hour-glass shape and squeezes through the confinement. Lastly the rear of the nucleus pushes forward resulting in the original ellipsoid shape. In general, the described deformation of the nucleus depends on dynamic interaction between the actin cytoskeleton and the nuclear envelope enabling transmission of force from the actin cytoskeleton to the nucleus. This interaction relies on the mechanical linkage between the actin filaments, microtubules, intermediate filaments and the nuclear membrane[121,125-127] (Figure 7). Linkers of the nucleocytoskeleton to cytoskeleton (LINC) complexes mediate the interaction between the nuclear membrane and the cytoskeleton[128]. Inner membrane proteins like SUN1/2 as well as the outer membrane proteins Nesprin-1/2, -3 are important components of the LINC complex interacting with the lamin network at the inner nuclear membrane[129]. Additionally, nuclear envelope transmembrane proteins, including the lamin B receptor (LBR) are involved in the anchoring of the nuclear membrane to the surrounding cytoskeleton[130].

Importantly, the nuclear shape as well as the nuclear envelope composition of neutrophil nuclei are different compared to other cell types, e.g. monocytes and T cells. Due to overexpression of LBR during granulopoiesis, neutrophil nuclei exhibit a multi-lobulated shape[131,132]. Human neutrophil nuclei consist of 2-6 nuclear lobes with a diameter of 2 μm which are connected by segments with a size of approximately 0.5 μm[133,134], whereas nuclei of murine neutrophils possess a ring-like shaped nucleus[135].
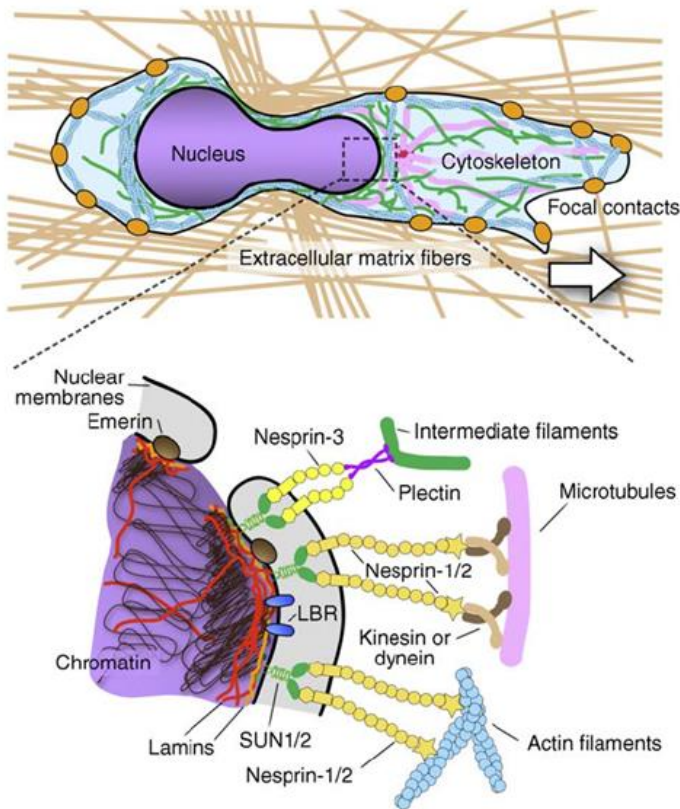
Figure 7. Schematics of the proteins involved in the connection between the cytoskeleton and the nucleus. Upper panel: Mesenchymal cell migration through a narrow pore smaller than the cell diameter within a 3D tissue (brown) shows an elongated nucleus at the rear of the migrating cell. In comparison, the nucleus is located in the front during amoeboid cell migration. The physical interaction of the cell with the extracellular matrix fibers is shown as orange spots (focal contacts). Lower panel: Components of the LINC complex namely SUN1/2 (green) and Nesprins (yellow) link the cytoskeleton filaments (intermediate filaments in green, microtubules in purple and actin filaments in light blue) to the nuclear membrane with its membrane proteins emerin (brown) and LBR (blue). Lamin network (red) at the inner nuclear membrane (adapted from Friedl, et al., 2011[121]).

Furthermore, neutrophil nuclei show low expression of LaminA/C and LINC complex proteins in the nuclear envelope leading to a high malleable nucleus which deforms and elongates during migration within 3D environments[132,136-138]. These unique characteristics enable neutrophils to migrate rapidly through constrictions being the first immune cells arriving at the sites of inflammation.

1.3   The myosin superfamily

The myosin (Myo) superfamily is a large and diverse family of F-actin based molecular motor proteins. The proteins are involved in a wide number of cellular functions, including cell adhesion and migration, membrane trafficking and signal transduction[139]. They consist of one or two heavy chains composed of a head (motor) domain binding actin in an ATP-dependent manner, a neck domain with a variable amount of IQ motifs binding light chains, calmodulin or calmodulin-like proteins and a tail domain with different binding sites determining the distinct function[139,140]. Most of the myosins are heterodimers and bind light chains via the characteristic consensus sequence

IQxxxRGxxxR of IQ motifs resulting in stability of the neck region[141]. Based on their structural similarity of the head (motor) domain, 267 myosins from 67 species are divided into 24 classes[142]. Some myosins are exclusively expressed in plants (e.g. MyoVIII) or in vertebrates (e.g. MyoX), however the majority is found in all eukaryotes[143]. Figure 8 shows the evolutionary tree of the first 18 myosin classes evolved and their structure of the heavy chains[143].
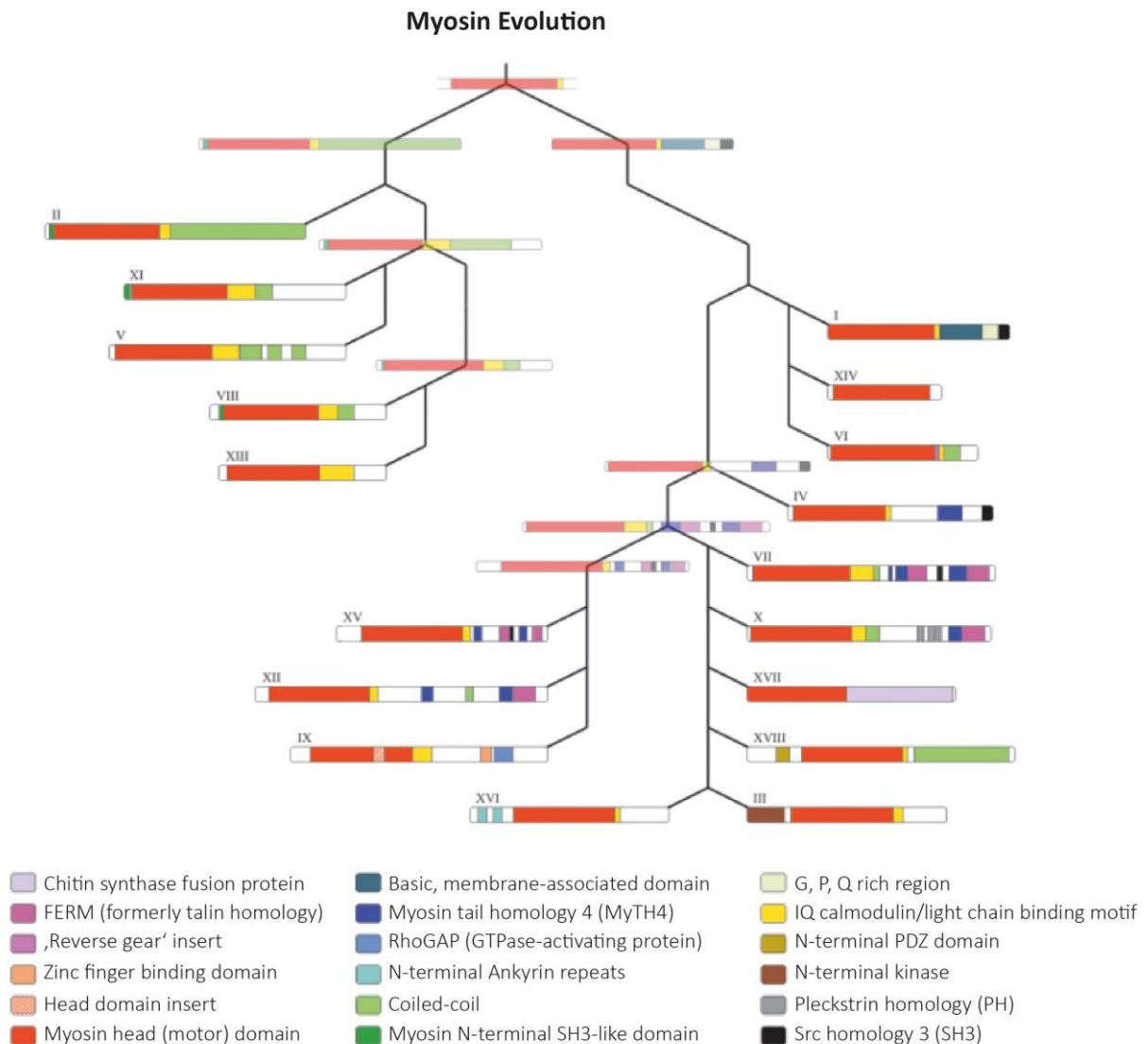
Figure 8. The evolutionary tree of the myosin superfamily. Schematics of the heavy chain of 18 myosin classes. Bright colors demonstrate examples from each myosin class. Light colors represent putative ancestral myosins not existing to date, however necessary to draw the diagram of the evolutionary pathways. Different colors indicate the different structural domains. FERM, four-point-one, ezrin, radixin, moesin; PDZ domain, post synaptic density protein, drosophila disc large tumor suppressor, zonula occludens-1 protein domain (adapted from Thompson et al., 2002[143]).

The myosin head (motor) domain is an ATPase which represents a mechanochemical enzyme converting energy released by ATP hydrolysis to force for cell movement along the actin cytoskeleton[144]. The tail domain contains different conserved protein domains for protein-protein interaction, kinase activity, or lipid binding which dictate the specific function of the myosin. Some tails contain heptad repeat sequences allowing the formation of coiled-coil structures leading to dimerization of two heavy chains as seen for the most studied conventional MyoII[139]. The muscle MyoII is involved in muscle contraction, whereas the non-muscle MyoII plays an important role in cytokinesis and cell migration[145,146]. Besides MyoII which is characterized by the formation of bipolar filaments by homo-oligomerization of the tail domain, all other classes are termed unconventional myosins and do not form filaments[147]. Due to membrane binding domains in the tail domain, unconventional myosins (e.g. MyoI and MyoV) are implicated in membrane-related processes, like endocytosis and vesicle trafficking[148,149].

1.3.1 Unconventional class I myosins (MyoI)

Unconventional class I myosins (MyoI) are highly conserved and widely expressed in almost all eukaryotic species. There are eight MyoI heavy-chain genes in mice and humans, six genes encode short-tailed forms (Myo1a, b, c, d, g, h) and two encode long-tailed forms (Myo1e, f)[150]. Myo1e and Myo1f are mainly expressed in hematopoietic cells, and Myo1a is found in the intestine. The other members of MyoI namely Myo1b, c, d, g, h are found in almost all cell types[148]. MyoI consist of a heavy chain containing the three typical structural domains, the head, neck and tail domain (Figure 8) and a basic tail homology 1 (TH1) domain with a pleckstrin homology domain binding different anionic phospholipids in various cellular membranes[151-154]. The long-tailed myosins encode an additional proline-rich TH2 domain and a TH3 domain with a SH3 domain mediating protein-protein interactions[139,155].

In general, class I myosins are involved in many membrane-associated functions due to their potential to link membranes to the actin cytoskeleton, including endocytosis, cell signaling and cell motility[156-158]. Myo1a localizes to the intestinal brush border domain consisting of microvilli in the apical surface of the intestine where it connects the microvilli membrane to the cytoskeleton and regulates membrane tension[159]. Furthermore, Myo1a was identified in Golgi-derived vesicles suggesting a crucial impact of Myo1a in vesicle trafficking[160,161]. The tail domain of Myo1b has 47 % homology to the Myo1a tail domain and was found to localize to endosomes and lysosomes indicating its contribution to the transport of vesicles[162,163]. Studies using recombinant Myo1c

demonstrated that basic tail domains bind specifically to phosphatidylinositol (4,5)-bisphosphate instead to the predicted acidic phosphatidylserine[153]. Myo1c was reported to play an important role in glucose transporter 4-containing vesicle movement[164] and in the transport of vascular endothelial growth factor receptor-2 to the plasma membrane[165]. Myo1d is mainly expressed in the brain and studies using a Myo1d blocking antibody demonstrated an important role of Myo1d in the membrane recycling pathway[166]. Myo1g is expressed in T lymphocytes where it plays an important role in T cell migration by generating membrane tension. It has also been shown that Myo1g enhances T cell-DC interactions during lymph node surveillance[167,168]. Furthermore it is expressed in B lymphocytes where it is involved in the regulation of actin remodeling[169] and in FcR-mediated phagocytosis[170]. Until now there is nothing known in the literature about the localization and function of Myo1h[151]. The two long-tailed members Myo1e and Myo1f are highly expressed in immune cells. Natural killer cells, DCs and macrophages express both long-tailed isoforms, whereas B cells only express Myo1e and neutrophils only express Myo1f[1,171]. In contrast to Myo1f, Myo1e is more widely expressed, and plays a role in clathrin-mediated endocytosis[172] as well as in Toll-like receptor 4 (TLR4)-mediated macrophage spreading and antigen presentation as it regulates major histocompatibility complex (MHC) class II surface expression[173].

1.3.2   Myosin 1f

Myo1f is expressed in the spleen, mesenteric lymph nodes, thymus and lung[1]. The protein consists of the motor domain, followed by an IQ motif, a TH1 domain and at its C-terminal end it encodes a SH3 domain (Figure 9).

Figure 9. Schematics of the domain structure of Myo1f. Myo1f consists of the motor domain (blue) which is an ATP and actin binding domain, followed by an IQ motif (orange) and a TH1 domain (green) which is involved in binding of membrane phosphoinositides. At its C-terminal end, the protein contains a SH3 domain (red) which is crucial for protein-protein interactions. Numbers indicate amino acids where the domains start and end.

Studies in the amoeboid organism *Dictyostelium discoideum* demonstrated that the deletion of several forms of MyoI, including MyoA, MyoB and MyoF resulted in impaired cell migration[174-176]. Since neutrophils and *Dictyostelium discoideum* exhibit similar migration modes it has been hypothesized that Myo1f is crucial for neutrophil migration. Indeed, Myo1f$^{-/-}$ mice fail to control infection by *Listeria monocytogenes* due to an impaired neutrophil accumulation at the site of inflammation. Furthermore, it has been demonstrated that the genetic absence of Myo1f results in an increased neutrophil adhesion to ICAM-1 via β_2 integrins under static conditions *in vitro.* In summary, Myo1f seems to be critically involved in neutrophil recruitment and innate host defense against infection[1].

2. AIM OF THE THESIS

Myo1f is the only long-tailed isoform of the Myosin I family expressed in neutrophils reported so far. It has been previously shown that Myo1f$^{-/-}$ neutrophils exhibit an abnormally increased adhesion to the β_2 integrin ligand ICAM-1 as well as decreased 2D migration velocity under static conditions *in vitro.* Furthermore, Myo1f$^{-/-}$ mice show an increased susceptibility to infection with *Listeria monocytogenes* due to impaired neutrophil accumulation at sites of inflammation[1]. However, the role of Myo1f for the different steps of the neutrophil recruitment cascade is still elusive.

Therefore, the first aim of this study was to identify the role of Myo1f for neutrophil rolling and adhesion under physiological flow conditions *in vitro* and *in vivo* using flow chamber assays and intravital microscopy. The second aim of this study was to analyze the impact of Myo1f for neutrophil extravasation in different *in vivo* models, including the TNFα-induced cremaster model, the peritonitis model, and the acute lung injury (ALI) model. The third aim of this study was to analyze the role of Myo1f for migration of neutrophils in 2D environments. The last aim of this study was to uncover the role of Myo1f for migration of neutrophils in 3D environments, i.e. transmigration and interstitial migration.

In summary, this study will not only improve the understanding of the function of Myo1f in neutrophil trafficking but may provide new concepts for therapeutic strategies in the treatment of neutrophil-driven acute or chronic inflammatory diseases.

3. MATERIALS

3.1 Mouse strains

Myo1f$^{-/-}$ mice were maintained on a C57BL/6 background. C57BL/6 wild type (Myo1f$^{+/+}$) mice were obtained from Charles River Laboratories. All animal experiments were conducted in accordance with the German federal animal protection laws and approved by the Bavarian Government (Regierung von Oberbayern, Munich, Germany).

3.2 Chemicals

Name	Supplier	Name	Supplier
2-mercaptoethanol	Sigma Aldrich, Germany	May-Grünwald solution	AppliChem, Germany
acetic acid	Applichem, Germany	manganese (II) chloride tetrahydrate	AppliChem, Germany
agarose	Genaxxon, Germany	methanol	Th. Geyer, Germany
ampicillin	AppliChem, Germany	midori Green	Nippon, Japan
bovine serum albumine (BSA)	Sigma Aldrich, Germany	modified eagle's minimum essential medium (Opti-MEM)	Gibco, Life Technologies, Germany
bromphenole blue	AppliChem, Germany	mowiol	Sigma Aldrich, Germany
calcium chloride (CaCl$_2$)	AppliChem, Germany	PageRuler™ prestained protein ladder	Thermo Fisher Scientific, Germany
collagen type I, rat tail	IBIDI, Germany	paraformaldehyde	Sigma Aldrich, Germany
crystal violet	Sigma Aldrich, Germany	paramethoxyamphetamine (PMA)	Merck, Germany
dimethyl sulfoxide (DMSO)	AppliChem, Germany	penicillin	Biochrom, Germany
diisopropyl phosphofluoridate (DFP)	Sigma Aldrich, Germany	percoll	Sigma Aldrich, Germany
dithiothreitol (DTT)	AppliChem, Germany	phosphate buffered saline (PBS)	Biochrom, Germany
Dulbecco's modified eagle medium (DMEM)	Biochrom, Germany	phenol red	Biochrom, Germany

Name	Supplier	Name	Supplier
ethanol absolute	Th. Geyer, Germany	poly-L-Lysin	Merck, Germany
ethylenediamine-tetraacetic acid (EDTA)	AppliChem, Germany	protease inhibitor Mix B	Sigma Aldrich, Germany
Eukitt quick-hardening mounting medium	Sigma Aldrich, Germany	Roswell Park Memorial Institute 1640 (RPMI)	Biochrom, Germany
fetal calf serum (FCS)	Biochrom, Germany	salmonella eneritidis	Sigma Aldrich, Germany
fluorescence microbeads	Polysciences, Germany	sodium chloride (NaCl)	AppliChem, Germany
GeneRuler™ 100 bp DNA ladder	Fermentas, USA	sodium hydrogen carbonate (Na$_2$HCO$_3$)	AppliChem, Germany
GeneRuler™ 100 bp DNA ladder	Nippon, Japan	sodium dodecyl sulfate (SDS)	AppliChem, Germany
Giemsa's azur eosin methylene blue	Sigma Aldrich, Germany	sodium fluoride	Sigma Aldrich, Germany
glucose	AppliChem, Germany	sodium dihydrogen carbonate (NaH$_2$PO$_4$)	Sigma Aldrich, Germany
glutaraldehyde solution	Sigma Aldrich, Germany	sodium orthovanadate	Sigma Aldrich, Germany
glycine	AppliChem, Germany	streptomycin	Biochrom, Germany
Hank's balanced salt solution	Biochrom, Germany	TritonX-100	Sigma Aldrich, Germany
HEPES	AppliChem, Germany	tris-HCl	Applichem, Germany
hydrochloric acid, 37% (HCl)	AppliChem, Germany	TRITC-Dextran	Sigma Aldrich, Germany
lipofectamin 2000	Thermo Fisher Scientific, Germany	Trizma®base (tris)	Applichem, Germany
lipopolysaccharide (LPS) from *Salmonella eneritidis*	Sigma Aldrich, Germany	trypsin/EDTA	Biochrom, Germany
manganese chloride (MnCl$_2$)	AppliChem, Germany	Tween 20	Sigma Aldrich, Germany
magnesium chloride (MgCl$_2$)	AppliChem, Germany	xylol	AppliChem, Germany

3.3   Recombinant proteins

Name	Supplier
rmCXCL1	R&D Systems, USA
murine fibrinogen	Innovative Research, USA
rmICAM1 without Fc	Stemcell, Germany
rmICAM-1/Fc	R&D Systems, USA
rmP-selectin with Fc	R&D Systems, USA
rmTNFα	R&D Systems, USA
human fibrinogen	R&D Systems, USA
human fibrinogen Alexa-647	Thermo Fisher Scientific, Germany
hICAM-1	R&D Systems, USA
interleukin-8 (IL-8)	R&D Systems, USA
N-formyl-L-methionyl-L-leucyl-phenylalanine (fMLP)	Sigma Aldrich, Germany

3.4   Antibodies

Antigen	Dye	Reactivity	Clone	Company
β actin	-	mouse anti-human	C4	Santa Cruz Biotechnology, USA
CD11a	Alexa Fluor 594	rat anti-mouse	2D7	BioLegend, USA
CD11a	PE	rat anti-mouse	2D7	BD Biosciences, USA
CD11a	-	rat anti-mouse	M17/4	eBioscience, USA
CD11b	PE	rat anti-mouse	M1/70	eBioscience, USA
CD11b	-	rat anti-mouse	M1/70	eBioscience, USA
CD18	PE	rat anti-mouse	C71/16	BD Biosciences, USA
GFP	-	rabbit anti-human	FL	Santa Cruz Biotechnology, USA
Hoechst 33342	-	-	-	Thermo Scientific, USA
IgG1	PE	mouse anti-human	H2	Southern Biotech, USA
isotype control	PE	rat anti-mouse	IgG2a, κ	BD Biosciences, USA
isotype control	PE	rat anti-mouse	IgG2b, κ	eBioscience, USA
Ly6-G	FITC	rat anti-mouse	1A8	BioLegend, USA
Myo1f	-	mouse anti-human	B-5	Santa Cruz Biotechnology, USA

Antigen	Dye	Reactivity	Clone	Company
Myo1f	-	rabbit anti-mouse	polyclonal	custom-made, Davids Biotechnology, Germany
Phalloidin	Alexa Fluor 546	-	-	Thermo Fisher Scientific, Germany
secondary antibody	Alexa Fluor 647	donkey anti-rabbit	-	Thermo Fisher Scientific, Germany
secondary infrared	680 RD	donkey anti-rabbit	-	Li-Cor Biotechnology, USA
secondary infrared	800 CW	donkey anti-mouse	-	Li-Cor Biotechnology, USA
Sir-Actin	-	-	-	Spirochrome, Switzerland

3.5 Media

Name	Ingredients	Name	Ingredients
DMEM+	DMEM GlutaMAX™ 4.5 g/l glucose 10% (v/v) fetal calf serum 100 U/ml penicillin 100 µg/ml streptomycin	RPMI 1640	10% (v/v) fetal calf serum 100 U/ml penicillin 100 µg/ml streptomycin
DMEM	10% (v/v) fetal calf serum 100 U/ml penicillin 100 µg/ml streptomycin		

3.6 Buffers and Solutions

Name	Ingredients	Name	Ingredients
1x adhesion medium (ADM)	1.2 mM Ca^{2+} 1 mM Mg^{2+} 0.25 % BSA 0.1 % glucose 20 mM Hepes pH 7.4 in Hank's balanced salt solution	50x TAE buffer	2 M tris 1 M sodium acetate 62.5 mM EDTA pH 8.5

Name	Ingredients	Name	Ingredients
10x ADM	12 mM Ca^{2+} 10 mM Mg^{2+} 2.5 % BSA 1 % glucose 200 mM Hepes pH 7.4 in Hank's balanced salt solution	agarose gel solution	1x TAE buffer 1-2% (w/v) agarose 1 µg/ml midori green
10x DNA sample buffer	0.1% (w/v) bromophenol blue 50% (v/v) glycerol 0.1 M EDTA pH 8.0	**BD FACS™ lysing solution**	Dilution 1:10 in H_2O
10x running buffer	2 M glycine 250 mM tris 1% (w/v) SDS	**cell lysis buffer**	25 mM tris-HCl pH 7.4 150 mM NaCl 0.5 mM EDTA 1 % TritonX-100 1% (w/v) sodium deoxycholate 1 mM DTT 1x Protease Inhibitor (Sigma) 1 mM DFP 20 mM sodium fluoride 2 mM sodium orthovanadate
1x SDS sample buffer	200 mM tris-HCl 400 mM DTT 8% (w/v) SDS 0.4% (w/v) bromophenol blue 40% (v/v) glycerol 10% (v/v) 2-mercaptoethanol pH 6.8	**WB blocking solution**	1x TBS 5% (w/v) skim milk powder 0.02% (v/v) Tween 20
10x TBS buffer	250 mM tris-HCl 1.5 M NaCl	**WB washing buffer (TBST)**	1x TBS 0.02% (v/v) Tween 20
1x transfer buffer	25 mM tris 192 mM glycine 20% (v/v) methanol		

3.7 Cell lines

Name	Description	Source
b.End3	immortalized mouse brain endothelial cell line	ATCC®CRL-2299™, Manassas, VA
HL-60	human promyelocytic leukemia cell line	ATCC®CRL-240™, Manassas, VA
WEHI-3B	murine myelomonocytic leukemia cell line	DSMZ ACC 26, Germany

3.8 Software

Name	Company
Adobe Photoshop and Illustrator	Adobe, USA
Chemotaxis and Migration Tool	IBIDI, Germany
EndNote X7.4	Clarivate Analytics, USA,
FACS Diva	BD Biosciences, USA
FlowJo 7.6	Treestar, USA
ImageJ	NIH, USA
Leica Application Suites	Leica, Germany
Prism 6	GraphPad, USA
Slidebook 6.0.8	3i, USA

3.9 Equipment

Name	Company
AxioCam Hsm camera	Zeiss, Germany
Axiotech Vario intravital microscope	Zeiss, Germany
Axiovert 200M microscope	Zeiss, Germany
Confocal scanner unit CSU-X1	Yokogawa Electric Corporation, Japan
Coulter A C T counter	Coulter Corporation, USA

Name	Company
EM CCD camera	Photometrics, USA
Examiner spinning disk confocal microscope	Zeiss, Germany
FACS BD Canto II cytometer	BD Bioscience, USA
Odyssey® CLx imaging system	Li-Cor Biotechnology, USA
ProCyte Dx hematology analyzer	IDEXX Laboratories, Germany
PowerWave HT microplate reader	Biotek, USA
SP8X WLL microscope	Leica Biosystems, Germany

3.10 IBIDI chambers

- µ-Slides Chemotaxis3D chamber
- µ–Slide membrane ibiPore flow chamber
- µ-Slide VI 0.1 flow chamber
- µ-Slide VI 0.4 flow chamber

4. METHODS

4.1 Genotyping

To identify the genetic background of Myo1f$^{+/+}$ and Myo1f$^{-/-}$ mice, DNA of tail biopsies was extracted and analyzed by Polymerase Chain Reaction (PCR). Total DNA was isolated using the PCRBIO Rapid Extract PCR kit (PCRBiosystems, United Kingdom) according to the manufacturer's instructions. PCR was carried out using FastGene® Optima HotStart ReadyMix according to the manufacturer's protocol (Table 1) and specifically designed primers (Table 2) to distinguish Myo1f$^{+/+}$ and Myo1f$^{-/-}$ mice (Figure 10). In homozygous Myo1f$^{-/-}$ mice exon 5 and 6 were eliminated on both alleles, therefore the PCR product differed in length between Myo1f$^{+/+}$ and Myo1f$^{-/-}$ DNA. The PCR protocol included a primary denaturation step at 95 °C for 3 min, followed by cycles of 15 s at 95 °C (denaturation), 15 s at the annealing temperature of the primers (hybridization) and 60 s at 72 °C (extension) and a final extension step of 7 min 72 °C. In all performed PCR reactions an annealing temperature of 52 °C was used.
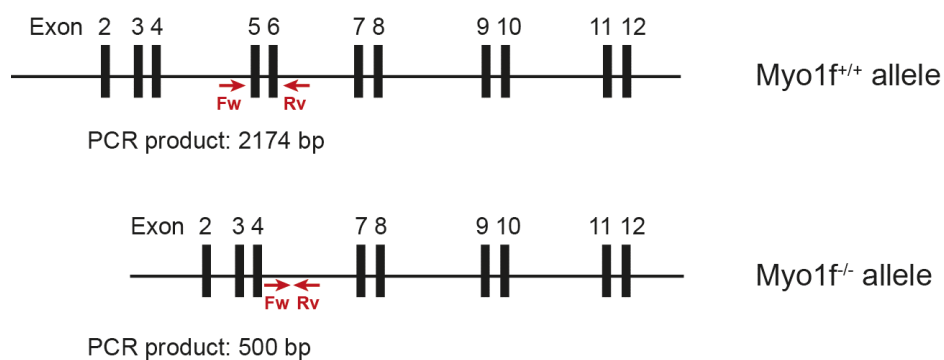
Figure 10. Schematic representation of Myo1f$^{+/+}$ and Myo1f$^{-/-}$ alleles. The red arrows show the specific primers (Fw, forward; Rv, reverse) used to distinguish between Myo1f$^{+/+}$ and Myo1f $^{-/-}$ DNA according to specific length of the PCR product.

DNA fragments were separated according to their size by agarose gel electrophoresis (2 % agarose in 1x TAE buffer), stained by adding 1 µg/mL Midori Green to the fluid gel before the run and visualized by UV light (260 nm). As a size standard, 100 bp DNA ladder was run on the same gel. The PCR with the specific primer pair resulted in a PCR product size of 2174 bp for the Myo1f$^{+/+}$ allele and product size of 500 bp for the Myo1f$^{-/-}$ allele.

Table 1. PCR components

Components	Final concentration
2x FastGene® Optima HotStart ReadyMix with dye	1x
Forward primer (10 µM)	0.5 µM
Reverse primer (10 µm)	0.5 µM
Template DNA	2 µL of isolated DNA
H_2O	x µL

Table 2. Primers used for genotyping

Name	Oligonucleotide 5' – 3'	Tm [°C]	Supplier
Myo1f Fw	ATGTCTTCAGGCTTGGCAAC	51.8	Metabion, Germany
Myo1f Rv	TCGCTGACCATCCACTTACA	51.8	Metabion, Germany

4.2 HL-60 cells

4.2.1 Culture and differentiation of HL-60 cells

The human promyelocytic leukemia cell line HL-60 was cultured in RPMI 1640 growth medium, supplemented with 10 % FCS, penicillin (100 U/mL), and streptomycin (100 µg/mL) at 37 °C in 5 % CO_2. To differentiate HL-60 cells towards neutrophil-like cells (dHL-60), $1x10^6$ cells were cultured in 10 mL RPMI 1640 (+10 % FCS, penicillin, streptomycin) medium supplemented with 1.3 % DMSO for 6 days[177,178]. HL-60 cells stably expressing an EGFP-tagged Myo1f fusion protein used in this study were generated by Phillip Löhr using lentiviral transduction[127].

4.2.2 Cryopreservation and resuscitation of frozen cells

For long term storage, cells were centrifuged at 300 g for 5 min and suspended in a mix of 90 % (v/v) FCS, and 10 % (v/v) dimethyl sulfoxide. Subsequently, cryotube aliquots were put in a NALGENE™ Cryo 1°C Freezing Container (Thermo Fisher Scientific, Germany) allowing freezing at constant rate of approximately -1°C per minute and kept at -80°C overnight before storing them

at -196 °C in liquid nitrogen. In order to re-cultivate frozen cell line stocks, cryotubes were quickly thawed in a water bath at 37 °C and washed once with 10 ml RPMI 1640 growth medium before culture.

4.2.3 Western Blot analysis

After puromycin selection, expression of the 152 kDa EGFP-fusion protein was analyzed by immunoblotting technique. Therefore, 10×10^6 infected HL-60 cells were lysed in 300 µL cytosolic cell lysis buffer supplemented with 1 mM DFP, 20 mM sodium fluoride and protease inhibitor cocktail at 4 °C for 30 min[179]. Cellular debris was removed by centrifugation at 1600 g for 5 min and supernatants containing soluble total protein were mixed with 2x SDS sample buffer, reduced and denatured by boiling at 95 °C for 10 min. Proteins were separated according to their molecular weight and charged by SDS-PAGE following the method by Laemmli[180]. Total protein lysates and PageRuler™ Prestained Protein ladder were loaded on polyacrylamide gels of a 10 % separating gel and a 4 % stacking gel. Electrophoresis was done in 1x running buffer at 80 - 120 V. For immunological identification of separated proteins, electrophoretic transfer of proteins on nitrocellulose transfer membrane was carried out by the semi-dry blotting technique. After blotting, membranes were incubated for at least 1 h in 10 ml blocking solution at room temperature on a rocking platform. Membranes were incubated with anti-human Myo1f antibody, anti-human β actin antibody and anti-human GFP antibody at 4 °C overnight. Detection was performed using near-infrared labeled secondary protein dyes and the Odyssey®CLx Imaging system.

4.3   Immunofluorescence and confocal microscopy

For the identification of the subcellular localization of the EGFP-Myo1f fusion protein as well as F-actin, adherent dHL-60 EGFP-Myo1f cells on immobilized fibrinogen (250 µg/µL) and stimulated with 100 nM fMLP for 15 min at 37 °C were fixed with 4 % paraformaldehyde (PFA). After permeabilization with 0.1 % Triton-X and blocking with 10 % BSA, Myo1f was stained using a custom-made anti-mouse Myo1f rabbit polyclonal antibody specifically recognizing the Myo1f C-terminal region of amino acids RPRRSAQAPTRAAPGPPRGLNRNGV, and a secondary Alexa Fluor 647 donkey anti-rabbit polyclonal antibody. Phalloidin 546 was used to visualize F-actin.

Cells were mounted in ProLong Diamond Antifade Mountan and imaged with a Leica SP8X upright confocal microscope using a Leica HC PL APO 63x/1.40 oil objective.

The morphology of the nucleus, the subcellular localization of Myo1f and Actin and the colocalization of both proteins in isolated primary human neutrophils were analyzed during migration within a 1.5 mg/mL collagen towards an fMLP (100 nM) gradient using spinning disk confocal microscopy. After migration within a collagen gel for 10 min primary human neutrophils were fixed with 4 % PFA, permeabilized with 0.2 % Triton-X and blocked with 1 % BSA. Myo1f was stained using the mentioned custom-made anti-mouse Myo1f rabbit polyclonal antibody labelled with Alexa Fluor 488. The nuclear dye Hoechst 33342 was used for nucleus staining (5 µM) and Alexa Fluor 546 Phalloidin was used for F-Actin staining. Images were acquired using an upright spinning disk confocal microscope and three lasers with an excitation wavelength of 405 nm, 488 nm and 561 nm.

4.4 Neutrophil recruitment *in vitro*

4.4.1 Isolation of murine neutrophils and human neutrophils

Myo1f$^{+/+}$ and Myo1f$^{-/-}$ bone marrow neutrophils obtained from femurs and tibias were loaded onto a discontinuous Percoll gradient (52 %/64 %/72 %)[181] and centrifuged for 30 min at 1000 g without break. Neutrophils enriched in the Percoll gradient interphase between 72 % and 64 % were collected and washed once in PBS. Isolated neutrophils were cultured for 24 h in RPMI 1640 medium supplemented with 20 % WEHI-3B-conditioned medium. Human blood was collected from healthy donors and anticoagulated with sodium citrate (0.3 %). Erythrocyte sedimentation was allowed in the presence of 40 % (v/v) autologous plasma. Neutrophils were isolated from the leukocyte-rich plasma using a discontinuous Percoll gradient (55 %/74 %) as described[182].

4.4.2 Cell number quantification

For cell culture experiments exact cell numbers of isolated murine neutrophils and dHL-60 cells were determined by counting viable cells using a Neubauer counting chamber and trypan blue for staining of dead cells.

4.4.3 Static adhesion assay

To investigate neutrophil adhesion under static conditions, a static adhesion assay was performed[183]. In detail, 1×10^5 neutrophils suspended in adhesion medium (ADM) were seeded into a 96-well plate and exposed to immobilized rmICAM-1 (12.5 µg/ml) or murine fibrinogen (50 µg/mL). Cells were allowed to adhere for 10 min at 37 °C and stimulated with 5 µg/ml rmCXCL1, 3 mM Mn^{2+}, 10 µM fMLP, 100 ng/mL TNF-α, or 100 ng/mL PMA at 37 °C for 10 min in triplicates. Adherent Myo1f$^{+/+}$ and Myo1f$^{-/-}$ neutrophils in percent of cells added (100 %) were calculated using a standard curve. The standard curve was prepared by adding 100 %, 80 %, 60 %, 40 %, 20 %, and 10 % of the cell suspension on poly-L-lysine coated wells (100 µg/mL) in triplicates. Samples and standard curve were fixed with 1 % glutaraldehyde and cells were stained with 0.1 % crystal ciolet. Absorbance was measured at a wavelength of 590 nm using a microplate reader.

4.4.4 Induction of adhesion under flow conditions

In order to study induction of adhesion under flow conditions, IBIDI µ-Slide VI 0.1 flow chambers were used as previously described [47]. In detail, flow chambers were coated overnight at 4 °C with 10 µg/mL rmP-selectin-Fc, 12.5 µg/ml rmICAM-1 and 5 µg/ml rmCXCL1 and blocked with 10 % casein for 2 h at room temperature. Myo1f$^{+/+}$ and Myo1f$^{-/-}$ neutrophils (5×10^5/sample) were resuspended in ADM and perfused through the flow chamber with a constant shear stress rate of 1 dyne/cm^2 for 9 min. Time-lapse videos were recorded using an Axiovert 200M microscope equipped with a Plan-Apochromat 20×/0.75NA objective, AxioCam HR digital camera, and a temperature-controlled environmental chamber. The number of rolling and adherent neutrophils was counted offline using ImageJ software.

4.4.5 2D migration assays

Mechanotactic crawling of Myo1f$^{+/+}$ and Myo1f$^{-/-}$ neutrophils was analyzed using IBIDI µ-Slide VI 0.1 flow chambers coated with 10 µg/mL rmP-selectin-Fc, 12.5 µg/ml rmICAM-1 and 5 µg/ml rmCXCL1 or with murine fibrinogen. To analyze crawling on fibrinogen, neutrophils were stimulated with fMLP (10 µM) for 10 min. The cells were perfused through the flow chamber and

allowed to adhere for 10 min at 37 °C. Flow was applied (1 dyne/cm^2) for 10 min and crawling was recorded by time-lapse microscopy with a time interval of 5 s.

Chemotactic migration was investigated in Zigmond chambers as described previously[184]. Briefly, Myo1f$^{+/+}$ and Myo1f$^{-/-}$ neutrophils were seeded onto coverslips coated with 50 μg/ml murine fibrinogen or with 12.5 μg/ml rmICAM-1. Cell migration towards a gradient of 10 μM fMLP or 100 ng/ml rmCXCL1 was analyzed for 10 min. Migration velocity, Euclidean distance and accumulated distance were analyzed offline using ImageJ software and its implemented manual tracking plugin. Single cell migration tracks and Rose Plots were generated using ImageJ's chemotaxis and migration software provided by IBIDI.

4.4.6 Live cell imaging of *in vitro* transmigration under flow conditions

Transmigration of Myo1f$^{+/+}$ and Myo1f$^{-/-}$ neutrophils was analyzed in IBIDI μ–Slide membrane ibiPore flow chambers. The device is shown in (Figure 11). F-Actin of Myo1f$^{+/+}$ and Myo1f$^{-/-}$ neutrophils was stained overnight at 37 °C in 5 % CO$_2$ using Sir Actin[185] (100 nM). Additionally, Myo1f$^{+/+}$ and Myo1f$^{-/-}$ neutrophils were labelled with a non-function blocking Alexa Fluor 594 conjugated anti-CD11a antibody (clone 2D7) for 15 min at room temperature. Neutrophils were perfused through the rmICAM-1 (12.5 μg/mL) and rmP-selectin (10 μg/mL) coated flow chamber with 1 dyne/cm^2 shear stress for 60 min.
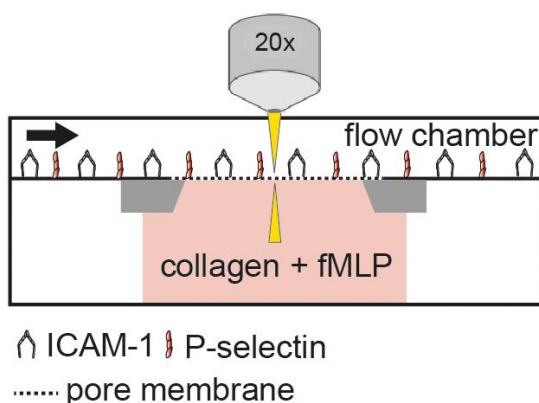
Figure 11. Schematic representation of the μ–Slide membrane ibiPore flow chamber. The IBIDI flow chamber consists of a flow chamber coated with rmICAM-1 (12.5 μg/mL) and rmP-selectin (10 μg/mL), a membrane with pores with a pore size of 5 μm and a subjacent collagen gel with fMLP (10 μM) as chemoattractant. Arrow indicates the direction of flow (adapted from IBIDI).

Time-lapse video microscopy with an average time interval of 30 s was performed using an upright spinning disk confocal microscope equipped with a confocal scanner unit CSU-X1, an EM CCD camera and a 20x/1.0NA water immersion objective. 3D images out of 70 z-stacks with a step size of 0.55 µm were acquired using two lasers with an excitation wavelength of 561 nm and 633 nm. To analyze transmigrated Myo1f$^{+/+}$ and Myo1f$^{-/-}$ neutrophils an orthogonal projection of the acquired z-stacks was generated using Slidebook 6.0.8 Software (3i, USA). The number of transmigrated cells was counted and shown as percentage of all cells in the field of view (FOV, 100 %)[127].

4.4.7   Transmigration under static conditions

To analyze transendothelial migration of Myo1f$^{+/+}$ and Myo1f$^{-/-}$ neutrophils *in vitro*, transwell assays were performed using transwell polycarbonate filters with a pore size of 8 µm. Brain-derived b.End3 endothelial cells were seeded on transwell filters and cultured for 48 h until a monolayer had formed. The lower compartment of the transwell system was either filled with ADM alone or complemented with CXCL1 (100 ng/mL). After 30 min of equilibration, 5x10^5 neutrophils resuspended in ADM, were added to the upper compartment and allowed to migrate for 45 min at 37 °C. As control the transwell filters were left uncoated. Transmigrated neutrophils were collected from the lower compartment and counted under the microscope.

In a second set of experiments, the morphology of the nucleus was analyzed during transmigration. Myo1f$^{+/+}$ and Myo1f$^{-/-}$ neutrophils were labeled with the nuclear dye Hoechst 33342 (5 µM) at 37 °C for 5 min. Stained cells were applied to rmICAM-1 (12.5 µg/mL) and rmP-selectin (10 µg/mL) coated transwell filters with a pore size of 3 µm in the upper compartment. In the lower compartment, ADM supplemented with fMLP (10 µM) as chemoattractant was added. Cells were allowed to transmigrate through the filters into the lower compartment. Transmigration was stopped after 5, 10 and 15 min by adding 4 % PFA for 15 min. After fixation membranes were cut out and mounted with Mowiol. Confocal microscopy was performed using a Leica SP8X WLL microscope, equipped with a 405 nm laser, a WLL2 laser (470 - 670 nm) and an acusto-optical beam splitter. Images were acquired using a 63x1.4 objective. Morphology of the nucleus was analyzed offline by measuring the nucleus area using ImageJ software.

4.4.8 Chemotaxis in a 3D collagen gel

3D migration of Myo1f^{+/+} and Myo1f^{-/-} neutrophils

Analysis of 3D chemotaxis was performed in IBIDI μ-Slides Chemotaxis3D chambers according to the manufacturer's protocol (IBIDI). Myo1f^{+/+} and Myo1f^{-/-} neutrophils (4x10^5/sample) were seeded into collagen gels with different concentrations of rat tail collagen type I (Table 3). The collagen solution was filled into the channel of the IBIDI μ-Slides Chemotaxis3D chambers. After gelation for 5 min at 37 °C the reservoirs were filled with ADM alone or ADM supplemented with CXCL1 (100 ng/mL). Time-lapse video microscopy was performed every 14 s for 30 min at 37 °C using an Axiovert 200M microscope. Analysis of the migration velocity was performed using ImageJ software and its implemented manual tracking plugin. Single cell migration tracks and Rose Plots were generated using ImageJs chemotaxis and migration software provided by IBIDI.

Table 3. Collagen gel preparation

Compound	Collagen concentration (mg/mL)	
	1.5	3.0
	Volumes (μL)	
10x ADM	10	10.5
H_2O	40	-
$NaHCO_3$	2	1.5
1x ADM	25	19
Collagen type I, rat tail 5 mg/mL	45	90
Cell suspension	25	25

Morphology of the nucleus during 3D migration of Myo1f^{+/+} and Myo1f^{-/-} neutrophils

In a second set of 3D chemotaxis experiments, the morphology of the nucleus during 3D chemotaxis was analyzed. Myo1f^{+/+} and Myo1f^{-/-} neutrophils were stained at 37 °C for 5 min using the nuclear dye Hoechst 33342 (5 μM) and 3D chemotaxis was performed in a 1.5 mg/mL collagen gel with a CXCL1 (100 ng/mL) chemoattractant gradient. Analysis of the shape of the nucleus during 3D migration was performed using spinning disk confocal microscopy. The mean nuclear elongation factor per FOV and time point were determined and subsequently normalized to the overall smallest value to calculate the change in elongation within the next 10 min of observation[127].

Shape of the nucleus and localization of Myo1f and F-Actin in dHL-60 cells during 3D migration

In a third set of experiments, dHL-60 cells stably expressing an EGFP-Myo1f fusion protein and an upright spinning disk confocal microscope to study the subcellular localization of Myo1f and F-Actin during 3D migration were utilized. Therefore the cells were stained for F-Actin (100 nM, Sir Actin) overnight at 37 °C in 5 % CO_2. In addition, cells were labelled with the nuclear dye Hoechst 33342 for 5 min at 37 °C to study the morphology of the nucleus during 3D migration in a 1.5 mg/mL collagen gel with fMLP (100 nM) as chemoattractant. Images were acquired using Slidebook 6.0.8 Software and by using three lasers with an excitation wavelength of 488 nm, 561 nm and 633 nm[127].

4.5 Confocal reflection contrast imaging of 3D collagen gels

Collagen fibers within hydrated non-fixed and unstained 3D collagen gels were visualized by confocal reflection contrast microscopy. The experiments were performed at the bioimaging core facility of the Biomedical Center with an inverted Leica SP8X WLL microscope, equipped with a 405 nm laser, a WLL2 laser (470 – 670 nm) and an acusto-optical beam splitter (AOBS). Briefly, collagen fibers were visualized by detecting the reflection of the 546 nm laser light with a photomultiplier tube and setting the AOBS to reflection mode. Live cell imaging was performed with a Leica HC PL APO 63x/1.40 oil objective for 10 - 20 min[127].

4.6 Fluorescence activated cell sorting (FACS) experiments

4.6.1 Analysis of the expression of surface proteins on neutrophils and dHL-60 cells

For analysis of surface expression of CD11a (LFA-1, αL, clone M17/4), CD11b (Mac-1, αM, clone M1/70), and CD18 (β2, clone C71/16) by flow cytometry, Myo1f^{+/+} and Myo1f^{-/-} neutrophils were suspended in ADM ($2.5x10^5$/sample) supplemented with 5 µL (1 µg) antibody or isotype control and stimulus. The cells were either stimulated with CXCL1 (100 ng/mL) or fMLP (10 µM) for 20 min at 37 °C or left untreated as control. Afterwards cells were fixed using FACS lysing solution (dilution 1:10 in H_2O) for 10 min on ice and washed twice in ice-cold PBS (centrifugation 800 g, 10 min, 4 °C). For flow cytometry analysis, a FACS BD Canto II machine was used. Data was analyzed using FlowJo software.

Analysis of surface expression of CD11a, CD11b, CD18 and CD162 of undifferentiated and differentiated (1.3 % DMSO for 6 days) HL-60 wt and HL-60 EGFP-Myo1f was performed using flow cytometry. Cells were stained with PE-conjugated mouse anti-human CD11a (clone G43-25B), PE-conjugated mouse anti-human CD11b (clone IRCF44), PE-conjugated mouse anti-human CD18 (clone 6.7) and APC-conjugated mouse anti-human CD162 (clone FLEG) or PE-conjugated IgG1 or APC-conjugated IgG2a isotype control antibodies. Fluorescence intensities were recorded using an LSRFortessa flow cytometer (BD Bioscience) and data was analyzed offline using FlowJo software.

4.6.2 ICAM-1 and fibrinogen binding assays

LFA-1 specific rmICAM-1/Fc binding assay was performed by flow cytometry as described previously[41,47]. Myo1f^{+/+} and Myo1f^{-/-} neutrophils ($2x10^5$/sample) were incubated with a function blocking anti-mouse CD11b antibody (30 µg/mL, clone M1/70). To analyze specific LFA-1 binding to soluble ICAM-1, control samples were additionally incubated with a functional blocking anti-mouse CD11a antibody (30 µg/mL, cloneM17/4). All function blocking antibodies were incubated for 15 min at room temperature. Subsequently, cells were stimulated with CXCL1 (100 ng/mL), fMLP (10 µM), Mn^{2+} (3 mM) or left untreated in the presence of rmICAM-1/Fc (20 µg/mL) and PE-labeled mouse anti-human IgG$_1$ gamma chain specific antibody (10 µg/mL, clone H2) at 37 °C for 3 min. After 3 min of stimulation, cells were fixed by adding FACS lysing solution (dilution 1:10 in H_2O) on ice for 10 min. After washing twice with ice-cold PBS, flow cytometry analysis was performed using a FACS BD Canto II machine. For analysis of LFA-1 specific rmICAM-1/Fc binding, the anti-CD11a antibody-treated control was used defining 95 % of neutrophils as negative for LFA-1 binding to rmICAM-1/Fc. This threshold was used for all samples and the percentage of neutrophils for positive LFA-1 specific rmICAM-1/Fc binding was calculated accordingly.

To study Mac-1 binding to fibrinogen, Myo1f^{+/+} and Myo1f^{-/-} neutrophils ($2x10^5$/sample) were stimulated with CXCL1 (100 ng/mL), fMLP (10 µM), Mn^{2+} (3 mM) or left untreated in the presence of Alexa Fluor 647-conjugated human fibrinogen (150 µg/mL) at 37 °C for 20 min. As negative control, fibrinogen binding to Mac-1 was blocked by adding 2 mM EDTA. The analysis for specific Mac-1 binding to fibrinogen was done as described above for LFA-1 specific rmICAM-1/Fc binding. Briefly, we defined a threshold of the mean fluorescence intensity in the EDTA control defining 95 % of cells as negative and calculated the percentage of neutrophils positive for fibrinogen binding accordingly.

4.7 *In vivo* **assays**

4.7.1 Intravital microscopy of the mouse cremaster muscle

To investigate neutrophil recruitment *in vivo*, intravital microscopy of the mouse cremaster muscle was performed as described previously[186]. After cannulation of the carotid artery (carotic catheter plastic tube ID: 0.28 mm; OD: 0.61 mm) of anesthetized mice (125 mg/kg ketamine and 25 mg/kg xylazin 2 %), the cremaster muscle was dissected and moisturized with PBS thermo-equilibrated at 37 °C. In postcapillary venules with a diameter of 20-40 mm, mean rolling velocities, number of rolling and adherent cells per mm were imaged with an intravital microscope and recorded by a digital camera. Leukocytes attached >30 s were defined as adherent, and centerline velocity of red blood cells was analyzed using fluorescent microbeads with a diameter of 1 mm. Flow was calculated as a mean of the length of at least three microspheres recorded with a defined exposure time and calculated offline. Rheological parameters, venular diameter, venular vessel segment length, and number of rolling and adherent leukocytes were analyzed using ImageJ software. Leukocyte counts were obtained from whole blood samples.

Trauma-induced cremaster model

In this model, mild inflammation was induced by exteriorization of the mouse cremaster muscle of $Myo1f^{+/+}$ and $Myo1f^{-/-}$ mice[187].

TNFα-induced cremaster model

Briefly, 2 h after intrascrotal (i.s.) injection of rmTNF-α (500 ng/animal), the cremaster muscle was dissected, and rolling flux fraction and number of adherent neutrophils were determined by intravital microscopy.

CXCL-induced cremaster model

To analyze CXCL1-induced adhesion, rolling flux fraction (rolling cell/min divided by all neutrophils passing the vessel/min) and number of adherent leukocytes were measured 1, 3, 6, and 9 min following systemic application of CXCL1 (600 ng) via the carotid artery and were compared with control values obtained from the same vessels prior to CXCL1 injection.

4.7.2   Histological analysis of TNFα-stimulated mouse cremaster whole mounts

Cremaster whole mounts were prepared 2.5 h after i.s. injection of rmTNFα (500 ng). The cremaster muscle was fixed with 4 % PFA and stained with Giemsa's azur eosin methylene blue as described[188]. Number of perivascular leukocytes was counted using a microscope with a 100X/1.4 NA oil immersion objective.

4.7.3   Peritonitis model

Myo1f^{+/+} and Myo1f^{-/-} mice were injected intraperitoneally (i.p.) with CXCL1 (600 ng/animal). After 4 h, mice were sacrificed and the peritoneal cavity was flushed with 5 mL ice-cooled PBS. Total number of extravasated leukocytes in the peritoneal lavage was analyzed using a Coulter A C T counter. The number of extravasated neutrophils were quantified with a PE-labeled rat α-mouse Ly6-G antibody (clone 1A8) and subsequent flow cytometry.

4.7.4   Lipopolysaccharide (LPS)-induced lung injury model

The experiment was performed as described previously[189,190]. Briefly, mice were exposed to aerosolized LPS (500 µg/mL) from *Salmonella eneritidis* (Sigma Aldrich, Germany) dissolved in 0.9 % NaCl, or to aerosolized NaCl for control for 30 min. Injection of a FITC-labeled rat α-mouse Ly6-G antibody (clone 1A8) and 100 µL TRITC-Dextran (30 mg/mL) via the tail vein was performed 30 min prior euthanasia. Mice were sacrificed 4 h after inhalation and the bronchoalveolar lavage (BAL) was obtained by cannulation of the trachea. Lungs were removed, minced and digested to obtain a single cell suspension. The number of neutrophils in the BAL and the lung tissue (interstitium and pulmonary vasculature) were analyzed by flow cytometry. To assess vascular leakage, TRITC-Dextran extravasation was used to measure vascular permeability. The fluorescence of 100 µL BAL supernatant (Fluor^{BAL}) and of 50 µL serum (Fluor^{serum}) was measured. The clearance volume, i.e. the permeability of the alveolar-capillary barrier can be calculated using the following equation[191]: V (µL) = ((Fluor^{BAL}/100 µL)*BAL volume (µL))/(Fluor^{serum}/50 µL)

4.8   Statistical analysis

All data were analyzed and plotted using GraphPad Prism 6 software (GraphPad Software Inc.) and shown as means ± SEM. Statistical significance for pairwise comparison of experimental groups was determined using an unpaired Student's t test. For multiple comparisons, a 2-way ANOVA with Sidak's multiple comparisons test (comparison of all experimental groups against each other) was used. P values < 0.05 were considered as statistically significant[127].

5. RESULTS

5.1 Role of Myo1f in neutrophil rolling and adhesion *in vitro* and *in vivo*

5.1.1 Neutrophil rolling and adhesion under static and flow conditions *in vitro*

The genetic absence of Myo1f has been shown to cause increased neutrophil adhesion to the β_2 integrin ligand ICAM-1 under static conditions[1]. In the present study adhesion was investigated using neutrophils isolated from the bone marrow of Myo1f^{+/+} and Myo1f^{-/-} mice. Upon stimulation with the chemokine ligand CXCL1, adhesion of Myo1f^{+/+} neutrophils on immobilized rmICAM-1 was increased from 3.1 ± 1 % in the unstimulated control to 50.5 ± 6 % (Figure 12a). Stimulation with Mn^{2+} which stabilizes the high affinity conformation of the β_2 integrins[39] increased adhesion from 3.1 ± 1 % to 24.7 ± 9 %. Similarly, the bacterial peptide fMLP induced adhesion from 3.1 ± 1 % to 42.9 ± 8 % and the inflammatory mediator TNFα from 3.1 ± 1 % to 47.8 ± 11 % in Myo1f^{+/+} neutrophils. In comparison to Myo1f^{+/+} neutrophils, adhesion of Myo1f^{-/-} neutrophils was significantly increased by about 20 % upon stimulation with all of the above mentioned stimuli. Thus, the present data confirmed the observation by Kim et al[1]. Similarly, Mac-1-dependent adhesion to immobilized fibrinogen was analyzed using Myo1f^{+/+} and Myo1f^{-/-} neutrophils. Adhesion of Myo1f^{+/+} neutrophils was increased from 0.5 ± 0.2 % in the unstimulated control to 12.8 ± 2 % upon CXCL1 stimulation, to 8.1 ± 1 % upon Mn^{2+} stimulation, to 13 ± 2 % upon fMLP stimulation and to 8 ± 2 % upon TNFα stimulation (Figure 12b). Adhesion of Myo1f^{-/-} neutrophils was significantly increased upon stimulation with Mn^{2+} compared to Myo1f^{+/+} neutrophils. The same trend was detectable upon stimulation with CXCL1, fMLP and TNFα, although the increase of adhesion in Myo1f^{-/-} neutrophils compared to Myo1f^{+/+} neutrophils was not significant. Next, neutrophil rolling and induction of adhesion were analyzed under physiological flow conditions using flow chambers and Myo1f^{+/+} and Myo1f^{-/-} neutrophils. Neutrophils were perfused through rmICAM-1, rmP-selectin and CXCL1 coated flow chambers with 1 dyne/cm^2 shear stress. Here, analysis of the number of rolling and adherent neutrophils revealed no difference in the induction of adhesion between Myo1f^{+/+} and Myo1f^{-/-} neutrophils (Figure 12c, d).
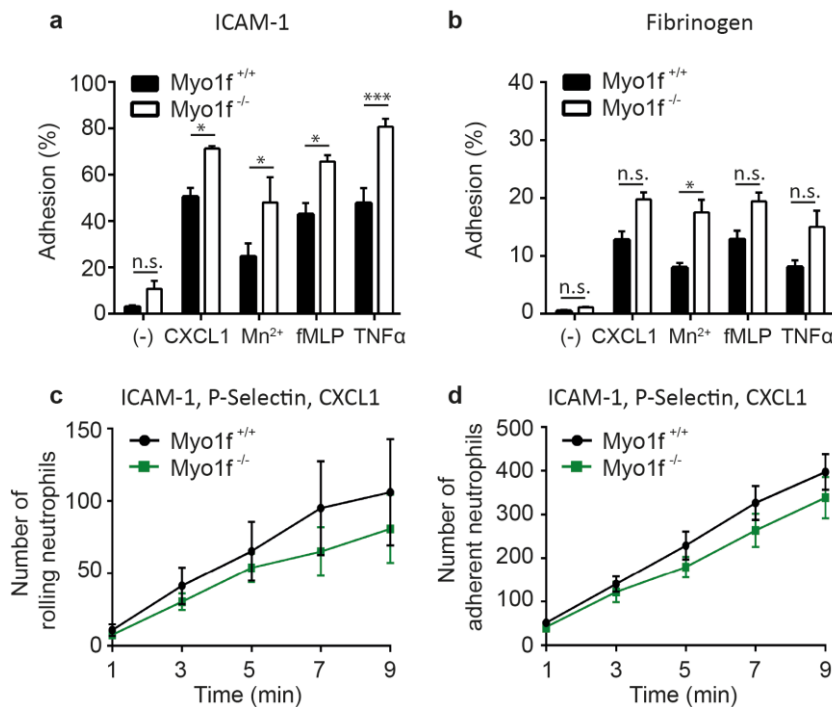
Figure 12. Adhesion of Myo1f$^{+/+}$ and Myo1f$^{-/-}$ neutrophils under static and flow conditions. (a,b) Neutrophils adherent to immobilized (a) rmICAM-1 (12.5 µg/mL), or (b) fibrinogen (50 µg/mL) upon stimulation with CXCL1 (100 ng/mL), Mn^{2+} (3 mM), fMLP (10 µM), or TNFα (20 ng/mL) for 10 min in percent of total neutrophils added (100 %). n = 4. Mean ± SEM. * $p<0.05$, *** $p<0.001$, n.s. not significant (One-way ANOVA, Sidak's multiple comparison test). (c,d) Number of (c) rolling and (d) adherent Myo1f$^{+/+}$ and Myo1f$^{-/-}$ neutrophils under flow conditions (1 dyne/cm^2) on immobilized rmICAM-1 (12.5 µg/mL), rmP-selectin (10 µg/mL) and CXCL1 (5 µg/mL) at indicated time points. n = 6. Mean ± SEM (modified from Salvermoser et al., 2018[127]).

5.1.2 Surface expression and affinity regulation of β₂ integrins

To study the question whether increased adhesion of Myo1f$^{-/-}$ neutrophils under static conditions was due to differently expressed β₂ integrins in Myo1f$^{+/+}$ and Myo1f$^{-/-}$ neutrophils, the surface expression of CD11a (alpha-subunit of LFA-1, αL), CD11b (alpha-subunit of Mac-1, αM) and CD18 (beta-subunit) was analyzed using flow cytometry. Analysis of mean fluorescence intensities revealed similar surface expression levels of CD11a, CD11b and CD18 in unstimulated Myo1f$^{+/+}$ and Myo1f$^{-/-}$ neutrophils (Figure 13a). Additionally, surface expression of CD11a showed no differences upon stimulation with CXCL1 and fMLP between Myo1f$^{+/+}$ and Myo1f$^{-/-}$ neutrophils as expected (Figure 13a, left graph). Upregulation of Mac-1 (CD11b/CD18) upon stimulation with CXCL1 or fMLP was not affected in the genetic absence of Myo1f indicating that increased adhesion under static condition was not due to dysregulated β₂ integrin expression (Figure 13a, middle and right panel).

Next, the impact of Myo1f on LFA-1 (CD11a/CD18) and Mac-1 (CD11b/CD18) affinity regulation was analyzed by flow cytometry. Binding of soluble ICAM-1 by Myo1f$^{+/+}$ and Myo1f$^{-/-}$ neutrophils in the presence of a function blocking anti-Mac-1 antibody was used to study LFA-1 affinity regulation (Figure 13b). As expected, ICAM-1 binding to Myo1f$^{+/+}$ neutrophils was increased from 5.1 ± 2 % in the unstimulated control to 33.0 ± 18 % upon CXCL1 stimulation, to 44.1 ± 17 % upon fMLP stimulation and to 27.3 ± 21 % upon Mn^{2+} stimulation. Similar results were obtained using Myo1f$^{-/-}$ neutrophils indicating that the affinity regulation of LFA-1 was intact in the genetic absence of Myo1f.
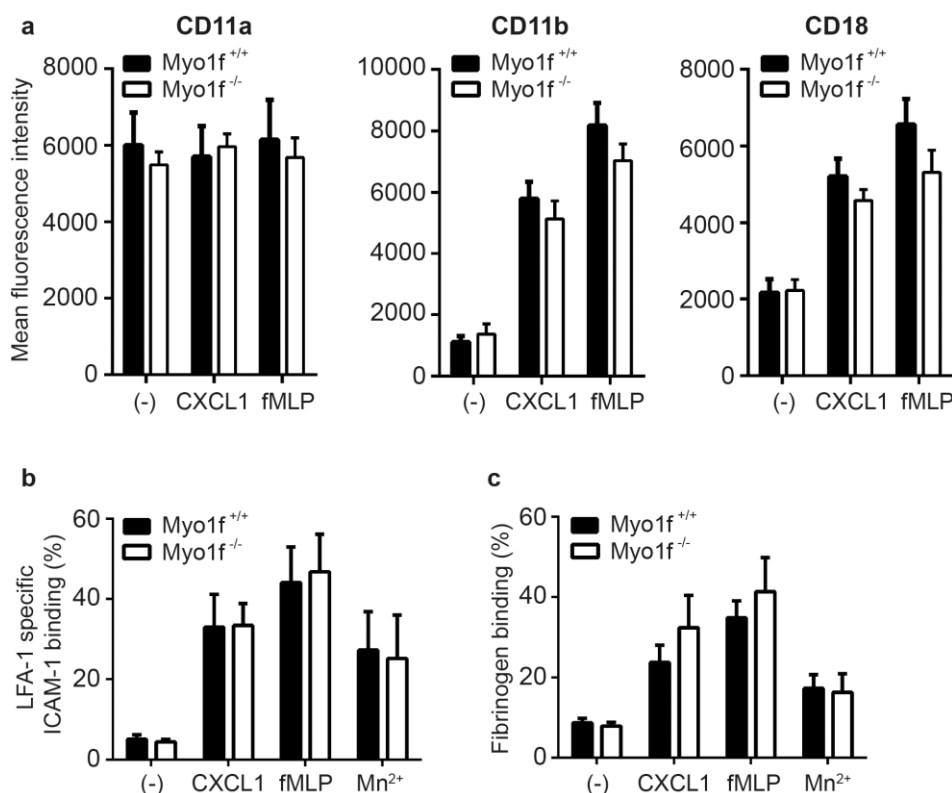
Figure 13. Surface expression and affinity regulation of β$_2$ integrins in Myo1f$^{+/+}$ and Myo1f$^{-/-}$ neutrophils. (a) Flow cytometric analysis of neutrophil surface expression of CD11a, CD11b, and CD18 before (-) and after stimulation with CXCL1 (100 ng/mL) and fMLP (10 μM) for 20 min. n = 4. Mean ± SEM. (b) Flow cytometric analysis of LFA-1 specific ICAM-1 binding to unstimulated (-) Myo1f$^{+/+}$ and Myo1f$^{-/-}$ neutrophils, or upon stimulation with CXCL1 (100 ng/mL), fMLP (10 μM), and Mn^{2+} (3 mM) for 3 min. Data show the percentage of cells binding ICAM-1 in a LFA-1-specific manner calculated by a threshold defining 95 % of neutrophils treated with an anti-LFA-1 antibody as negative. (c) Mac-1 affinity regulation was measured by fibrinogen binding to unstimulated (-) Myo1f$^{+/+}$ and Myo1f$^{-/-}$ neutrophils, or upon stimulation with CXCL1 (100 ng/mL), fMLP (10 μM), or Mn^{2+} (3 mM) for 20 min using flow cytometry analysis. Data show the percentage of cells binding soluble fibrinogen calculated by a threshold defining 95 % of EDTA-treated (2 mM) neutrophils as negative. n = 6. Mean ± SEM.

Binding of soluble fibrinogen by Myo1f^{+/+} and Myo1f^{-/-} neutrophils indicated Mac-1 affinity regulation (Figure 13c).Fibrinogen binding was increased from $4.4 \pm 1\%$ in the unstimulated control to $33.4 \pm 12\%$ upon CXCL1 stimulation, to $46.8 \pm 18\%$ upon fMLP stimulation and to $25.2 \pm 24\%$ upon Mn^{2+} stimulation in Myo1f^{+/+} neutrophils. In the genetic absence of Myo1f binding of soluble fibrinogen was not different indicating that the affinity regulation of Mac-1 was normal in Myo1f^{-/-} neutrophil. Thus, Myo1f was dispensable for surface expression and affinity regulation of LFA-1 and Mac-1.

5.1.3 Neutrophil rolling and adhesion *in vivo*

To study the biological importance of Myo1f for adhesion in the situation *in vivo*, neutrophil trafficking was analyzed by imaging cremaster muscle venules of Myo1f^{+/+} and Myo1f^{-/-} mice using intravital microscopy.

	Mice	Venules	Diameter (µm)	Length (µm)	Centerline velocity (µm/s)	Shear rate (s⁻¹)	WBC (µL⁻¹)
Myo1f^{+/+}	4	14	29±4	255±6	878±192	1048±376	5600±779
Myo1f^{-/-}	5	12	27±4	252±14	925±220	1137±342	5720±593
			n.s.	n.s.	n.s.	n.s.	n.s.
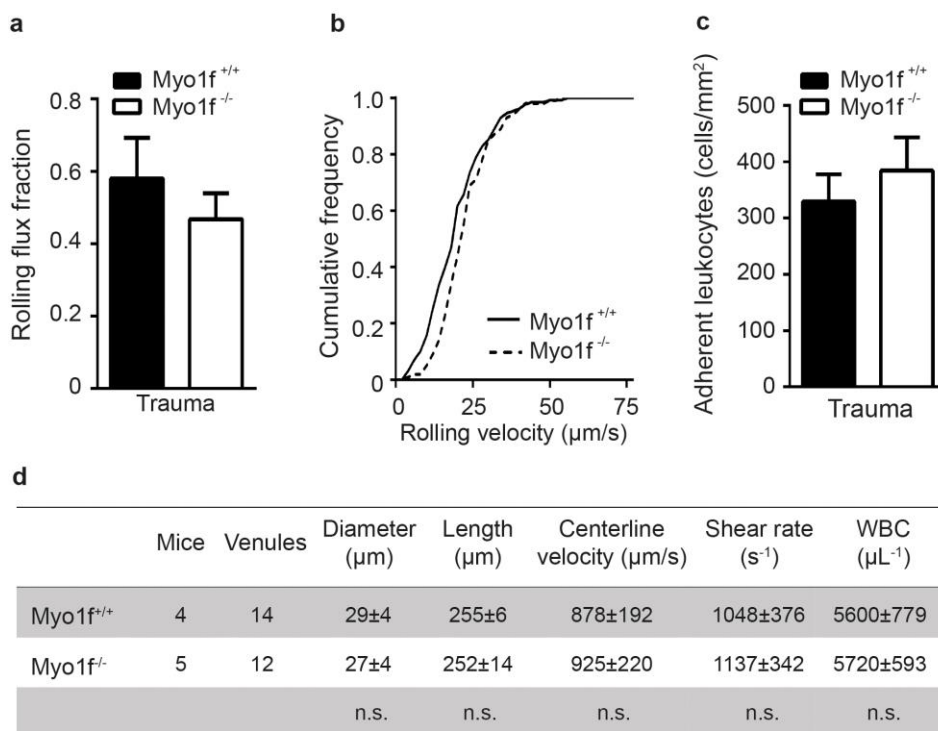
Figure 14. Leukocyte rolling and adhesion in the trauma-induced mouse cremaster muscle model of acute inflammation. (a-c) Intravital microscopy of postcapillary venules in the mouse cremaster model after surgical dissection of the cremaster muscle. (a) Rolling flux fraction, (b) rolling velocity, and (c) number of adherent leukocytes were analyzed offline. n = 14 venules from 4 Myo1f^{+/+} mice and n = 12 venules from 5 Myo1f^{-/-} mice. Mean ± SEM. (d) Hemodynamic and microvascular parameters of cremaster muscle venules in the trauma model. n.s. not significant.

In the trauma model, a mild inflammation was induced by surgical preparation and exteriorization of the mouse cremaster muscle. In this model, leukocyte rolling is mainly mediated by P-selectin mobilized onto the inflamed endothelium[187]. Leukocyte rolling flux fraction, rolling velocity as well as the number of adherent leukocytes revealed no differences in Myo1f^{+/+} and Myo1f^{-/-} mice (Figure 14a-c). Hemodynamic and microvascular parameters were similar in both mouse strains (Figure 14d).

Next, an acute inflammation was induced in the cremaster muscle by i.s. injection of TNFα. Upon TNFα application, P- and E-selectin expression is induced on the endothelial surface leading to slow leukocyte rolling and leukocyte adhesion[192]. Within 2.5 h after stimulation, no differences in the leukocyte rolling flux fraction and in the rolling velocity as well as in the number of adherent leukocytes in Myo1f^{-/-} and Myo1f^{+/+} mice were observed (Figure 15a-c). Hemodynamic and microvascular parameters were not altered in the genetic absence of Myo1f (Figure 15d).

	Mice	Venules	Diameter (µm)	Length (µm)	Centerline velocity (µm/s)	Shear rate (s⁻¹)	WBC (µL⁻¹)
Myo1f^{+/+}	4	15	29±4	255±4	1090±328	1094±327	4525±1310
Myo1f^{-/-}	3	12	29±4	262±10	925±220	1070±183	5900±954
			n.s.	n.s.	n.s.	n.s.	n.s.
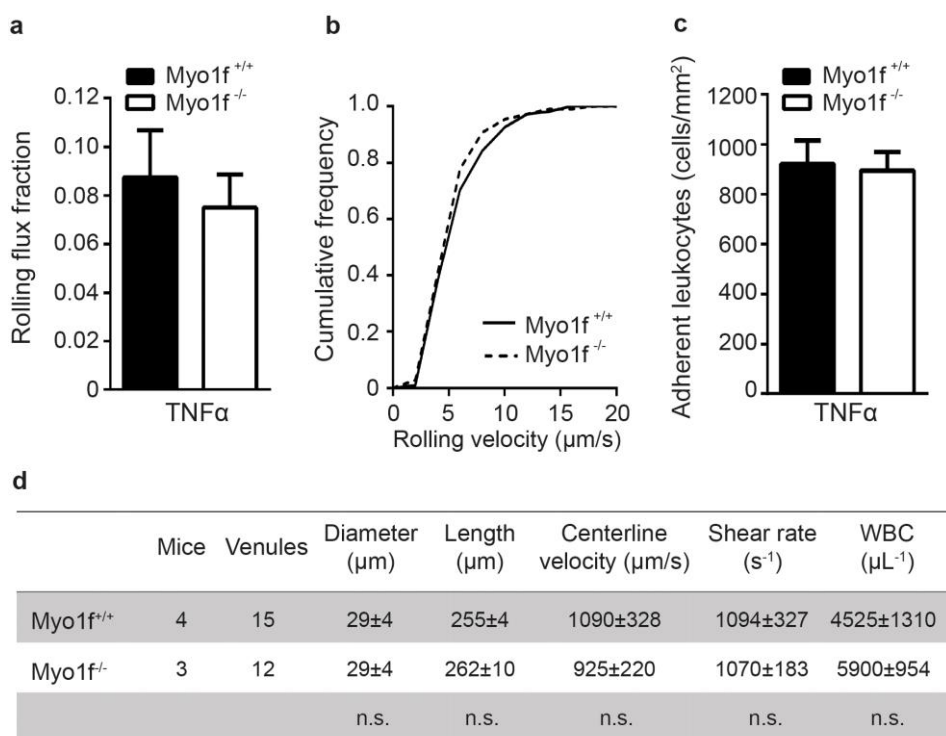
Figure 15. Leukocyte rolling and adhesion in the TNFα-stimulated mouse cremaster muscle model of acute inflammation. (a, b) Intravital microscopy of postcapillary venules in the mouse cremaster muscle 2.5 h after i.s. injection of TNFα (500 ng). (a) Rolling flux fraction, (b) rolling velocity, and (c) number of adherent leukocytes were analyzed offline. n = 15 venules from 4 Myo1f^{+/+} mice and n = 12 venules from 3 Myo1f^{-/-} mice. Mean ± SEM. (d) Hemodynamic and microvascular parameters of cremaster muscle venules 2.5 h after i.s. TNFα injection. n.s. not significant (modified from Salvermoser et al., 2018[127]).

To study the role of Myo1f for LFA-1-dependent neutrophil trafficking, rolling and adhesion was analyzed in the mouse cremaster model upon intravenous (i.v.) administration of CXCL1, which activates LFA-1 resulting in firm neutrophil arrest[193]. Here, the same vessel was recorded before and 1, 3, 6 and 9 min after i.v. injection of 600 ng CXCL1. As expected, upon stimulation with CXCL1 for 1 min, leukocyte rolling flux fraction decreased from 0.26 ± 0.08 to 0.09 ± 0.04, whereas the number of adherent leukocytes per mm^2 vessel increased from 231.2 ± 35 to 526.3 ± 131 in Myo1f$^{+/+}$ mice (Figure 16a, b). As CXCL1 stimulation leads to transient leukocyte adhesion[193], the rolling flux fraction gradually increased within the next 3, 6, 9 min of stimulation as expected. Accordingly, the number of adherent leukocytes decreased in Myo1f$^{+/+}$ mice within the observation period after 3, 6 and 9 min of stimulation.

	Mice	Venules	Diameter (µm)	Length (µm)	Centerline velocity (µm/s)	Shear rate (s^{-1})	WBC (µL^{-1})
Myo1f$^{+/+}$	4	4	33±2	253±4	1381±230	1037±120	6843±3400
Myo1f$^{-/-}$	4	5	30±2	252±1	1312±213	1064±166	6860±906
			n.s.	n.s.	n.s.	n.s.	n.s.
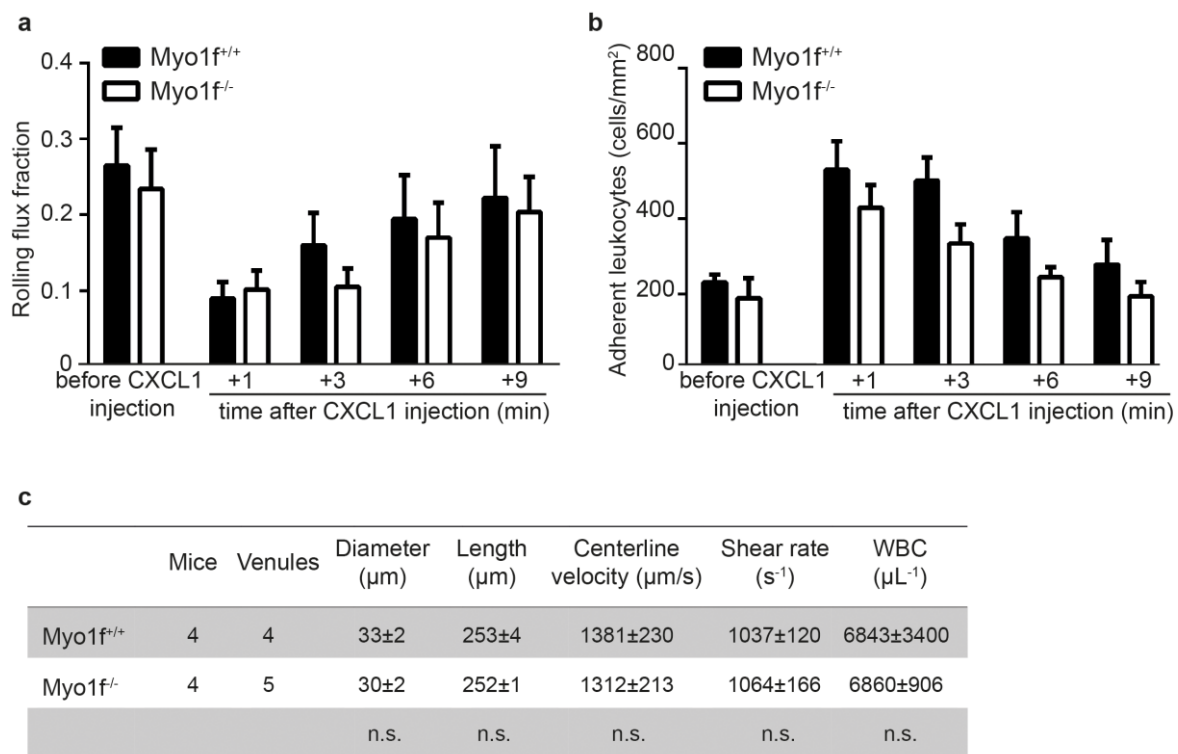
Figure 16. Leukocyte rolling and adhesion in the mouse cremaster muscle model upon systemic administration of CXCL1. (a) Leukocyte rolling flux fraction, and (b) number of adherent leukocytes in postcapillary cremaster muscle venules were measured at different time points in each vessel: before CXCL1 injection and 1, 3, 6, and 9 min after systemic administration of CXCL1 (600 ng) via the carotic artery. n = 4 venules from 4 Myo1f$^{+/+}$ mice and n = 5 venules from 4 Myo1f$^{-/-}$ mice. Mean ± SEM. (c) Hemodynamic and microvascular parameters of cremaster muscle venules before CXCL1 injection. n.s. not significant (modified from Salvermoser et al., 2018[127]).

The same was true for Myo1f$^{-/-}$ mice indicating that Myo1f was not required for leukocyte firm adhesion upon CXCL1-triggered β$_2$ integrin activation. Similarly, no differences between the hemodynamic and microvascular parameters were observed between both mice strains (Figure 16c).

5.2   Neutrophil extravasation during acute inflammation

5.2.1   Neutrophil extravasation in the TNFα-inflamed mouse cremaster model

To investigate the role of Myo1f for neutrophil extravasation from the blood vessel into the inflamed cremaster tissue, the number of extravasated neutrophils in the TNFα-stimulated mouse cremaster muscle model was counted in Myo1f$^{+/+}$ and Myo1f$^{-/-}$ mice. The exteriorized cremaster muscles were fixed with 4 % PFA, stained by Giemsa's azur eosin methylene blue and analyzed using bright-field microscopy. Microscopic inspection of the histological samples demonstrated substantial neutrophil extravasation in the TNFα-stimulated cremaster muscle of Myo1f$^{+/+}$ mice (Figure 17a).
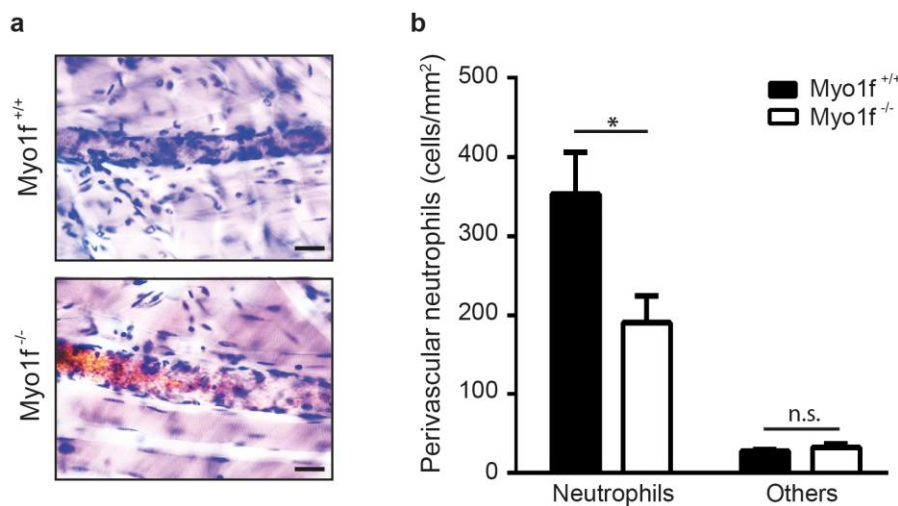
Figure 17. Extravasation of Myo1f$^{+/+}$ and Myo1f$^{-/-}$ neutrophils into TNFα-inflamed mouse cremaster tissue. (a, b) Whole mounts of TNFα-stimulated mouse cremaster muscles fixed with 4 % PFA and stained with Giemsa's azur eosin methylene blue. (a) Representative images of postcapillary venules of Myo1f$^{+/+}$ and Myo1f$^{-/-}$ cremaster whole mounts. Scale bar = 20 μm. (b) Quantification of perivascular neutrophils and other leukocyte subtypes (others). n = 18 vessels from 3 Myo1f$^{+/+}$ mice and n = 17 vessels from 3 Myo1f$^{-/-}$ mice. Mean ± SEM. * p<0.05, n.s. not significant (2-way ANOVA, Sidak's multiple comparison test, modified from Salvermoser et al., 2018[127]).

In the genetic absence of Myo1f, neutrophil accumulation in the inflamed cremaster tissue was reduced. Quantitative analysis revealed that 353.2 ± 52 neutrophils extravasated into the inflamed cremaster tissue in Myo1f$^{+/+}$ mice (Figure 17b). In comparison to Myo1f$^{+/+}$ mice, extravasation was significantly diminished to 190.6 ± 34 neutrophils in Myo1f$^{-/-}$ mice. The number of other extravasated leukocyte subtypes, e.g. monocytes and eosinophils was not altered in the genetic absence of Myo1f. These data suggested that Myo1f played an important role in neutrophil extravasation into the inflamed cremaster muscle tissue.

5.2.2 Neutrophil extravasation into the inflamed peritoneum

To study the role of Myo1f for neutrophil extravasation in acute peritonitis induced by i.p. injection of CXCL1, the number of extravasated neutrophils into the inflamed peritoneum of Myo1f$^{+/+}$ and Myo1f$^{-/-}$ mice was analyzed. In the peritoneal lavage $1.34 \pm 0.5 * 10^6$ neutrophils were counted in Myo1f$^{+/+}$ mice 4 h after CXCL1 injection (Figure 18). The number of extravasated neutrophils was significantly reduced to $0.21 \pm 1 * 10^6$ neutrophils in the genetic absence of Myo1f. Thus, the ability of Myo1f$^{-/-}$ neutrophils to extravasate into the peritoneal cavity was almost completely abolished compared to Myo1f$^{+/+}$ neutrophils.
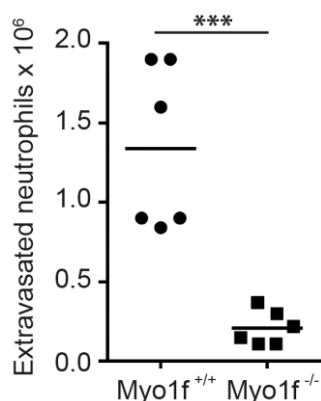
Figure 18. Extravasation of Myo1f$^{+/+}$ and Myo1f$^{-/-}$ neutrophils into the inflamed peritoneal cavity. Total number of neutrophils in the peritoneal lavage 4 h after i.p. injection of CXCL1 (600 ng). n = 6. Mean ± SEM. *** p<0.001 (Unpaired Student's t-test, modified from Salvermoser et al., 2018[127]).

5.2.3 Recruitment of neutrophils into the inflamed lung

Next, the role of Myo1f in the LPS-induced ALI model mimicking a bacterial infection was evaluated. In this model, the recruitment of activated neutrophils into the lung is an essential step during the inflammatory response[190]. ALI was induced in Myo1f$^{+/+}$ and Myo1f$^{-/-}$ mice by exposure

to aerosolized LPS or aerosolized 0.9 % NaCl for negative control for 30 min and neutrophil transmigration from the lung vasculature into the interstitium and the bronchoalveolar space was analyzed. Intravascular, interstitial, and alveolar myeloid cells were quantified 4 h after inhalation. Neutrophil extravasation was calculated as ratio between interstitial and intravascular neutrophils and was dramatically increased from 0.15 ± 0.04 to 1.86 ± 0.6 in LPS-treated Myo1f^{+/+} mice compared to NaCl-treated Myo1f^{+/+} mice (Figure 19a, left panel). The same was true for neutrophils extravasated from the lung vasculature to the bronchoalveolar space in Myo1f^{+/+} mice upon LPS treatment compared to NaCl treatment where the ratio increased from 0.02 ± 0.01 to 0.61 ± 0.19 (Figure 19a, right panel). In comparison to Myo1f^{+/+} mice, ratios of neutrophils extravasated into the interstitium or the bronchoalveolar space were significantly decreased to approximately 30 % in the genetic absence of Myo1f (Figure 19a). These data indicated that Myo1f was critical for neutrophil extravasation into the inflamed lungs. Lung damage during ALI was studied by measuring the increase in permeability of the alveolar-capillary barrier[194]. Here, TRITC-Dextran permeability measurements revealed a significantly impaired TRITC-Dextran clearance in Myo1f^{-/-} mice compared to Myo1f^{+/+} mice (Figure 19b). Thus, LPS-induced lung injury was decreased in the absence of Myo1f[127].
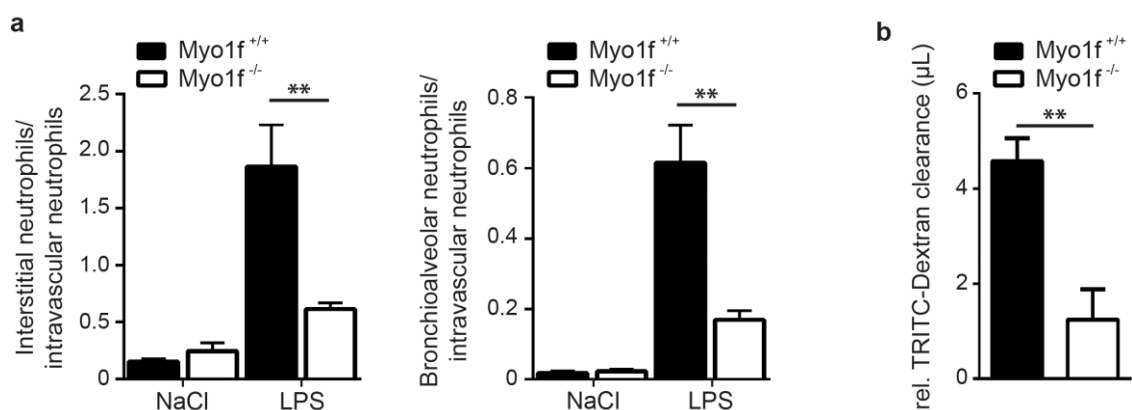
Figure 19. LPS-induced lung injury in Myo1f^{+/+} and Myo1f^{-/-} mice. (a) Ratios between Myo1f^{+/+} and Myo1f^{-/-} neutrophils extravasated into the interstitium (left panel) or the bronchioalveolar space (right panel) and neutrophils remaining in the lung vasculature 4 h after exposure to aerosolized 0.9 % NaCl or LPS for 30 min. n = 4. Mean ± SEM. ** p<0.001 (2-way ANOVA, Tukey's multiple comparison test). (b) Lung damage was assessed by quantification of TRITC-Dextran clearance. n = 4. Mean ± SEM. ** p<0.001 (Unpaired Student's t-test, modified from Salvermoser et al., 2018[127]).

5.3   The role of Myo1f in neutrophil migration

5.3.1   Neutrophil migration in 2D environments

To investigate the cellular defect underlying impaired extravasation in Myo1f^{-/-} mice, neutrophil spreading, polarization and migration were analyzed in 2D environments *in vitro*. Myo1f^{+/+} and Myo1f^{-/-} neutrophils were exposed to immobilized fibrinogen and stimulated with soluble fMLP or neutrophils were exposed to immobilized rmICAM-1 and CXCL1.
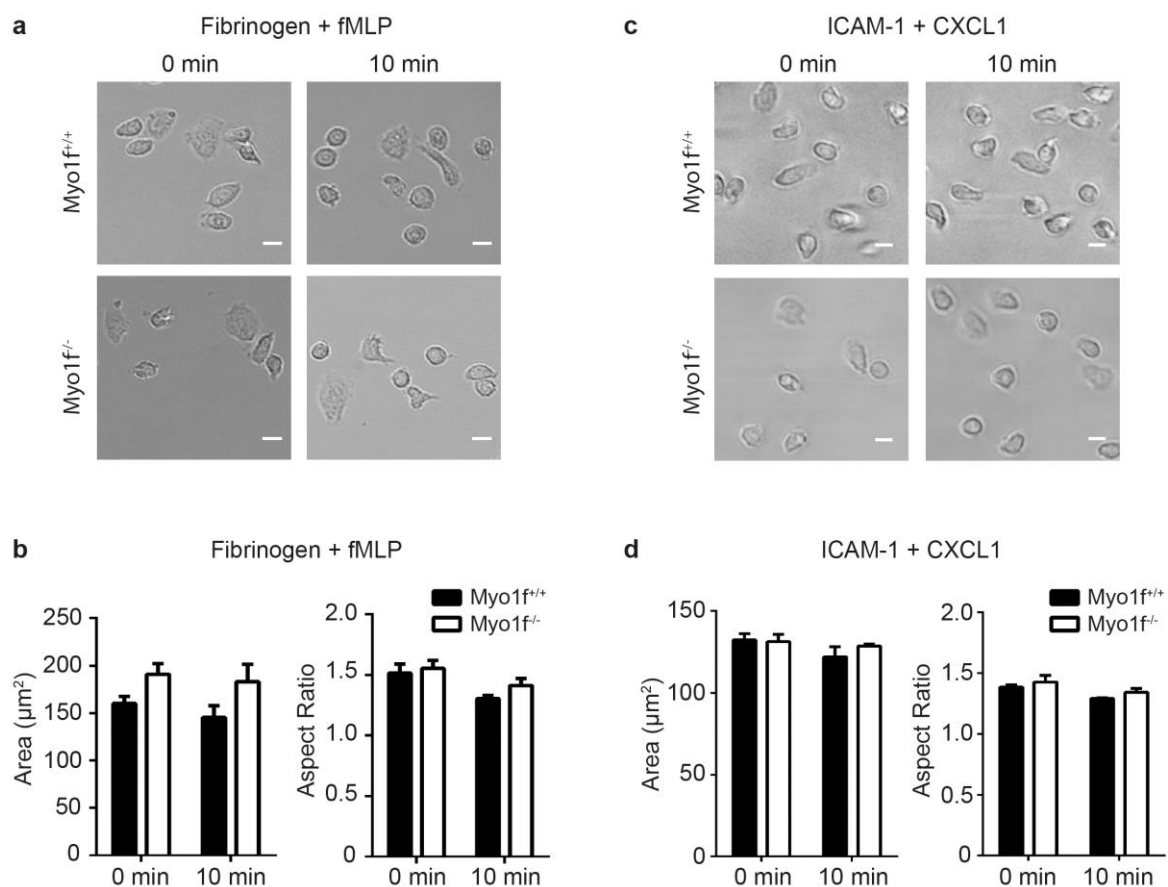
Figure 20. Spreading and polarization of Myo1f^{+/+} and Myo1f^{-/-} neutrophils under flow conditions. Spreading and polarization of Myo1f^{+/+} and Myo1f^{-/-} neutrophils analyzed in flow chambers coated with immobilized fibrinogen (50 µg/mL) in the presence of soluble fMLP (10 µM) or immobilized rmICAM-1 (12.5 µg/mL) and CXCL1 (5 µg/mL). (a, c) Representative microscopic images of adherent Myo1f^{+/+} and Myo1f^{-/-} neutrophils on (a) fibrinogen stimulated with soluble fMLP, or on (c) rmICAM-1 stimulated with immobilized CXCL1 before (0 min) and after application of shear stress for 10 min (10 min). (b, d) Spreading and polarization of adherent neutrophils were quantified by the measurement of cell area (left panel) and aspect ratio (right panel) at indicated time points. n = 3 (fibrinogen+fMLP) and n = 4 (rmICAM-1+CXCL1) independent experiments. Mean ± SEM (modified from Salvermoser et al., 2018[127]).

After 10 min at 37 °C, spreading and polarization were studied before and after the application of 1 dyne/cm² shear stress for 10 min. Microscopic inspection demonstrated a similar cell shape of Myo1f$^{+/+}$ and Myo1f$^{-/-}$ neutrophils before (0 min) and after 10 min of constant shear flow (10 min, Figure 20a, c). Quantitative analysis of cell area and aspect ratio revealed that fMLP-induced neutrophil spreading and polarization on immobilized fibrinogen were intact in the genetic absence of Myo1f (Figure 20b, d). Similar results were obtained upon exposure to immobilized rmICAM-1 and CXCL1.

Next, migration of Myo1f$^{+/+}$ and Myo1f$^{-/-}$ neutrophils which were exposed to immobilized fibrinogen and stimulated with soluble fMLP or to immobilized rmICAM-1 and CXCL was investigated under flow conditions. Analysis of single cell migration tracks revealed no differences in the migration behavior of Myo1f$^{+/+}$ and Myo1f$^{-/-}$ neutrophils (Figure 21a). Quantification of the Euclidean distance and migration velocity confirmed that migration was intact in the genetic absence of Myo1f (Figure 21b). In conclusion, Myo1f was dispensable for neutrophil spreading, polarization and migration under physiological flow conditions in 2D environments.
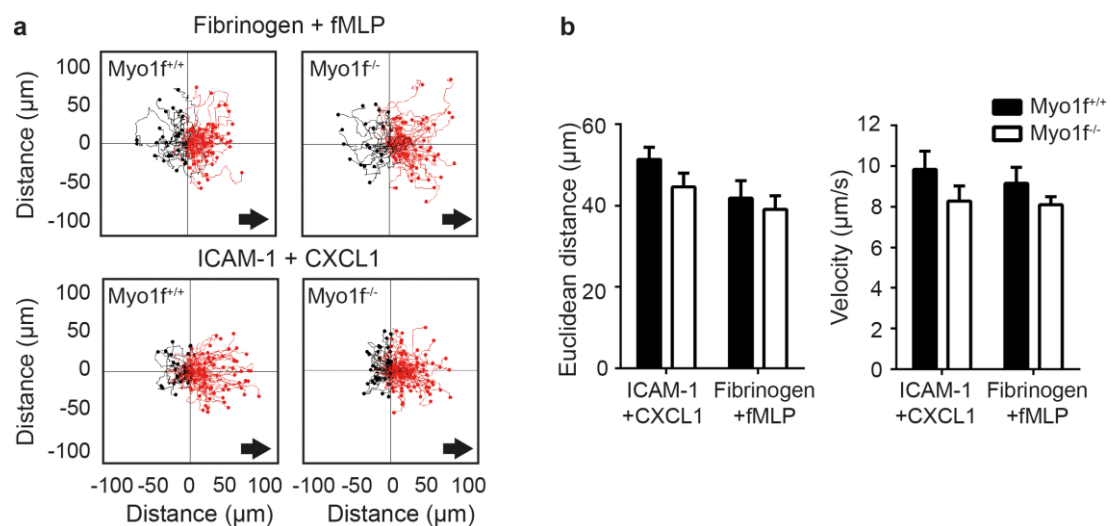
Figure 21. Migration of Myo1f$^{+/+}$ and Myo1f$^{-/-}$ neutrophils in 2D environments under flow conditions. Mechanotactic migration of Myo1f$^{+/+}$ and Myo1f$^{-/-}$ neutrophils under flow conditions (1 dyne/cm²) using flow chambers coated with immobilized fibrinogen (50 µg/mL) in the presence of fMLP (10 µM) or immobilized rmICAM-1 (12.5 µg/mL) and CXCL1 (5 µg/mL). (a) Single cell migration tracks after 10 min of flow. Arrows indicate the direction of flow. (b) Quantitative analysis of the mean Euclidean distance and the mean migration velocity. n = 4 (fibrinogen+fMLP), n = 5 (rmICAM-1+CXCL1). Mean ± SEM (modified from Salvermoser et al., 2018[127]).

To study the role of Myo1f for chemotactic migration in 2D environments, migration on immobilized fibrinogen towards an fMLP gradient or immobilized rmICAM-1 towards a CXCL1 gradient was analyzed using Zigmond chambers. Microscopic inspection demonstrated that the capacity of neutrophils to spread and polarize on immobilized fibrinogen or rmICAM-1 in the presence of fMLP or CXCL1 was not different in Myo1f$^{+/+}$ and Myo1f$^{-/-}$ neutrophils (Figure 22a, c). Similar to the behavior under flow conditions described above, quantitative analysis of cell area and aspect ratio showed intact neutrophil spreading and polarization in the genetic absence of Myo1f (Figure 22b, d).
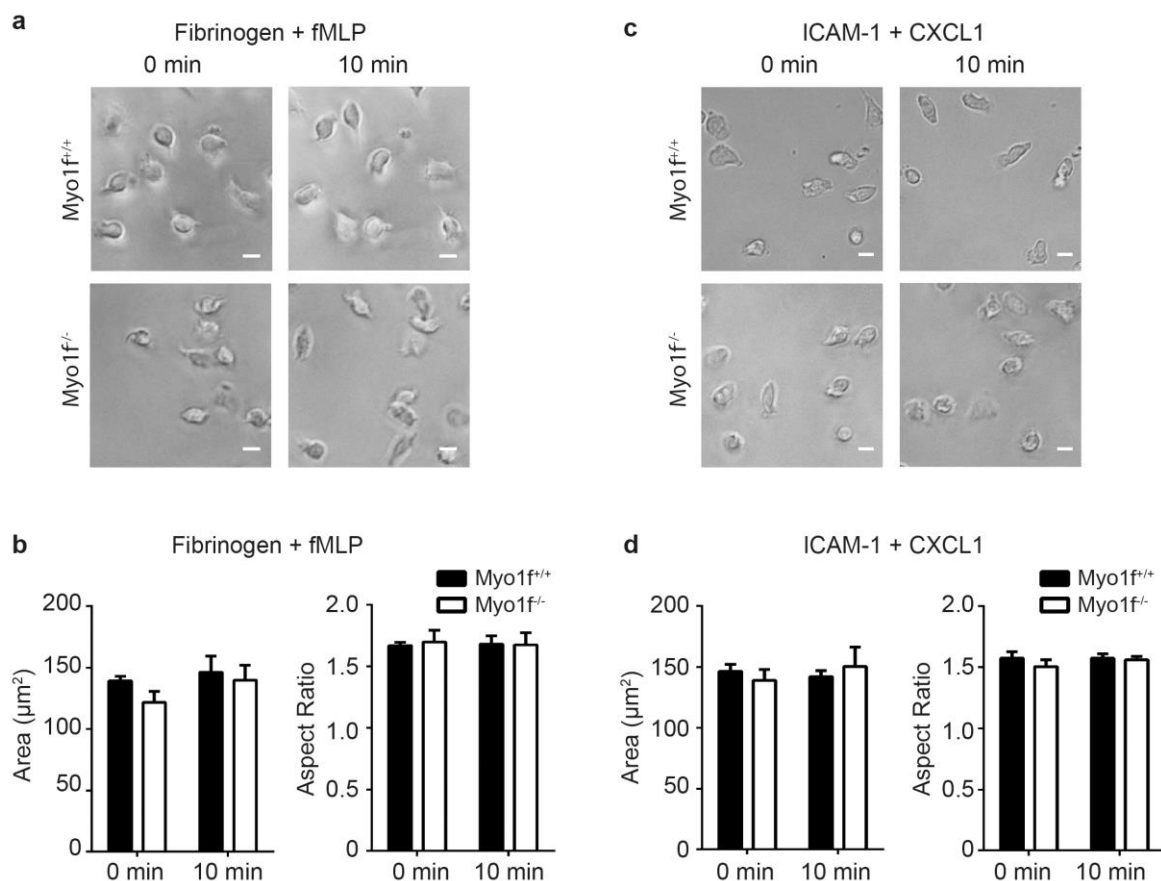
Figure 22. Neutrophil spreading and polarization during chemotaxis in 2D environments. Spreading and polarization of isolated Myo1f$^{+/+}$ and Myo1f$^{-/-}$ neutrophils during 2D chemotaxis were analyzed using Zigmond chambers coated with fibrinogen in the presence of an fMLP gradient or coated with rmICAM-1 in the presence of a CXCL1 gradient. (a, c) Representative microscopic images of adherent Myo1f$^{+/+}$ and Myo1f$^{-/-}$ neutrophils in (a) fibrinogen coated chambers with an fMLP gradient or in (c) rmICAM-1 coated chambers with a CXCL1 gradient at indicated time points. (b, d) Spreading and polarization of adherent neutrophils were quantified by measuring cell area (left panel) and aspect ratio (right panel) at indicated time points. n = 3 (fibrinogen+fMLP), n = 5 (rmICAM-1+CXCL1) independent experiments. Mean ± SEM (modified from Salvermoser et al., 2018[127]).

In addition, analysis of single cell migration tracks showed no difference in chemotactic migration of Myo1f^{-/-} neutrophils compared to Myo1f^{+/+} neutrophils (Figure 23a). Quantitative analysis of the Euclidean distance and the migration velocity confirmed that migration was intact in the genetic absence of Myo1f (Figure 23b). Thus, chemotactic migration in 2D environments was unaffected in Myo1f^{-/-} neutrophils.
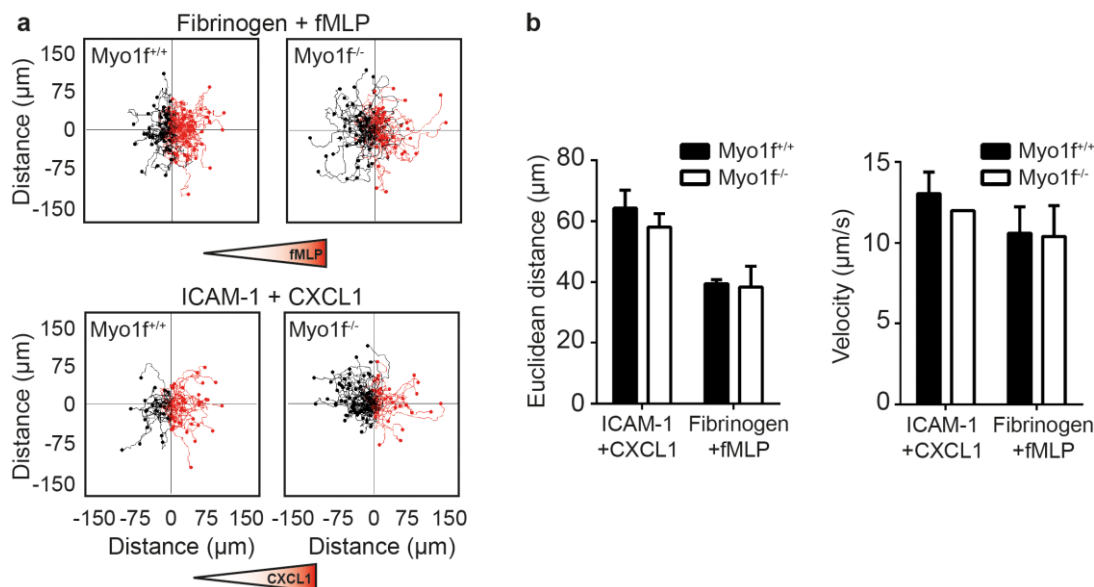
Figure 23. Chemotactic migration of Myo1f^{+/+} and Myo1f^{-/-} neutrophils in 2D environments. Chemotaxis of isolated Myo1f^{+/+} and Myo1f^{-/-} neutrophils was analyzed using Zigmond chambers coated with fibrinogen in the presence of an fMLP gradient or coated with rmICAM-1 in the presence of a CXCL1 gradient. (a) Single cell migration tracks of Myo1f^{+/+} and Myo1f^{-/-} neutrophils. (b) Quantitative analysis of the mean Euclidean distance and the migration velocity. n = 3 (fibrinogen+fMLP), n = 5 (rmICAM-1+CXCL1). Mean ± SEM (modified from Salvermoser et al., 2018[127]).

5.3.2   Myo1f in neutrophil transmigration

After successful migration on the inflamed endothelium, neutrophils emigrate through the endothelium and the underlying BM to enter the interstitial space. Therefore, the role of Myo1f for the process of neutrophil transmigration was analyzed under static and flow conditions. Transmigration under physiological flow conditions (1 dyne/cm^2) was studied by utilizing an *in vitro* system consisting of µ–Slide membrane ibiPore flow chambers and live cell spinning disk confocal microscopy. The flow chamber coated with rmICAM-1 and rmP-selectin was separated from a collagen gel containing 10 µM fMLP as chemoattractant by a 300 nm thick membrane with 5 µm pores. Myo1f^{+/+} and Myo1f^{-/-} neutrophils were perfused through the rmICAM-1 and

rmP-selectin coated flow chamber with 1 dyne/cm^2 shear stress and transmigration was investigated in real-time (four-dimensional). Cross-sectional images of time-lapse video microscopy measurements were generated to count the number of neutrophils located within the flow chamber (flow chamber), stuck within the pores (pores), or fully transmigrated into the collagen gel (collagen gel) after 60 min of stimulation (Figure 24a). Images demonstrated successful transmigration of Myo1f$^{+/+}$ neutrophils into the lower collagen compartment. In comparison to Myo1f$^{+/+}$ neutrophils, Myo1f$^{-/-}$ neutrophils showed impaired transmigration into the lower collagen compartment and the majority of neutrophils were found within the flow chamber or stuck within the pores. Quantitative analysis of neutrophils located within the flow chamber (flow chamber), stuck within the pores (pores), or fully transmigrated into the collagen gel (collagen gel) demonstrated that 60 ± 12 % of Myo1f $^{+/+}$ neutrophils transmigrated into the collagen gel while 11 ± 9 % of cells remained within the flow chamber, and 29 ± 8 % of neutrophils were located within the pore after stimulation for 60 min (Figure 24b)[127].
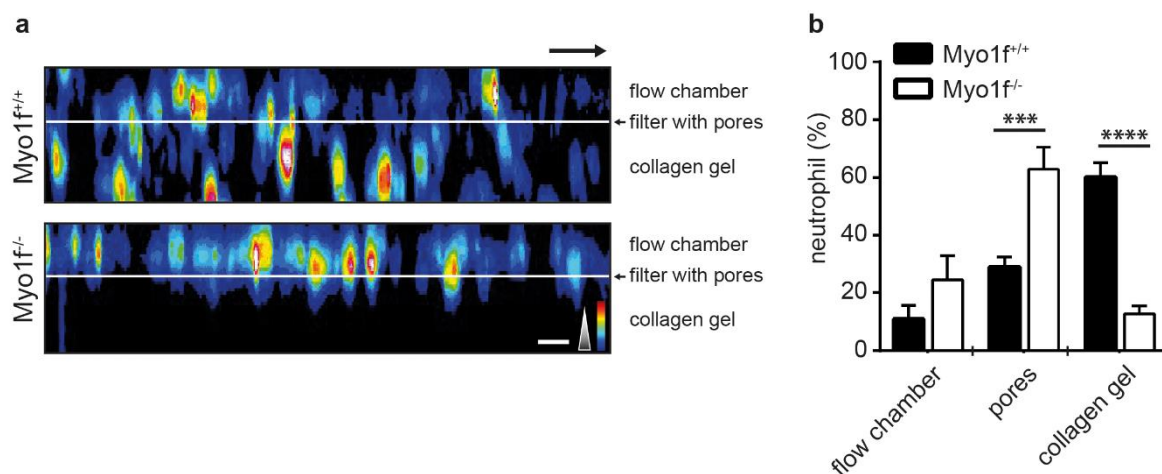
Figure 24. Neutrophil transmigration under flow conditions. Transmigration of Myo1f$^{+/+}$ and Myo1f$^{-/-}$ neutrophils under 1 dyne/cm^2 shear stress into an fMLP-containing collagen gel was analyzed using rmICAM-1 (12.5 µg/mL) and rmP-selectin (10 µg/mL) coated µ-Slide membrane ibiPore flow chambers and spinning disk confocal microscopy. (a) Orthogonal view of representative pseudo-colored time-lapse images demonstrating the localization of neutrophils during the process of transmigration into an fMLP-containing collagen gel after stimulation for 60 min. Scale bar = 10 µm. Color scales, heat map. Triangle indicates orientation of fMLP gradient. Arrow indicates direction of flow. (b) Quantitative analysis of transmigrating Myo1f$^{+/+}$ and Myo1f$^{-/-}$ neutrophils respective to their position in percent of all neutrophils analyzed (100 %). n = 4 independent experiments (with a total of 240 Myo1f$^{+/+}$ neutrophils and 220 Myo1f$^{-/-}$ neutrophils analyzed). Mean ± SEM. *** p <0.001, **** p<0.0001 (2-way ANOVA, Sidak's multiple comparison test, modified from Salvermoser et al., 2018[127]).

This was in sharp contrast to Myo1f^{-/-} neutrophils. Here, neutrophil transmigration into the collagen gel was significantly diminished to 13 ± 7 % in the genetic absence of Myo1f. Accordingly, significantly more Myo1f^{-/-} neutrophils stuck within the pores (63 ± 18 %) or remained in the flow chamber (25 ± 15 %) compared to Myo1f^{+/+} neutrophils[127].

The impact of Myo1f for TEM under static conditions was investigated using transwell chambers with 8 µm pores coated with a monolayer of endothelial b.End3 cells. CXCL1 was used as chemoattractant in the lower compartment. Similar to the findings under physiological flow conditions, CXCL1 induced substantial transmigration in Myo1f^{+/+} neutrophils compared to unstimulated Myo1f^{+/+} neutrophils (Figure 25a). The number of transmigrated Myo1f[-/] neutrophils upon CXCL1 stimulation was significantly reduced compared to transmigration of Myo1f^{+/+} neutrophils. Accordingly, CXCL1 stimulation induced substantial transmigration of Myo1f^{+/+} neutrophils in uncoated filters, whereas transmigration of Myo1f^{-/-} neutrophils was significantly diminished (Figure 25b). In summary, Myo1f was indispensable for neutrophil transmigration through narrow pores[127].
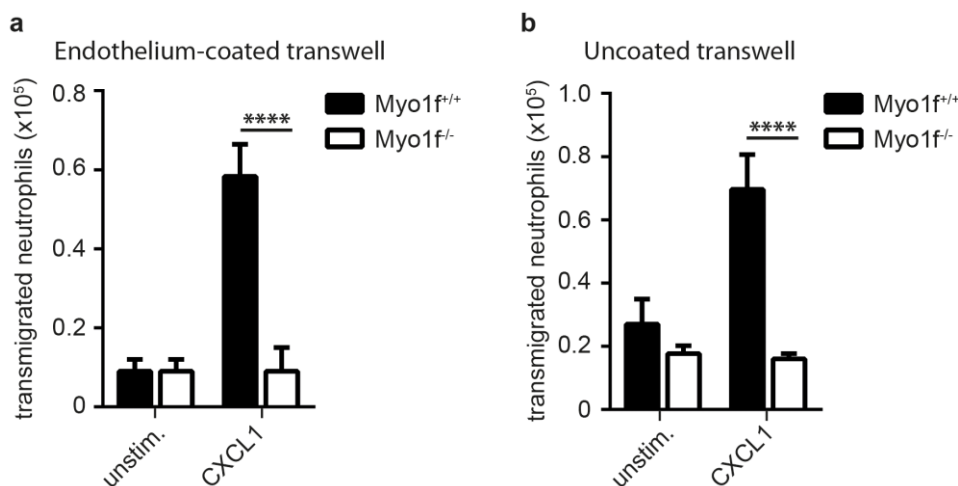
Figure 25. TEM of Myo1f^{+/+} and Myo1f^{-/-} neutrophils. Transmigration of neutrophils studied in transwell assays using filters with 8 µm pore sizes. Neutrophils were exposed to CXCL1 (100 ng/mL) as chemoattractant or left unstimulated. (a) Transwell filters coated with a monolayer of brain-derived b.End3 endothelial cells or (b) left uncoated as control. n = 4. Mean ± SEM. **** $p < 0.0001$ (2-way ANOVA, Sidak's multiple comparison test, modified from Salvermoser et al., 2018[127]).

5.3.3 Neutrophil migration in 3D collagen networks

After successful transmigration through the endothelial barrier and the BM, neutrophils migrate in the interstitial tissue to sites of inflammation or injury[195,196]. To investigate the role of Myo1f in this context, 3D migration of Myo1f^{+/+} and Myo1f^{-/-} neutrophils within a collagen gel was studied using 3D chemotaxis chambers. Here, analysis of single cell migration tracks of Myo1f^{+/+} neutrophils revealed a reduced migration capacity in a high-density collagen gel (3 mg/mL) compared to a low-density (1.5 mg/mL) collagen gel in response to a CXCL1 chemoattractant gradient (Figure 26a). Quantitative analysis demonstrated that the migration velocity significantly decreased from 8.1 ± 0.5 µm/min in a 1.5 mg/mL collagen gel to 5.1 ± 0.8 µm/min in a 3.0 mg/mL collagen gel in Myo1f^{+/+} neutrophils (Figure 26b).
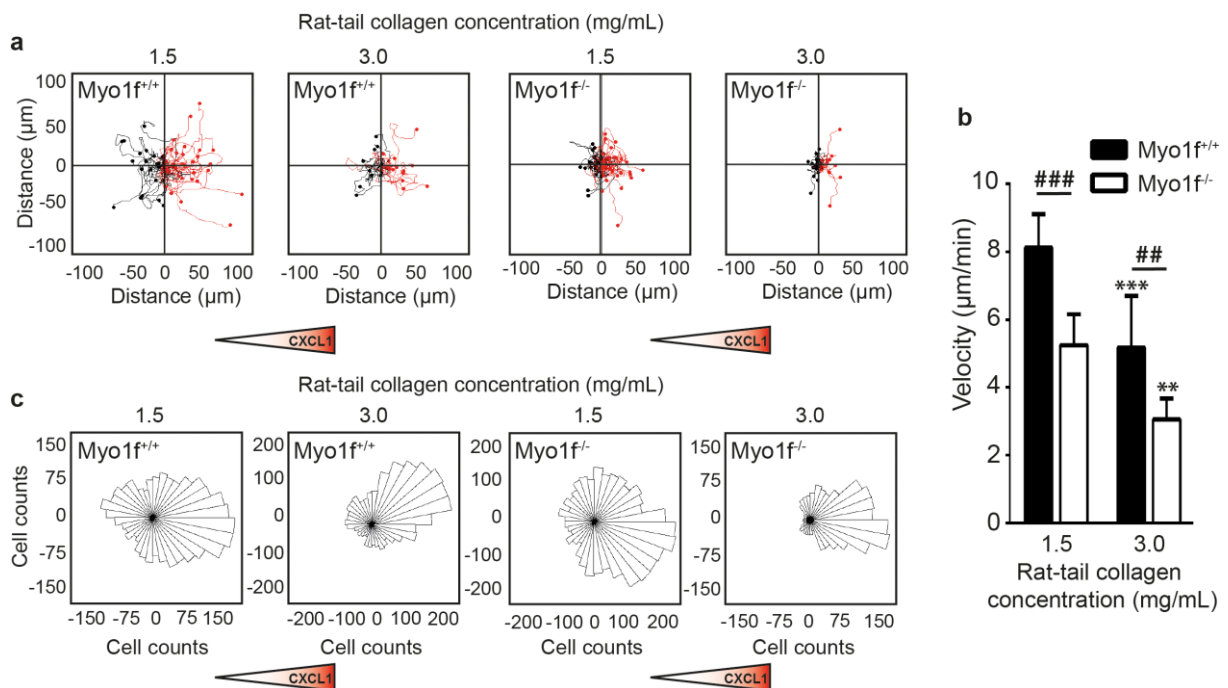
Figure 26. The role of Myo1f for neutrophil migration in 3D collagen networks. (a, b) Chemotactic migration of Myo1f^{+/+} and Myo1f^{-/-} neutrophils in 3D collagen gels towards a CXCL1 (100 ng/mL) gradient using µ-Slides Chemotaxis3D chambers. (a) Single cell migration tracks in 3D collagen gels with different collagen concentrations. Triangles indicate orientation of the gradient. (b) Quantitative analysis of mean migration velocity. n = 4. ## p<0.01, ### p<0.001, ** p<0.01, *** p<0.001 versus rat-tail collagen concentration 1.5 mg/mL (2-way ANOVA, Sidak's multiple comparison test). (c) Rose diagrams indicating the distribution of migration vectors of tracked Myo1f^{+/+} and Myo1f^{-/-} neutrophils. The radius of each sector represents the cell number. Triangles indicate orientation of the gradient (modified from Salvermoser et al., 2018[127]).

These data indicated that the increased density of the collagen meshwork caused a decreased migration velocity in Myo1f^{+/+} neutrophils. In the genetic absence of Myo1f, the migration velocity was significantly reduced from 5.2 ± 0.5 µm/min in 1.5 mg/mL collagen gels to 3.1 ± 0.3 µm/mL in 3.0 mg/mL collagen gels. Moreover, the migration velocities in both densities of the collagen gels upon stimulation with CXCL1 were significantly decreased in Myo1f^{-/-} compared to Myo1f^{+/+} neutrophils indicating that migration within 3D collagen gels critically involved Myo1f. Analysis of Rose diagrams, showing the frequency of the migration vectors of tracked Myo1f^{+/+} and Myo1f^{-/-} neutrophils in each direction, revealed that the sensing of the chemoattractant was still intact in Myo1f^{-/-} neutrophils and similar to Myo1f^{+/+} neutrophils (Figure 26c). Together, these data demonstrated that in contrast to migration in 2D environments which was independent of Myo1f, Myo1f was indispensable for migration in 3D environments[127].

5.4   Dynamic regulation of the nuclear shape during migration in 3D environments

Migration within a 3D environment requires rapid changes of the cell shape as well as deformation of the nucleus[67,120]. Therefore, the impact of Myo1f for squeezing of the neutrophil nucleus during 3D migration was analyzed in the last part of the study.

5.4.1   Morphology of the nucleus during transmigration

To investigate the impact of Myo1f for squeezing neutrophils through restrictive sites during the process of transmigration, transwell assays were performed and the morphology of the nucleus was analyzed. Microscopic inspection of cytospins of freshly isolated unstimulated Myo1f^{+/+} and Myo1f^{-/-} neutrophils showed a similar morphology of the nuclei in both cell populations (Figure 27a). The role of Myo1f in nuclear morphometry during transmigration was studied using Myo1f^{+/+} and Myo1f^{-/-} neutrophils stained with the nuclear dye Hoechst 33342. Here, neutrophils were seeded on rmICAM-1 and rmP-selectin coated transwell filters with fMLP as chemoattractant in the lower compartment. Confocal immunofluorescence images show the morphology of Myo1f^{+/+} and Myo1f^{-/-} nuclei during transmigration (Figure 27b). The area of the nuclei of Myo1f^{-/-} neutrophils with 64.3 ± 6 µm^2 was significantly larger compared to the area of the nuclei of Myo1f^{+/+} neutrophils with 39.3 ± 3 µm^2 upon fMLP stimulation for 5 min (Figure 27c, left panel). Similar effects were observed at later time-points[127].
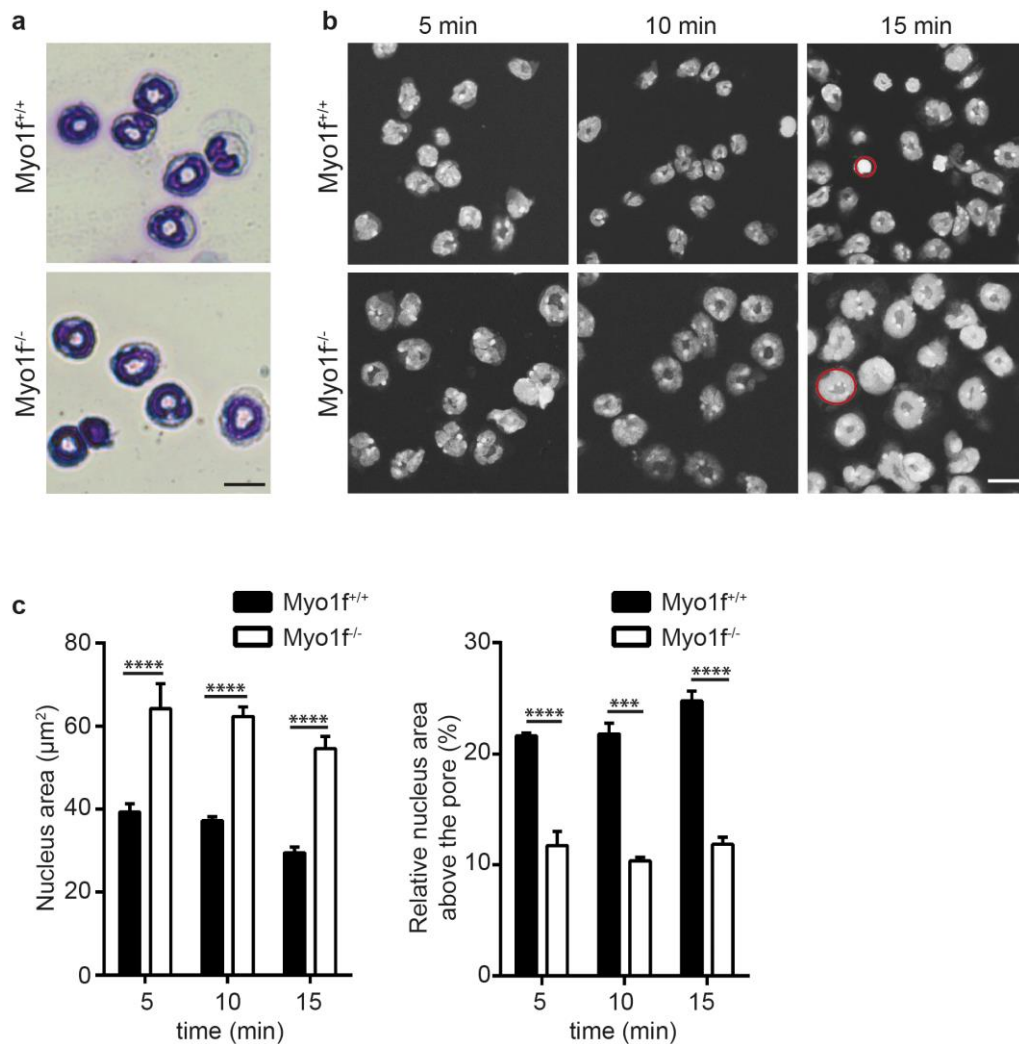
Figure 27. The morphology of Myo1f+/+ and Myo1f-/- nuclei during transmigration. (a) Micrographs of the morphology of Myo1f+/+ and Myo1f-/- nuclei after cytospin and May-Grünwald-Giemsa staining. Scale bar = 10 μm. (b, c) Morphology of the nucleus was analyzed during transmigration using rmICAM -1 (12.5 μg/mL) and rmP-selectin (10 μg/mL) coated transwell filters. Myo1f+/+ and Myo1f-/- neutrophils were labeled with the nuclear dye Hoechst 33342 (5 μM), fixed and imaged after 5, 10 and 15 min upon fMLP stimulation. (b) Representative microscopic images of the morphology of the nuclei at indicated time points. Scale bar = 10 μm. Red circle indicates area of the nucleus in Myo1f+/+ and Myo1f-/- neutrophils. (c) Quantification of the total (left graph) and relative (right graph) area of the nuclei of Myo1f+/+ and Myo1f-/- neutrophils above the pore upon stimulation with fMLP at indicated time points. n = 3 independent experiments with a total of 76 Myo1f+/+ and 78 Myo1f-/- neutrophils at each time point. Mean ± SEM. n.s. not significant, ** P <.01, *** P <.001, **** P <.0001 (2-way ANOVA, Sidak's multiple comparison test, modified from Salvermoser et al., 2018[127]).

Here, the area of the nucleus of Myo1f+/+ neutrophils was 37.2± 1 μm^2 at 10 min and 30.5± 2 μm^2 at 15 min, whereas the area of the nucleus of Myo1f-/- neutrophils was significantly larger with 62.3± 3 μm^2 at 10 min and 55.5± 4 μm^2 at 15 min. Accordingly, the nucleus area located above the

pores relative to the whole nucleus area (100 %) was significantly larger in Myo1f^{+/+} neutrophils compared to Myo1f^{-/-} neutrophils (Figure 27c, right panel) suggesting that Myo1f was important for neutrophil transmigration by squeezing the nucleus through narrow spaces[127].

5.4.2 Localization of Myo1f during 3D migration in a collagen network

The restrictive barriers in the collagen meshwork that neutrophils pass while migrating through this confined environment were visualized using live cell imaging by reflection and confocal fluorescence microscopy. Representative confocal reflection and fluorescence images show a primary human neutrophil migrating through a meshwork of collagen fibers (Figure 28).
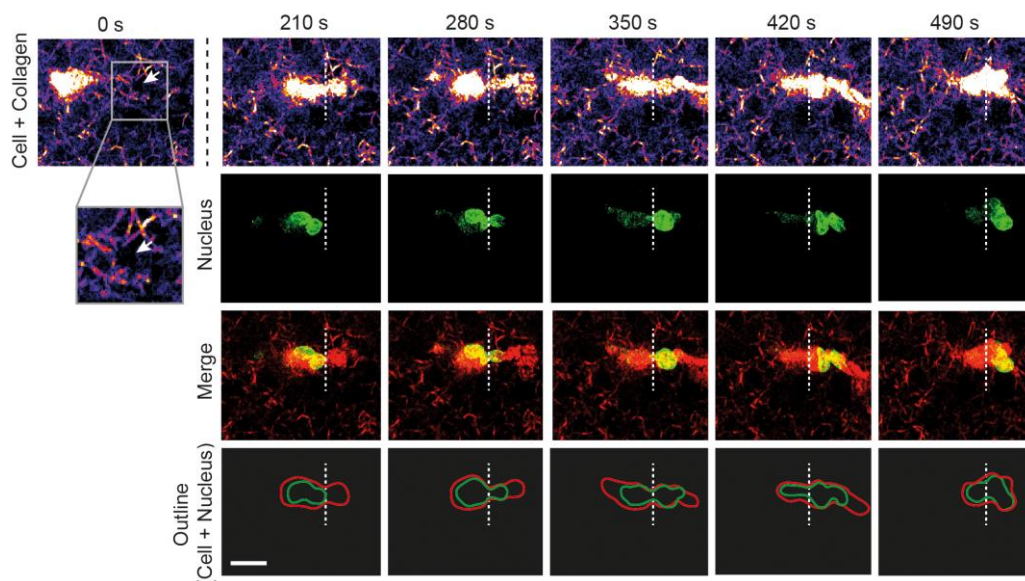
Figure 28. Migration of primary human neutrophil within a 3D collagen gel. Live cell imaging of a primary human neutrophil migrating within a 1.5 mg/mL collagen gel towards an fMLP (100 nM) gradient using confocal reflection/fluorescence microscopy. Confocal images demonstrate a human neutrophil stained with the nuclear dye Hoechst 33342 (5 µM) migrating through the meshwork of collagen fibers at indicated time points. The architecture of the collagen meshwork and the cell body were visualized by confocal reflection microscopy (fire and red). The shape of the nucleus during 3D migration is shown by confocal fluorescence microscopy (green). Merge (yellow) indicates the reflection image (red) and the nucleus (green). Schematic outline of the morphology of the nucleus (green) and the cell body (red) during migration in a collagen gel. Neutrophil localization is normalized to the pore (white dotted line and white arrow). Scale bar = 10 µm (modified from Salvermoser et al., 2018[127]).

As expected, the migration through restrictive spaces (white dotted line) was initiated by the formation of a small nuclear lobe inserted into the narrow pore preparing the deformation of the nucleus to squeeze the whole neutrophil through the pore (280 s)[124]. This step was followed by the elongation of the nucleus (350 s- 420 s). After successful squeezing through the narrow pore, the nucleus refolded back into an ellipsoid, multi-lobular shape (490 s)[127].

To delineate the potential interplay between Myo1f, Actin and the nucleus during migration in 3D collagen gels, their subcellular localization was studied by spinning disk confocal microscopy using HL-60 cells stably expressing an EGFP-Myo1f fusion protein. After differentiation of HL-60 EGFP-Myo1f cells towards neutrophil-like cells by addition of DMSO for 6 days, cells were stained with the nuclear dye Hoechst 33342 and Sir Actin to stain F-actin and exposed to an fMLP gradient in a 1.5 mg/mL collagen gel. As expected and similar to human neutrophils, the nucleus of dHL-60 EGFP-Myo1f cells formed a nuclear lobe to initiate migration through a permissive site (0 s). Subsequently, the nucleus elongated and deformed (30 s – 60 s) to squeeze through the narrow pore and refolded into a roundish shape after successful squeezing (Figure 29a). During the initiation and deformation phases, Myo1f was mainly accumulated at the front and the rear of the polarized cell and redistributed throughout the lamellipodium in the remodeling phase. Actin was found to form a ring-like structure around the nucleus while the initiation and deformation phase. After passing the narrow space an open actin formation remained at the rear of the cell while the remodeling phase. Importantly, during the initiation (0 s) and deformation phase (30-60 s) Myo1f and Actin colocalized at the constriction sites as well as at the rear and the front of the cell. This observation suggested a role of Myo1f for bringing the nucleus into shape to migrate within a defined 3D collagen meshwork[127]. The deformation of the nucleus as well as the localization and the colocalization of Myo1f and Actin during the different phases initiation phase (0 s), deformation phase (30 s-60 s) and remodeling phase (90 s) of migration within confined 3D environments, are shown in the schematic representation of the dHL-60 EGFP-Myo1f cell in Figure 29b[127].

The localization of Myo1f and Actin during the different phases cells undergo while migrating through a meshwork of collagen fibers was confirmed using isolated primary human neutrophils (Figure 29c).
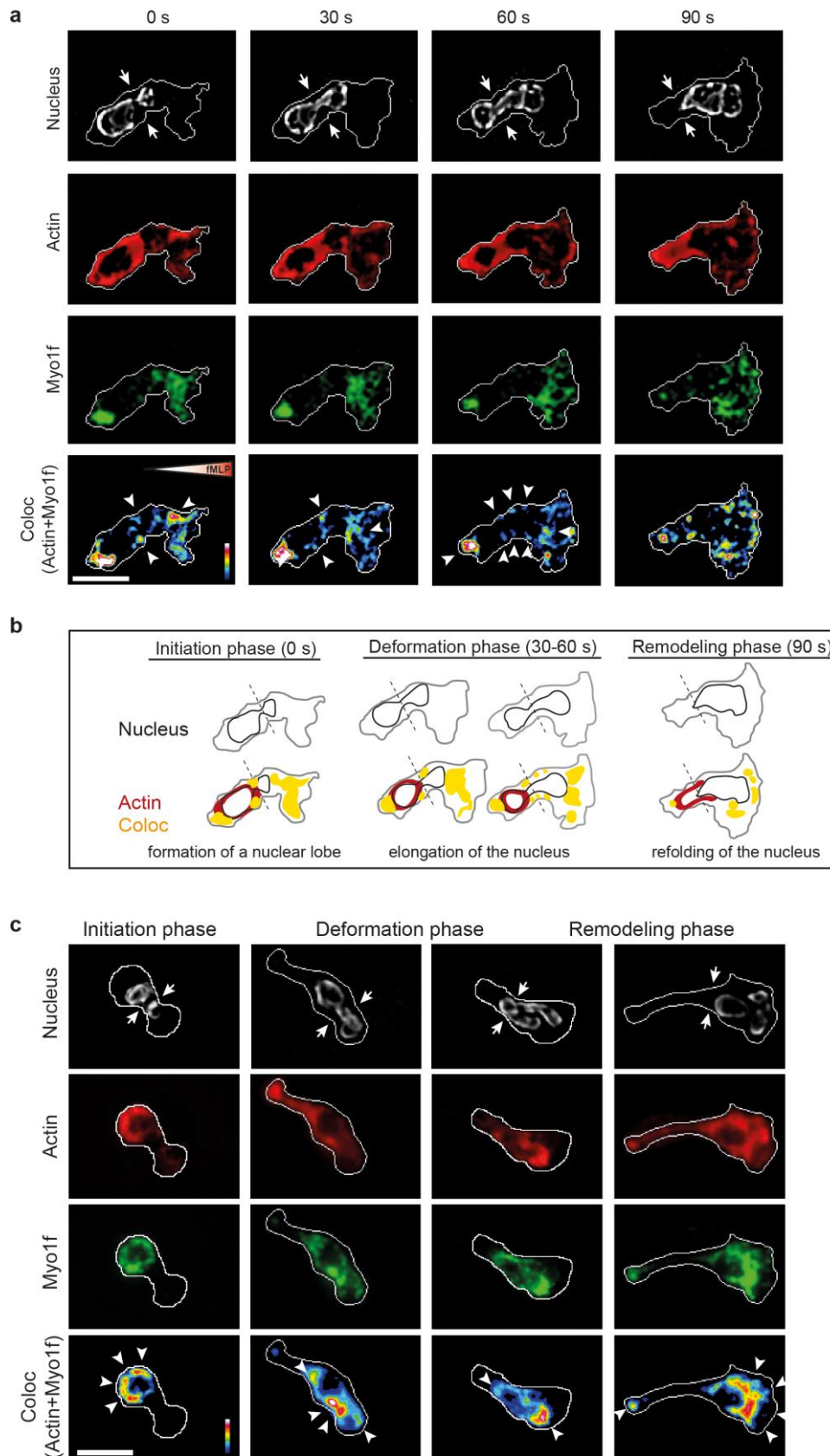
Figure 29. Localization of Myo1f and Actin during migration in a 3D collagen meshwork. Migration of (a) dHL-60 EGFP-Myo1f cells and (b) isolated primary human neutrophils was analyzed in a meshwork of collagen fibers using spinning disk confocal microscopy. (a) Live cell

imaging of a migrating dHL-60 EGFP-Myo1f towards an fMLP (100 nM) gradient. Still images demonstrate the morphology of the nucleus (grey), the subcellular localization of Myo1f (green) and Actin (red), as well as the colocalization of Myo1f and Actin (white arrow heads). Representative cell from 3 independent experiments. Color scale, heat map. Triangle indicates the orientation of an fMLP (100 nM) gradient. Scale bar = 10 μm. (b) Schematic outline of the morphology of the nucleus (black), localization of Actin (red) and Myo1f (green), and colocalization of Actin and Myo1f (yellow) of the dHL-60 EGFP-Myo1f cell during migration in a collagen gel at indicated time points. The neutrophil shape is indicated in grey. (c) Analysis of 3D migration of isolated primary human neutrophils in a collagen gel towards an fMLP (100 nM) gradient using spinning-disk confocal microscopy. After migration within the collagen gel for 10 min, neutrophils were fixed with 4 % PFA, permeabilized with 0.2 % Triton-X and stained with the nuclear dye Hoechst 33342 (5 μM), SiR-actin (100 nM) and for endogenous Myo1f using a polyclonal rabbit anti-human Myo1f antibody and a secondary Alexa-Fluor 488 antibody. Pseudo-colored images demonstrating the morphology of the nucleus (grey), the subcellular localization of Actin (red) and Myo1f (green), as well as the colocalization of Actin and Myo1f (arrow heads) during the different migration phases: initiation phase, deformation phase and remodeling phase. Arrows indicate constriction site. Representative cell from 3 independent experiments. Scale bar = 10 μm. Color scales, heat map (modified from Salvermoser et al., 2018[127]).

Similar to dHL-60 EGFP-Myo1f cells, the formation of a nuclear lobe during the initiation phase, the elongation of the nucleus during the deformation phase as well as the refolding of the nucleus into a roundish morphology during the remodeling phase were observed. In addition, colocalization of Myo1f and Actin at the rear and the front as well as at the constriction sites was detected in primary human neutrophils. This was in line with the observed colocalization of Myo1f and Actin in dHL-60 EGFP-Myo1f cells[127].

5.4.3   The role of Myo1f for the deformation of the nucleus during 3D migration

To study the functional impact of Myo1f during 3D migration in detail, Hoechst 33342 -labeled neutrophils were imaged during migration in a collagen gel towards a CXCL1 gradient using reflection and confocal fluorescence microscopy (Figure 30). As expected, real-time reflection and fluorescence microscopic images revealed that the nucleus of Myo1f$^{+/+}$ neutrophils deformed during migration in a collagen meshwork. Starting from a roundish shaped nucleus, a nuclear lobe was formed after 280 s, followed by elongation and deformation of the nucleus at 350 s to squeeze through the narrow pore in the meshwork of collagen fibers and refolded into a roundish morphology after passing the pore at 420 s. In sharp contrast to Myo1f$^{+/+}$ neutrophils, Myo1f$^{-/-}$ neutrophils failed to deform their nuclei during 3D migration. The nucleus kept a roundish

morphology without almost no detectable shape change during the entire recording time suggesting that the lack of nucleus deformation was the reason for the defective 3D migration in the genetic absence of Myo1f[127].
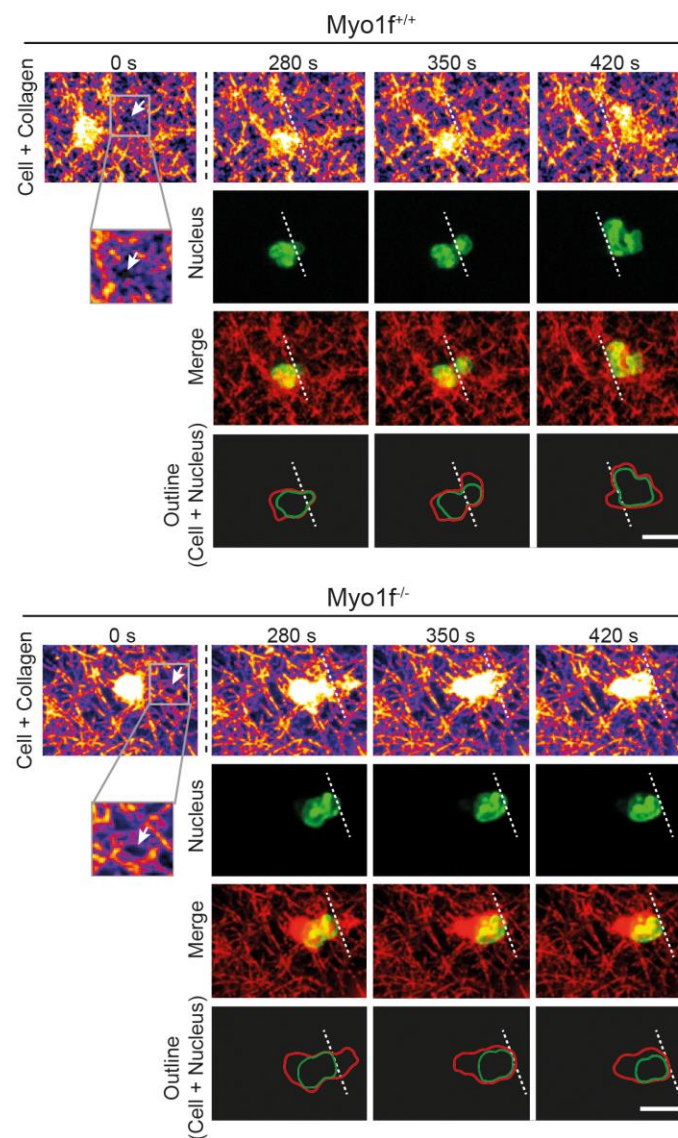
Figure 30. Migration of Myo1f$^{+/+}$ and Myo1f$^{-/-}$ neutrophils within a 3D collagen gel. Live cell imaging of Myo1f$^{+/+}$ and Myo1f$^{-/-}$ neutrophils migrating within a 1.5 mg/mL collagen gel towards CXCL1 (100 ng/mL) gradient using confocal reflection/fluorescence microscopy. Confocal images demonstrate Myo1f$^{+/+}$ and Myo1f$^{-/-}$ neutrophils stained with the nuclear dye Hoechst 33342 (5 µM) migrating through the meshwork of collagen fibers at indicated time points. The architecture of the collagen meshwork and the cell body are visualized by confocal reflection microscopy (fire and red). The shape of the nucleus during 3D migration is shown by confocal fluorescence microscopy (green). Merge (yellow) indicates the reflection image (red) and the nucleus (green). Schematic outline of the morphology of the nucleus (green) and the cell body (red) during migration in a collagen gel. Neutrophil localization is normalized to the pore (white dotted line and white arrow). Scale bar = 10 µm (modified from Salvermoser et al., 2018[127]).

To study the localization of Actin and the morphology of the nucleus during migration in a collagen gel, Myo1f^{+/+} and Myo1f^{-/-} neutrophils were stained with the nuclear dye Hoechst 33342 as well as Sir-Actin and 3D migration was analyzed using spinning disk confocal microscopy (Figure 31a). Similar to the results observed in dHL-60 EGFP-Myo1f cells, an Actin ring was formed around the back of the Myo1f^{+/+} nucleus during the elongation of the nucleus. In comparison to Myo1f^{+/+} neutrophils this ring-like Actin structure was not observed in Myo1f^{-/-} neutrophils.
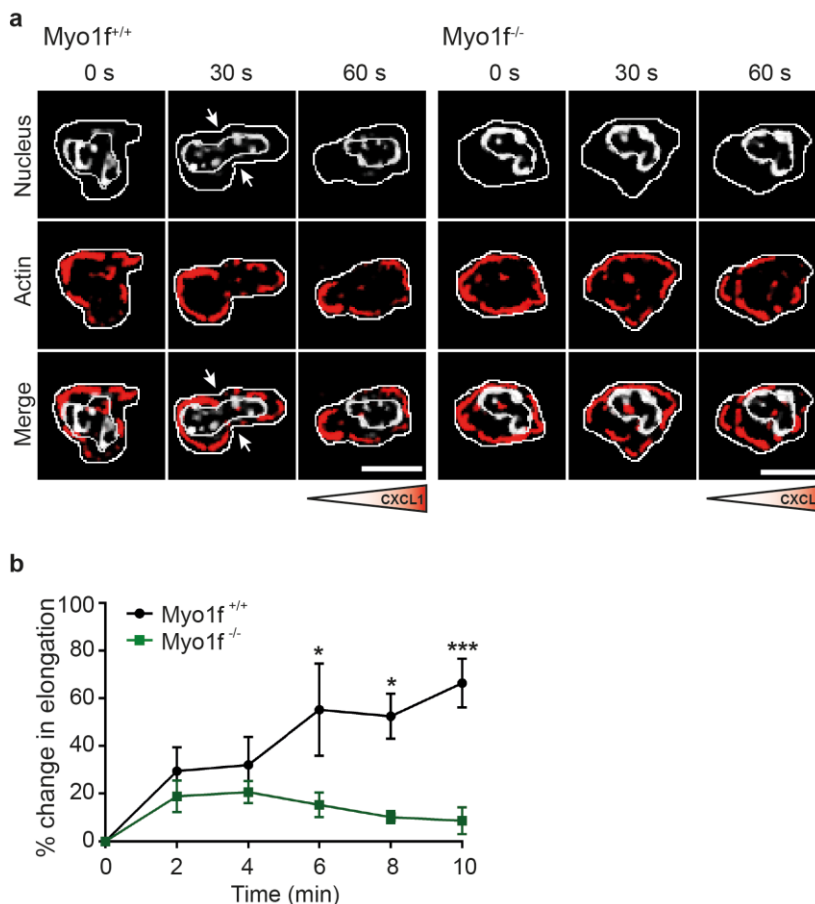
Figure 31. Shape change of Myo1f^{+/+} and Myo1f^{-/-} nuclei during migration in 3D collagen gels. (a, b) Migration of Myo1f^{+/+} and Myo1f^{-/-} neutrophils in a 1.5 mg/mL collagen gel towards a CXCL1 (100 ng/mL) gradient was analyzed using μ-Slides Chemotaxis 3D chambers. The neutrophils were stained with the nuclear dye Hoechst 33342 (5 μM) and Sir Actin (100 nM) and the shape of the nucleus was determined using spinning disk confocal microscopy. (a) Representative fluorescence time-lapse microscopy images of Myo1f^{+/+} and Myo1f^{-/-} neutrophils indicated the morphology of the nucleus (white) as well as the localization of actin (red) during 3D migration at indicated time points. Scale bar = 10 μm. Triangles indicate orientation of the gradient. (b) Percentage of change in nucleus elongation during neutrophil 3D migration at indicated time points. n = 3 independent experiments. * $p < 0.05$, *** $p < 0.001$ (2-way ANOVA, Sidak's multiple comparison test, modified from Salvermoser et al., 2018[127]).

For quantitative analysis of change in nucleus elongation, a basic shape change factor defining shape elongation was used. Here, a shape change factor of 0 indicated a rounded nucleus and 1 represented an elongated nucleus. The mean nuclear shape change factor per time point was analyzed and normalized to the overall smallest value to calculate the percent change in nuclear shape within the following 10 min of observation (Figure 31b)[127]. However, this change in nucleus elongation was almost not existent in Myo1f$^{-/-}$ neutrophils, indicating that the shape change of the nucleus for successful migration in a 3D collagen network did not occur in the genetic absence of Myo1f. These results demonstrated that Myo1f$^{-/-}$ neutrophils were not able to exhibit efficient nucleus deformation resulting in hampered migration through physical barriers in the meshwork of collagen fibers[127].

6. DISCUSSION

Neutrophils play an essential role in the innate immune response as they are the first leukocytes arriving at the site of inflammation. The neutrophil recruitment from the blood stream into the inflamed tissue and to the site of injury or infection follows a multi-step cascade of consecutive events[14]. There is evidence that the unconventional Myo1f is involved in neutrophil recruitment during the acute inflammatory response by affecting neutrophil adhesion under static conditions and neutrophil accumulation at the site of inflammation[1]. However, the role of Myo1f under physiological flow conditions as well as the mechanism of the action of Myo1f remained elusive. In the present study, the functional importance of Myo1f for neutrophil trafficking during the acute inflammatory response was analyzed in detail.

6.1 The role of Myo1f in neutrophil rolling and adhesion

A previous study by Kim et al. demonstrated that Myo1f$^{-/-}$ neutrophils displayed increased adhesion under static conditions *in vitro*[1]. In the present study, the genetic absence of Myo1f resulted in increased neutrophil adhesion to the β_2 integrin ligand ICAM-1 upon stimulation with diverse stimuli, including the chemokine CXCL1, Mn^{2+} which stabilizes the high affinity conformation of the β_2 integrins[39], the chemotactic peptide fMLP as well as the cytokine TNFα. These *in vitro* results under static conditions were in line with the data obtained by Kim and co-workers[1]. In addition, adhesion to the Mac-1 ligand fibrinogen was increased in the genetic absence of Myo1f upon stimulation (compare Figure 12).

To study whether this effect was due to differently expressed β_2 integrins, surface expression of CD11a, CD11b and CD18 was analyzed in unstimulated neutrophils and after stimulation with CXCL1 and fMLP. Surface expression of LFA-1 and Mac-1 was similar between Myo1f$^{+/+}$ and Myo1f$^{-/-}$ neutrophils showing that altered β_2 integrin surface expression was not responsible for increased adhesion under static conditions in the situation *in vitro* (compare Figure 13). However, neutrophil adhesion was analyzed under static conditions by Kim and co-workers[1] and therefore it did not reflect the actual physiological situation *in vivo*. Here, neutrophils need to resist shear forces of the blood stream while they adhere to the endothelial surface[99]. In contrast to the study by Kim et al.[1], the present study analyzed the physiological function of Myo1f for neutrophil trafficking under flow conditions *in vitro* and *in vivo*. Neutrophil rolling and adhesion on rmICAM-1, rmP-selectin and CXCL1 coated flow chambers was investigated under 1 dyne/cm^2 shear stress

representing the physiological conditions in postcapillary venules[197]. However, no difference in induction of adhesion between Myo1f^{-/-} and Myo1f^{+/+} neutrophils was observed. (Figure 12). Taken together, these data suggest that Myo1f functions differently under static and flow conditions highlighting the importance of the experimental conditions when analyzing neutrophil trafficking.

Moreover, the biological relevance of Myo1f for leukocyte rolling and adhesion was studied *in vivo* using three different inflammatory models in the mouse cremaster muscles of Myo1f^{+/+} and Myo1f^{-/-} mice. In the trauma-induced model of inflammation, rolling flux fraction as well as the number of adherent leukocytes of Myo1f^{+/+} mice were similar to values reported in earlier studies[193,198,199]. Interestingly, leukocyte rolling and adhesion in this model of inflammation was not altered in the genetic absence of Myo1f (compare Figure 14). Intrascrotal injection of the proinflammatory cytokine TNFα causes the upregulation of E-selectin, P-selectin, ICAM-1 as well as CXCL1 expression on the endothelium leading to slow leukocyte rolling and arrest[192,199]. These events are mediated by talin-dependent activation of LFA-1 into an intermediate ligand affinity E(+) H(-) conformation[41,42,200,201]. Accordingly, the rolling flux fraction decreased and the number of adherent leukocytes increased 2.5 h after i.s. TNFα application in Myo1f^{+/+} mice as expected. The genetic absence of Myo1f did not affect leukocyte rolling and adhesion in TNFα stimulated mouse cremaster postcapillary venules suggesting that Myo1f was dispensable for LFA-1 activation into the intermediate ligand affinity E(+) H(-) conformation, slow leukocyte rolling and arrest *in vivo* (compare Figure 15). Chemokine signaling through GPCRs leads to the binding of both talin and kindlin-3 to the cytoplasmic tail of LFA-1 inducing the LFA-1 high ligand affinity E(+) H(+) conformation. Extended, fully activated LFA-1 binds endothelial ICAM-1 and ICAM-2 which results in firm neutrophil adhesion[41,44,198]. In the present study, chemokine-induced firm leukocyte adhesion was investigated by i.v. injection of CXCL1 into Myo1f^{+/+} and Myo1f^{-/-} mice. As expected, the number of adherent leukocytes was dramatically increased in Myo1f^{+/+} mice. Similarly, leukocyte adhesion in Myo1f^{-/-} mice was increased after CXCL1 application indicating that LFA-1 activation and subsequent firm leukocyte adhesion does not require Myo1f (compare Figure 16). Affinity regulation of LFA-1 and Mac-1 was evaluated *in vitro* using isolated Myo1f^{+/+} and Myo1f^{-/-} neutrophils (compare Figure 13). LFA-1 specific ICAM-1 binding which reports the high-affinity conformation of LFA-1[41,44] was not altered in the genetic absence of Myo1f supporting the finding that Myo1f is not relevant for the affinity regulation of LFA-1. Fibrinogen binding to Myo1f^{+/+} and Myo1f^{-/-} neutrophils was used to investigate Mac-1 affinity regulation. Here, no difference in binding of soluble fibrinogen was detected in Myo1f^{-/-}

neutrophils when compared to Myo1f^{+/+} neutrophils. Similar to Mac-1, the integrin CD11c/CD18 also binds fibrinogen. However CD11c/CD18 expression is rather low on neutrophils and Mac-1 represents the main fibrinogen receptor on these cells[202]. These data demonstrate that Myo1f was dispensable for the regulation of the β_2 integrins LFA-1 and Mac-1 in murine neutrophils under physiological conditions *in vitro* as well as in the situation *in vivo*.

6.2   Neutrophil extravasation in different *in vivo* inflammation models

Although the absence of Myo1f did not affect neutrophil rolling and adhesion under physiological flow conditions, Myo1f was found to be fundamentally important for neutrophil extravasation into inflamed tissues in three different experimental models. Here, analysis of the TNFα stimulated mouse cremaster muscle model, the CXCL1-induced peritonitis model and the LPS-triggered lung injury model revealed severely compromised neutrophil extravasation to the site of inflammation in Myo1f^{-/-} mice compared to Myo1f^{+/+} mice (compare Figure 17-19). Importantly, the white blood cell counts in the circulation were similar between Myo1f^{+/+} and Myo1f^{-/-} mice, indicating that neutrophil recruitment from the bone marrow into the blood stream was not hampered by the genetic absence of Myo1f, whereas the extravasation from the blood stream to sites of inflammation was dependent on Myo1f.

The observed extravasation defect in Myo1f^{-/-} mice was in line with a previous report by Kim et al., where Myo1f^{-/-} mice were shown to be more susceptible to infection with *Listeria monocytogenes*[1]. The authors speculated that the failure to control bacterial infection was attributed to increased neutrophil adhesion causing impaired neutrophil accumulation at the site of inflammation. As mentioned above, increased adhesion was only observed under static conditions whereas adhesion under flow conditions was normal. Thus, one can speculate that increased adhesion under static condition occurred coincidentally and did not represent the mechanism influencing neutrophil extravasation upon inflammation and therefore did not represent the reason for the increased susceptibility to *Listeria monocytogenes* infection.

In the present study, TNFα stimulation in the mouse cremaster muscle of Myo1f^{+/+} mice led to leukocyte accumulation in the inflamed tissue as expected[65,203]. Analysis of whole mount histology revealed that neutrophil extravasation but not extravasation of other leukocyte subtypes was impaired in the genetic absence of Myo1f suggesting a pivotal impact of Myo1f for neutrophil extravasation in response to TNFα. In line with the results obtained in the cremaster model, neutrophil extravasation was observed to be significantly compromised in the experimental

models of acute peritonitis and acute lung injury, pointing again towards the importance of Myo1f for neutrophil extravasation. Neutrophil recruitment into the peritoneal cavity can be induced by i.p. injection of pathogens, inflammatory cytokines, thioglycollate or CXCL1[204,205]. Studies using CD18-deficient or CD11a-deficient mice showed that neutrophil recruitment into the inflamed peritoneum is β_2 integrin dependent[206-208]. In contrast neutrophil recruitment into the lungs can occur in a β_2 integrin dependent or independent regulated by the stimulus applied[209,210]. Since Myo1f^{-/-} neutrophils failed to extravasate in all three different experimental models applied, these results suggest that Myo1f is not involved in the regulation of β_2 integrins but plays an important role in neutrophil extravasation independent on β_2 integrins.

By applying the ALI model, the impact of Myo1f for neutrophil recruitment in a clinical relevant disease was investigated. ALI and its most severe form, the acute respiratory distress syndrome (ARDS), are major problems in intensive care medicine and are associated with a high mortality rate[211]. The disease is characterized by the formation of pulmonary edema and impaired gas exchange eventually leading to respiratory failure[212]. ALI is initiated by injury of the endothelium as well as the epithelium of the lungs, leading to increased permeability of the alveolar-capillary barrier and infiltration of neutrophils into the bronchoalveolar space[213,214]. The severity of ALI and ARDS correlates with the infiltrated amount of neutrophils in the BAL. Accordingly, it has been shown that depletion of neutrophils decreased the severity of ALI suggesting that neutrophils are critically involved in the progression of the disease[215]. Further experiments demonstrated that infiltrated neutrophils damage the lung tissue by releasing proteinases, cationic peptides, cytokines and ROS[216]. Although recruitment of neutrophils into the lungs is essential for host defense, regulation of neutrophil activation and emigration might represent an option for treating ALI. However, it was reported that patients with neutropenia still developed ALI, thus indicating an additional neutrophil-independent mechanism of ALI development under specific conditions[217,218]. Nevertheless, various animal models and clinical data point towards a fundamental impact of neutrophil activation and recruitment during ALI[212]. In the present study, ALI was initiated by the inhalation of LPS, a component of the outer membrane of gram-negative bacteria, leading to neutrophil migration into the bronchoalveolar space[219]. Importantly, in Myo1f^{-/-} mice significantly less neutrophils were recruited into the lungs compared to Myo1f^{+/+} mice. As expected, lung damage assessed by TRITC-Dextran permeability measurements was decreased in the absence of Myo1f, suggesting that Myo1f represents an important novel player in neutrophil-driven ALI by mediating neutrophil migration.

In general, inhibitors of leukocyte trafficking are promising anti-inflammatory drugs for the treatment of inflammatory diseases and cancer[220,221]. In the last decade, several new therapeutics altering leukocyte trafficking were developed, whereas many clinical trials failed or are still ongoing[80,220]. For example, until now the treatment of ischemia-reperfusion injury in acute myocardial infarction by the blockade of neutrophil infiltration was not successful[222]. However, there are approved drugs like natalizumab, an anti-α_4 integrin monoclonal antibody which inhibits T cell recruitment into inflamed tissues in multiple sclerosis[223] and Crohn's disease[220,224,225]. The treatment of multiple sclerosis with natalizumab showed severe side effects, e.g. the development of progressive multifocal leukoencephalopathy. This example clearly demonstrates that the blockade of leukocyte trafficking as an anti-inflammatory therapy is a 'doubled-edge sword'[80]. On the one hand, inhibition of leukocyte trafficking can be effective in the treatment of various diseases, on the other hand blocking of leukocyte trafficking can cause an increased susceptibility to infections. Thus, in the future it is necessary to understand leukocyte trafficking in more detail to dampen side effects[80].

6.3 The impact of Myo1f in neutrophil migration

Controlled trafficking of leukocytes towards the sites of inflammation is fundamentally important for efficient innate and adaptive immune responses. To unravel the mechanism for the dramatic extravasation defect in the genetic absence of Myo1f, the role of Myo1f for neutrophil migration was examined. Since neutrophils migrate on the endothelial surface (2D) as well as in tissue (3D), it is of utmost importance to consider that the mode of migration may be different in 2D and 3D environments.

Neutrophil spreading, polarization and migration in 2D environments were found to be unaffected in the presence of the β_2 integrin ligand ICAM-1 or fibrinogen in Myo1f^{-/-} neutrophils under flow conditions *in vitro* (compare Figure 20-23). This was in contrast to the findings by Kim et al. where neutrophil spreading was analyzed under static conditions and shown to be increased in the genetic absence of Myo1f[1]. Furthermore, the study demonstrated decreased neutrophil migration on fibronectin and poly-lysine towards an fMLP chemoattractant[1]. These ligands are not specific for β_2 integrins, which could be the reason for the different outcome of the migration studies, since neutrophil migration in physiological 2D environments is dependent on adhesion via β_2 integrins[48,226]. These findings clearly demonstrate that experimental conditions are important for

the outcome of the experiment and further highlight that neutrophils employ highly specific mechanisms for adhesion, spreading and migration to resist shear forces under flow conditions. Another study analyzed the impact of Myo1f on TLR4-driven spreading response of macrophages. Downregulation of Myo1f in bone marrow-derived macrophages using siRNA severely reduced spreading upon LPS stimulation under static conditions[173]. These results suggest that the biological function of Myo1f may have evolved differently in diverse leukocyte subtypes.

Next, the impact of Myo1f for neutrophil migration within confined 3D environments was studied (compare Figure 24-26). During TEM and interstitial migration, neutrophils need to pass narrow pores ranging from 1 to 30 µm in diameter[227,228]. Accordingly, neutrophil transmigration was investigated using transwell chambers with pore sizes of 3 µm, 5 µm and 8 µm reflecting constrictions present in the actual *in vivo* situation[227]. Analysis of the number of neutrophils transmigrated into the lower compartment of a transmigration chamber supplemented with fMLP or CXCL1 revealed that Myo1f was critically involved in neutrophil transmigration. To further analyze the role of Myo1f for TEM, transwell filters were coated with a monolayer of endothelial b.End3 cells or left uncoated for comparison. CXCL1 stimulation induced transmigration of Myo1f$^{+/+}$ neutrophils through the bEnd.3-coated as well as through the non-coated filters as expected. In comparison to Myo1f$^{+/+}$ neutrophils, Myo1f$^{-/-}$ neutrophils failed to transmigrate through the endothelial barrier as well as through the uncoated pores. In both cases, this resulted in a diminished number of neutrophils detected in the lower compartment of the transwell chamber suggesting that neutrophil transmigration through narrow pores was dependent on Myo1f.

Neutrophil interstitial migration was studied in collagen gels which form fibrillary networks and therefore allow to study 3D migration. In general, the ECM consists of collagens, elastin, proteoglycans and noncollagenous glycoproteins forming a heterogeneous network in a tissue-specific manner[229]. The main component of interstitial tissue is type I collagen assembled into mechanically stable fibrils providing physical stability of the connective tissue[227]. *In vivo* interfibrillar spaces in tissues consisting of non-fiber forming molecules like proteoglycans, including the mouse cremaster tissue, have been shown to range from 2 to 30 µm[119,227]. Studies using collagen gels with a collagen concentration of 1.5 mg/mL (low-density) yielding pore cross sections of 10-12 µm^2 and a collagen concentration of 3.0 mg/mL (high-density) with pore cross sections ranging between 2-3 µm^2 demonstrated reduced migration speed in high-density collagen gels indicating that 3D migration depends on substrate porosity[68,119,127]. However, the exact structure of collagen gels is often not known due to various factors being essential for the

collagen architecture like the type of collagen, gelation time, temperature and pH[227,230-232]. In the present study, analysis of 3D migration experiments in collagen gels with different collagen concentrations confirmed that neutrophil migration was dependent on the density of the meshwork of collagen fibers which was in line with findings by Wolf et al[119]. Moreover, Myo1f^{-/-} neutrophils showed significantly decreased migration velocities in high- and low-density collagen gels compared to Myo1f^{+/+} neutrophils indicating that Myo1f was critically involved in neutrophil migration in 3D environments.

6.4 Requirement of Myo1f for the deformation of the nucleus

To identify the underlying mechanism causing defective migration in 3D environments, i.e. transmigration and interstitial migration, the impact of Myo1f on squeezing the neutrophil through narrow spaces was analyzed. For effective cell migration in 3D environments, rapid change of the cell shape as well as deformation of the nucleus are required[119]. A previous study demonstrated that the malleability of the neutrophil nucleus is indispensable during neutrophil migration through narrow pores within confined 3D environments[137].

Analysis of the nuclear morphology in transmigration as well as during migration in 3D collagen gels revealed that the absence of Myo1f almost completely abrogated the deformation of the nucleus suggesting that Myo1f was indispensable for neutrophil migration through narrow pores by regulating the deformation of the nucleus (compare Figure 27-31).

The mechanical linkage between the actin filaments and the nuclear membrane enables the dynamic interaction between the actin cytoskeleton and the nucleus and is required for cell locomotion and nucleus deformation during migration in 3D environments[120,121,125,126,233]. To study the putative role of Myo1f in the interaction between the actin cytoskeleton and the nucleus, an HL-60 cell line stably expressing an EGFP-Myo1f fusion protein was used allowing the identification of the interplay between Actin, Myo1f and the nucleus in these cells. HL-60 cells are human promyelocytic leukemia cells which proliferate independent of growth-factors and can be differentiated towards neutrophil-like cells by applying 1.3 % DMSO for 6 days[234-236]. DMSO differentiation results in the upregulation of various surface markers including different chemoattractant receptors for fMLP or LTB$_4$ as well as typical neutrophil surface markers like LFA-1, Mac-1 and L-selectin[237,238]. In addition, previous studies comparing dHL-60 cells with primary human neutrophils demonstrated high similarities between those two cell types[235,239-241].

Therefore, the HL-60 cell line is a suitable model to study neutrophil chemotaxis and motility *in vitro*.

Using this cell model as well as primary human neutrophils, three phases neutrophils undergo during migration through restrictive pores were defined in line with a recent study by Barzilai and co-workers[124] (Figure 29). The initiation phase was characterized by the formation of a small nuclear lobe inserting into the narrow pore to start migration. The deformation phase was defined by the elongation of the nucleus to squeeze the whole cell body through the constriction and the remodeling phase by refolding the nucleus into a spherical multi-lobular shape.

During the initiation and elongation phase, accumulated Myo1f was found at the rear and the front of the nucleus, suggesting that Myo1f functions in pushing and/or pulling of the nucleus through the permissive site. This was in line with previous studies demonstrating Myosin II being involved in pushing and pulling of the nucleus to squeeze the cell through constriction sites[124,242,243]. At the same time Actin was found to form a ring-like structure around the deformed nucleus during the first two phases of 3D migration. Studies using fibroblasts reported that the deformation of the nucleus is regulated by a dome-like actin cap located above and around the nucleus which is composed of thick, dynamic actomyosin filaments linked to the nucleus[244,245]. The physical nucleus-cytoskeleton interaction is required for the active deformation of the nucleus during migration in 3D environments by transmitting force from the cytoskeleton to the nucleus[128,245-247]. The observed actin ring during initiation and deformation phase suggested an existence of an actin filament structure involved in controlling the deformation of the nucleus in neutrophil-like HL-60 cells.

Importantly, the colocalization of Myo1f and Actin were found at the rear and the front of the nucleus as well as at the constriction, pointing towards a putative importance of Myo1f in the dynamic regulation of the nucleus morphology during migration through narrow pores. These findings were further supported by studying the nuclear morphology during migration in 3D collagen gels in the absence of Myo1f. Analysis of the nuclear shape change revealed that in contrast to Myo1f^{+/+} neutrophils, Myo1f^{-/-} neutrophils almost completely failed to exhibit rapid nucleus deformation resulting in compromised 3D migration through physical barriers in the meshwork of collagen fibers.

In addition to the low expression of LaminA/C in the nuclear envelope of neutrophils[136], studies using dHL-60 cells and primary human neutrophils demonstrated that several LINC complex proteins, including SUN1 and Nesprin 1/2 are profoundly downregulated in neutrophil nuclei[132,137,138]. These specific features lead to a flexible nuclear envelope structure resulting in a

highly malleable cell. Although neutrophils are easily deformable, the nucleus-cytoskeleton connection is essential for 3D migration by transmitting force from the cytoskeleton to the inside of the nucleus[247]. Thus, one can speculate that Myo1f has a similar function as the LINC complexes and links the cytoskeleton to the nuclear envelope via its TH1 domain to provide a high malleability of the nucleus[127]. However, further experiments are required to unravel the exact mechanism by which Myo1f exerts its function in regard to coupling the cytoskeleton to the nuclear membrane.
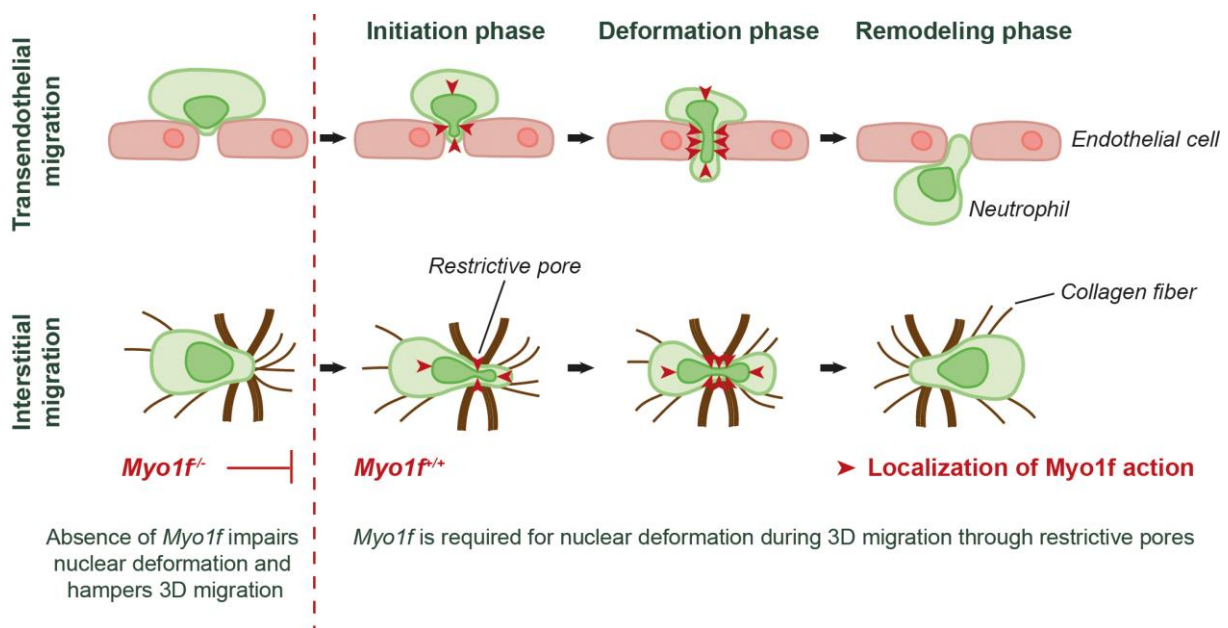
Figure 32. The fundamental role of Myo1f during TEM and interstitial migration. Neutrophils undergo three phases while they squeeze their nucleus through restrictive barriers including the initiation, the deformation and the remodeling phase during migration within 3D environments (transendothelial migration and interstitial migration). Myo1f was found to act at the rear and the front of the nucleus as well as at the constriction sites (red arrow heads) bringing the nucleus in shape for successful migration within 3D environments. Myo1f was critically involved in regulating the dynamic deformation of the nucleus during neutrophil migration through narrow pores. In the genetic absence of Myo1f, neutrophils fail to migrate through narrow pores as they are not able to deform their nuclei (modified from Salvermoser et al., 2018[127]).

In summary, the presented experimental data demonstrate that Myo1f plays a fundamental role in neutrophil extravasation to sites of inflammation. However, neutrophil rolling, induction of adhesion, spreading and polarization as well as migration in 2D environments are not altered in the genetic absence of Myo1f. Interestingly, studying neutrophil migration in 3D environments, i.e. transmigration and migration in 3D collagen networks, which relies on the

dynamic deformation of the nucleus to pass restrictive sites, indicates the specific importance of Myo1f for 3D migration of neutrophils. Thus, Myo1f is identified as a novel indispensable molecular player in the process of nuclear deformation during neutrophil trafficking in innate immunity (Figure 32).

7. REFERENCES

1. Kim SV, Mehal WZ, Dong X, et al. Modulation of cell adhesion and motility in the immune system by Myo1f. *Science.* 2006;314(5796):136-139.

2. Mestas J, Hughes CC. Of mice and not men: differences between mouse and human immunology. *J Immunol.* 2004;172(5):2731-2738.

3. Pillay J, den Braber I, Vrisekoop N, et al. In vivo labeling with 2H2O reveals a human neutrophil lifespan of 5.4 days. *Blood.* 2010;116(4):625-627.

4. Friedewald JJ, Rabb H. Inflammatory cells in ischemic acute renal failure. *Kidney Int.* 2004;66(2):486-491.

5. Kolaczkowska E, Kubes P. Neutrophil recruitment and function in health and inflammation. *Nat Rev Immunol.* 2013;13(3):159-175.

6. Brinkmann V, Reichard U, Goosmann C, et al. Neutrophil extracellular traps kill bacteria. *Science.* 2004;303(5663):1532-1535.

7. Belaaouaj A, McCarthy R, Baumann M, et al. Mice lacking neutrophil elastase reveal impaired host defense against gram negative bacterial sepsis. *Nat Med.* 1998;4(5):615-618.

8. van Wetering S, Tjabringa GS, Hiemstra PS. Interactions between neutrophil-derived antimicrobial peptides and airway epithelial cells. *J Leukoc Biol.* 2005;77(4):444-450.

9. Rada BK, Geiszt M, Kaldi K, Timar C, Ligeti E. Dual role of phagocytic NADPH oxidase in bacterial killing. *Blood.* 2004;104(9):2947-2953.

10. Borregaard N. Neutrophils, from marrow to microbes. *Immunity.* 2010;33(5):657-670.

11. Risau W. Mechanisms of angiogenesis. *Nature.* 1997;386(6626):671-674.

12. Theilgaard-Monch K, Knudsen S, Follin P, Borregaard N. The transcriptional activation program of human neutrophils in skin lesions supports their important role in wound healing. *J Immunol.* 2004;172(12):7684-7693.

13. Kamenyeva O, Boularan C, Kabat J, et al. Neutrophil recruitment to lymph nodes limits local humoral response to Staphylococcus aureus. *PLoS Pathog.* 2015;11(4):e1004827.

14. Ley K, Laudanna C, Cybulsky MI, Nourshargh S. Getting to the site of inflammation: the leukocyte adhesion cascade updated. *Nat Rev Immunol.* 2007;7(9):678-689.

15. Nourshargh S, Alon R. Leukocyte migration into inflamed tissues. *Immunity.* 2014;41(5):694-707.

16. Voisin MB, Nourshargh S. Neutrophil transmigration: emergence of an adhesive cascade within venular walls. *J Innate Immun.* 2013;5(4):336-347.

17. Yago T, Leppanen A, Qiu H, et al. Distinct molecular and cellular contributions to stabilizing selectin-mediated rolling under flow. *J Cell Biol.* 2002;158(4):787-799.

18. Mocsai A, Walzog B, Lowell CA. Intracellular signaling during neutrophil recruitment. *Cardiovasc Res.* 2015.

19. Weber M, Hauschild R, Schwarz J, et al. Interstitial dendritic cell guidance by haptotactic chemokine gradients. *Science.* 2013;339(6117):328-332.

20. Segal AW, Dorling J, Coade S. Kinetics of fusion of the cytoplasmic granules with phagocytic vacuoles in human polymorphonuclear leukocytes. Biochemical and morphological studies. *J Cell Biol.* 1980;85(1):42-59.

21. Segal AW, Geisow M, Garcia R, Harper A, Miller R. The respiratory burst of phagocytic cells is associated with a rise in vacuolar pH. *Nature.* 1981;290(5805):406-409.

22. Kruger P, Saffarzadeh M, Weber AN, et al. Neutrophils: Between host defence, immune modulation, and tissue injury. *PLoS Pathog.* 2015;11(3):e1004651.

23. Schymeinsky J, Sperandio M, Walzog B. The mammalian actin-binding protein 1 (mAbp1): a novel molecular player in leukocyte biology. *Trends Cell Biol.* 2011;21(4):247-255.

24. Shi Y, Evans JE, Rock KL. Molecular identification of a danger signal that alerts the immune system to dying cells. *Nature.* 2003;425(6957):516-521.

25. Nauseef WM, Borregaard N. Neutrophils at work. *Nat Immunol.* 2014;15(7):602-611.

26. Bevilacqua MP, Pober JS, Wheeler ME, Cotran RS, Gimbrone MA, Jr. Interleukin 1 acts on cultured human vascular endothelium to increase the adhesion of polymorphonuclear leukocytes, monocytes, and related leukocyte cell lines. *J Clin Invest.* 1985;76(5):2003-2011.

27. Gamble JR, Harlan JM, Klebanoff SJ, Vadas MA. Stimulation of the adherence of neutrophils to umbilical vein endothelium by human recombinant tumor necrosis factor. *Proc Natl Acad Sci U S A.* 1985;82(24):8667-8671.

28. McEver RP, Beckstead JH, Moore KL, Marshall-Carlson L, Bainton DF. GMP-140, a platelet alpha-granule membrane protein, is also synthesized by vascular endothelial cells and is localized in Weibel-Palade bodies. *J Clin Invest.* 1989;84(1):92-99.

29. McEver RP. Selectins: initiators of leucocyte adhesion and signalling at the vascular wall. *Cardiovasc Res.* 2015;107(3):331-339.

30. Moore KL, Stults NL, Diaz S, et al. Identification of a specific glycoprotein ligand for P-selectin (CD62) on myeloid cells. *J Cell Biol.* 1992;118(2):445-456.

31. Xia L, Sperandio M, Yago T, et al. P-selectin glycoprotein ligand-1-deficient mice have impaired leukocyte tethering to E-selectin under flow. *J Clin Invest.* 2002;109(7):939-950.

32. Ley K. The role of selectins in inflammation and disease. *Trends Mol Med.* 2003;9(6):263-268.

33. Arbones ML, Ord DC, Ley K, et al. Lymphocyte homing and leukocyte rolling and migration are impaired in L-selectin-deficient mice. *Immunity.* 1994;1(4):247-260.

34. Eriksson EE, Xie X, Werr J, Thoren P, Lindbom L. Importance of primary capture and L-selectin-dependent secondary capture in leukocyte accumulation in inflammation and atherosclerosis in vivo. *J Exp Med.* 2001;194(2):205-218.

35. Marshall BT, Long M, Piper JW, Yago T, McEver RP, Zhu C. Direct observation of catch bonds involving cell-adhesion molecules. *Nature.* 2003;423(6936):190-193.

36. Ramachandran V, Williams M, Yago T, Schmidtke DW, McEver RP. Dynamic alterations of membrane tethers stabilize leukocyte rolling on P-selectin. *Proc Natl Acad Sci U S A.* 2004;101(37):13519-13524.

37. Marki A, Gutierrez E, Mikulski Z, Groisman A, Ley K. Microfluidics-based side view flow chamber reveals tether-to-sling transition in rolling neutrophils. *Sci Rep.* 2016;6:28870.

38. Evans R, Patzak I, Svensson L, et al. Integrins in immunity. *J Cell Sci.* 2009;122(Pt 2):215-225.

39. Luo BH, Carman CV, Springer TA. Structural basis of integrin regulation and signaling. *Annu Rev Immunol.* 2007;25:619-647.

40. Fan Z, McArdle S, Marki A, et al. Neutrophil recruitment limited by high-affinity bent beta2 integrin binding ligand in cis. *Nat Commun.* 2016;7:12658.

41. Lefort CT, Rossaint J, Moser M, et al. Distinct roles for talin-1 and kindlin-3 in LFA-1 extension and affinity regulation. *Blood.* 2012;119(18):4275-4282.

42. Kuwano Y, Spelten O, Zhang H, Ley K, Zarbock A. Rolling on E- or P-selectin induces the extended but not high-affinity conformation of LFA-1 in neutrophils. *Blood.* 2010;116(4):617-624.

43. Li YF, Tang RH, Puan KJ, Law SK, Tan SM. The cytosolic protein talin induces an intermediate affinity integrin alphaLbeta2. *J Biol Chem.* 2007;282(33):24310-24319.

44. Lefort CT, Ley K. Neutrophil arrest by LFA-1 activation. *Front Immunol.* 2012;3:157.

45. Moser M, Bauer M, Schmid S, et al. Kindlin-3 is required for beta2 integrin-mediated leukocyte adhesion to endothelial cells. *Nat Med.* 2009;15(3):300-305.

46. Schymeinsky J, Gerstl R, Mannigel I, et al. A fundamental role of mAbp1 in neutrophils: impact on beta(2) integrin-mediated phagocytosis and adhesion in vivo. *Blood.* 2009;114(19):4209-4220.

47. Jakob SM, Pick R, Brechtefeld D, et al. Hematopoietic progenitor kinase 1 (HPK1) is required for LFA-1-mediated neutrophil recruitment during the acute inflammatory response. *Blood.* 2013;121(20):4184-4194.

48. Phillipson M, Heit B, Colarusso P, Liu L, Ballantyne CM, Kubes P. Intraluminal crawling of neutrophils to emigration sites: a molecularly distinct process from adhesion in the recruitment cascade. *J Exp Med.* 2006;203(12):2569-2575.

49. Sumagin R, Prizant H, Lomakina E, Waugh RE, Sarelius IH. LFA-1 and Mac-1 define characteristically different intralumenal crawling and emigration patterns for monocytes and neutrophils in situ. *J Immunol.* 2010;185(11):7057-7066.

50. Hallmann R, Zhang X, Di Russo J, et al. The regulation of immune cell trafficking by the extracellular matrix. *Curr Opin Cell Biol.* 2015;36:54-61.

51. Sorokin L. The impact of the extracellular matrix on inflammation. *Nat Rev Immunol.* 2010;10(10):712-723.

52. Bader BL, Smyth N, Nedbal S, et al. Compound genetic ablation of nidogen 1 and 2 causes basement membrane defects and perinatal lethality in mice. *Mol Cell Biol.* 2005;25(15):6846-6856.

53. Frieser M, Nockel H, Pausch F, et al. Cloning of the mouse laminin alpha 4 cDNA. Expression in a subset of endothelium. *Eur J Biochem.* 1997;246(3):727-735.

54. Kenne E, Soehnlein O, Genove G, Rotzius P, Eriksson EE, Lindbom L. Immune cell recruitment to inflammatory loci is impaired in mice deficient in basement membrane protein laminin alpha4. *J Leukoc Biol.* 2010;88(3):523-528.

55. Wu C, Ivars F, Anderson P, et al. Endothelial basement membrane laminin alpha5 selectively inhibits T lymphocyte extravasation into the brain. *Nat Med.* 2009;15(5):519-527.

56. Armulik A, Abramsson A, Betsholtz C. Endothelial/pericyte interactions. *Circ Res.* 2005;97(6):512-523.

57. Andreeva ER, Pugach IM, Gordon D, Orekhov AN. Continuous subendothelial network formed by pericyte-like cells in human vascular bed. *Tissue Cell.* 1998;30(1):127-135.

58. Nourshargh S, Hordijk PL, Sixt M. Breaching multiple barriers: leukocyte motility through venular walls and the interstitium. *Nat Rev Mol Cell Biol.* 2010;11(5):366-378.

59. van Buul JD, Allingham MJ, Samson T, et al. RhoG regulates endothelial apical cup assembly downstream from ICAM1 engagement and is involved in leukocyte trans-endothelial migration. *J Cell Biol.* 2007;178(7):1279-1293.

60. Barreiro O, Yanez-Mo M, Serrador JM, et al. Dynamic interaction of VCAM-1 and ICAM-1 with moesin and ezrin in a novel endothelial docking structure for adherent leukocytes. *J Cell Biol.* 2002;157(7):1233-1245.

61. Carman CV, Springer TA. A transmigratory cup in leukocyte diapedesis both through individual vascular endothelial cells and between them. *J Cell Biol.* 2004;167(2):377-388.

62. Wang S, Voisin MB, Larbi KY, et al. Venular basement membranes contain specific matrix protein low expression regions that act as exit points for emigrating neutrophils. *J Exp Med.* 2006;203(6):1519-1532.

63. Voisin MB, Probstl D, Nourshargh S. Venular basement membranes ubiquitously express matrix protein low-expression regions: characterization in multiple tissues and remodeling during inflammation. *Am J Pathol.* 2010;176(1):482-495.

64. Hyun YM, Sumagin R, Sarangi PP, et al. Uropod elongation is a common final step in leukocyte extravasation through inflamed vessels. *J Exp Med.* 2012;209(7):1349-1362.

65. Dangerfield JP, Wang S, Nourshargh S. Blockade of alpha6 integrin inhibits IL-1beta- but not TNF-alpha-induced neutrophil transmigration in vivo. *J Leukoc Biol.* 2005;77(2):159-165.

66. Proebstl D, Voisin MB, Woodfin A, et al. Pericytes support neutrophil subendothelial cell crawling and breaching of venular walls in vivo. *J Exp Med.* 2012;209(6):1219-1234.

67. De Bruyn PP. The amoeboid movement of the mammalian leukocyte in tissue culture. *Anat Rec.* 1946;95:177-191.

68. Lammermann T, Bader BL, Monkley SJ, et al. Rapid leukocyte migration by integrin-independent flowing and squeezing. *Nature.* 2008;453(7191):51-55.

69. Lammermann T, Germain RN. The multiple faces of leukocyte interstitial migration. *Semin Immunopathol.* 2014;36(2):227-251.

70. Anderson DC, Schmalsteig FC, Finegold MJ, et al. The severe and moderate phenotypes of heritable Mac-1, LFA-1 deficiency: their quantitative definition and relation to leukocyte dysfunction and clinical features. *J Infect Dis.* 1985;152(4):668-689.

71.   Bowen TJ, Ochs HD, Altman LC, et al. Severe recurrent bacterial infections associated with defective adherence and chemotaxis in two patients with neutrophils deficient in a cell-associated glycoprotein. *J Pediatr.* 1982;101(6):932-940.

72.   Phillips ML, Schwartz BR, Etzioni A, et al. Neutrophil adhesion in leukocyte adhesion deficiency syndrome type 2. *J Clin Invest.* 1995;96(6):2898-2906.

73.   Luhn K, Wild MK, Eckhardt M, Gerardy-Schahn R, Vestweber D. The gene defective in leukocyte adhesion deficiency II encodes a putative GDP-fucose transporter. *Nat Genet.* 2001;28(1):69-72.

74.   Svensson L, Howarth K, McDowall A, et al. Leukocyte adhesion deficiency-III is caused by mutations in KINDLIN3 affecting integrin activation. *Nat Med.* 2009;15(3):306-312.

75.   Pai SY, Kim C, Williams DA. Rac GTPases in human diseases. *Dis Markers.* 2010;29(3-4):177-187.

76.   Williams DA, Tao W, Yang F, et al. Dominant negative mutation of the hematopoietic-specific Rho GTPase, Rac2, is associated with a human phagocyte immunodeficiency. *Blood.* 2000;96(5):1646-1654.

77.   Ambruso DR, Knall C, Abell AN, et al. Human neutrophil immunodeficiency syndrome is associated with an inhibitory Rac2 mutation. *Proc Natl Acad Sci U S A.* 2000;97(9):4654-4659.

78.   Roberts AW, Kim C, Zhen L, et al. Deficiency of the hematopoietic cell-specific Rho family GTPase Rac2 is characterized by abnormalities in neutrophil function and host defense. *Immunity.* 1999;10(2):183-196.

79.   Mantovani A, Cassatella MA, Costantini C, Jaillon S. Neutrophils in the activation and regulation of innate and adaptive immunity. *Nat Rev Immunol.* 2011;11(8):519-531.

80.   Luster AD, Alon R, von Andrian UH. Immune cell migration in inflammation: present and future therapeutic targets. *Nat Immunol.* 2005;6(12):1182-1190.

81.   Friedl P, Brocker EB. The biology of cell locomotion within three-dimensional extracellular matrix. *Cell Mol Life Sci.* 2000;57(1):41-64.

82.   Tamariz E, Grinnell F. Modulation of fibroblast morphology and adhesion during collagen matrix remodeling. *Mol Biol Cell.* 2002;13(11):3915-3929.

83.   Rhee S, Grinnell F. Fibroblast mechanics in 3D collagen matrices. *Adv Drug Deliv Rev.* 2007;59(13):1299-1305.

84.   Friedl P, Wolf K. Proteolytic and non-proteolytic migration of tumour cells and leucocytes. *Biochem Soc Symp.* 2003(70):277-285.

85.   Friedl P, Wolf K. Proteolytic interstitial cell migration: a five-step process. *Cancer Metastasis Rev.* 2009;28(1-2):129-135.

86.   Wolf K, Muller R, Borgmann S, Brocker EB, Friedl P. Amoeboid shape change and contact guidance: T-lymphocyte crawling through fibrillar collagen is independent of matrix remodeling by MMPs and other proteases. *Blood.* 2003;102(9):3262-3269.

87.   Friedl P, Borgmann S, Brocker EB. Amoeboid leukocyte crawling through extracellular matrix: lessons from the Dictyostelium paradigm of cell movement. *J Leukoc Biol.* 2001;70(4):491-509.

88.   Bokoch GM, Gilman AG. Inhibition of receptor-mediated release of arachidonic acid by pertussis toxin. *Cell.* 1984;39(2 Pt 1):301-308.

89.   Lad PM, Olson CV, Smiley PA. Association of the N-formyl-Met-Leu-Phe receptor in human neutrophils with a GTP-binding protein sensitive to pertussis toxin. *Proc Natl Acad Sci U S A.* 1985;82(3):869-873.

90.   Pestonjamasp KN, Forster C, Sun C, et al. Rac1 links leading edge and uropod events through Rho and myosin activation during chemotaxis. *Blood.* 2006;108(8):2814-2820.

91.   Xu J, Wang F, Van Keymeulen A, et al. Divergent signals and cytoskeletal assemblies regulate self-organizing polarity in neutrophils. *Cell.* 2003;114(2):201-214.

92.   Li Z, Dong X, Wang Z, et al. Regulation of PTEN by Rho small GTPases. *Nat Cell Biol.* 2005;7(4):399-404.

93.   Malawista SE, de Boisfleury Chevance A. Random locomotion and chemotaxis of human blood polymorphonuclear leukocytes (PMN) in the presence of EDTA: PMN in close quarters require

neither leukocyte integrins nor external divalent cations. *Proc Natl Acad Sci U S A.* 1997;94(21):11577-11582.

94. Smith A, Bracke M, Leitinger B, Porter JC, Hogg N. LFA-1-induced T cell migration on ICAM-1 involves regulation of MLCK-mediated attachment and ROCK-dependent detachment. *J Cell Sci.* 2003;116(Pt 15):3123-3133.

95. Niggli V. Rho-kinase in human neutrophils: a role in signalling for myosin light chain phosphorylation and cell migration. *FEBS Lett.* 1999;445(1):69-72.

96. Lammermann T, Sixt M. Mechanical modes of 'amoeboid' cell migration. *Curr Opin Cell Biol.* 2009;21(5):636-644.

97. Friedl P, Weigelin B. Interstitial leukocyte migration and immune function. *Nat Immunol.* 2008;9(9):960-969.

98. Renkawitz J, Schumann K, Weber M, et al. Adaptive force transmission in amoeboid cell migration. *Nat Cell Biol.* 2009;11(12):1438-1443.

99. Begandt D, Thome S, Sperandio M, Walzog B. How neutrophils resist shear stress at blood vessel walls: molecular mechanisms, subcellular structures, and cell-cell interactions. *J Leukoc Biol.* 2017.

100. Phillipson M, Heit B, Parsons SA, et al. Vav1 is essential for mechanotactic crawling and migration of neutrophils out of the inflamed microvasculature. *J Immunol.* 2009;182(11):6870-6878.

101. Hepper I, Schymeinsky J, Weckbach LT, et al. The mammalian actin-binding protein 1 is critical for spreading and intraluminal crawling of neutrophils under flow conditions. *J Immunol.* 2012;188(9):4590-4601.

102. Fine N, Dimitriou ID, Rullo J, et al. GEF-H1 is necessary for neutrophil shear stress-induced migration during inflammation. *J Cell Biol.* 2016;215(1):107-119.

103. Krendel M, Zenke FT, Bokoch GM. Nucleotide exchange factor GEF-H1 mediates cross-talk between microtubules and the actin cytoskeleton. *Nat Cell Biol.* 2002;4(4):294-301.

104. Jacobelli J, Bennett FC, Pandurangi P, Tooley AJ, Krummel MF. Myosin-IIA and ICAM-1 regulate the interchange between two distinct modes of T cell migration. *J Immunol.* 2009;182(4):2041-2050.

105. Malawista SE, de Boisfleury Chevance A, Boxer LA. Random locomotion and chemotaxis of human blood polymorphonuclear leukocytes from a patient with leukocyte adhesion deficiency-1: normal displacement in close quarters via chimneying. *Cell Motil Cytoskeleton.* 2000;46(3):183-189.

106. Lammermann T, Afonso PV, Angermann BR, et al. Neutrophil swarms require LTB4 and integrins at sites of cell death in vivo. *Nature.* 2013;498(7454):371-375.

107. Woolf E, Grigorova I, Sagiv A, et al. Lymph node chemokines promote sustained T lymphocyte motility without triggering stable integrin adhesiveness in the absence of shear forces. *Nat Immunol.* 2007;8(10):1076-1085.

108. Renkawitz J, Sixt M. Mechanisms of force generation and force transmission during interstitial leukocyte migration. *EMBO Rep.* 2010;11(10):744-750.

109. Kienle K, Lammermann T. Neutrophil swarming: an essential process of the neutrophil tissue response. *Immunol Rev.* 2016;273(1):76-93.

110. Lammermann T. In the eye of the neutrophil swarm-navigation signals that bring neutrophils together in inflamed and infected tissues. *J Leukoc Biol.* 2016;100(1):55-63.

111. de Oliveira S, Rosowski EE, Huttenlocher A. Neutrophil migration in infection and wound repair: going forward in reverse. *Nat Rev Immunol.* 2016;16(6):378-391.

112. Soehnlein O, Lindbom L. Phagocyte partnership during the onset and resolution of inflammation. *Nat Rev Immunol.* 2010;10(6):427-439.

113. Buckley CD, Gilroy DW, Serhan CN, Stockinger B, Tak PP. The resolution of inflammation. *Nat Rev Immunol.* 2013;13(1):59-66.

114. Mathias JR, Perrin BJ, Liu TX, Kanki J, Look AT, Huttenlocher A. Resolution of inflammation by retrograde chemotaxis of neutrophils in transgenic zebrafish. *J Leukoc Biol.* 2006;80(6):1281-1288.

115. Yoo SK, Huttenlocher A. Spatiotemporal photolabeling of neutrophil trafficking during inflammation in live zebrafish. *J Leukoc Biol.* 2011;89(5):661-667.

116. Tauzin S, Starnes TW, Becker FB, Lam PY, Huttenlocher A. Redox and Src family kinase signaling control leukocyte wound attraction and neutrophil reverse migration. *J Cell Biol.* 2014;207(5):589-598.

117. Woodfin A, Voisin MB, Beyrau M, et al. The junctional adhesion molecule JAM-C regulates polarized transendothelial migration of neutrophils in vivo. *Nat Immunol.* 2011;12(8):761-769.

118. Hamza B, Wong E, Patel S, Cho H, Martel J, Irimia D. Retrotaxis of human neutrophils during mechanical confinement inside microfluidic channels. *Integr Biol (Camb).* 2014;6(2):175-183.

119. Wolf K, Te Lindert M, Krause M, et al. Physical limits of cell migration: control by ECM space and nuclear deformation and tuning by proteolysis and traction force. *J Cell Biol.* 2013;201(7):1069-1084.

120. Friedl P. Prespecification and plasticity: shifting mechanisms of cell migration. *Curr Opin Cell Biol.* 2004;16(1):14-23.

121. Friedl P, Wolf K, Lammerding J. Nuclear mechanics during cell migration. *Curr Opin Cell Biol.* 2011;23(1):55-64.

122. Wolf K, Wu YI, Liu Y, et al. Multi-step pericellular proteolysis controls the transition from individual to collective cancer cell invasion. *Nat Cell Biol.* 2007;9(8):893-904.

123. Lammerding J, Fong LG, Ji JY, et al. Lamins A and C but not lamin B1 regulate nuclear mechanics. *J Biol Chem.* 2006;281(35):25768-25780.

124. Barzilai S, Yadav SK, Morrell S, et al. Leukocytes Breach Endothelial Barriers by Insertion of Nuclear Lobes and Disassembly of Endothelial Actin Filaments. *Cell Rep.* 2017;18(3):685-699.

125. Maniotis AJ, Chen CS, Ingber DE. Demonstration of mechanical connections between integrins, cytoskeletal filaments, and nucleoplasm that stabilize nuclear structure. *Proc Natl Acad Sci U S A.* 1997;94(3):849-854.

126. Dahl KN, Ribeiro AJ, Lammerding J. Nuclear shape, mechanics, and mechanotransduction. *Circ Res.* 2008;102(11):1307-1318.

127. Salvermoser M, Pick R, Weckbach LT, et al. Myosin 1f is specifically required for neutrophil migration in 3D environments during acute inflammation. *Blood.* 2018;131(17):1887-1898.

128. Crisp M, Liu Q, Roux K, et al. Coupling of the nucleus and cytoplasm: role of the LINC complex. *J Cell Biol.* 2006;172(1):41-53.

129. Haque F, Lloyd DJ, Smallwood DT, et al. SUN1 interacts with nuclear lamin A and cytoplasmic nesprins to provide a physical connection between the nuclear lamina and the cytoskeleton. *Mol Cell Biol.* 2006;26(10):3738-3751.

130. Schirmer EC, Florens L, Guan T, Yates JR, 3rd, Gerace L. Nuclear membrane proteins with potential disease links found by subtractive proteomics. *Science.* 2003;301(5638):1380-1382.

131. Hoffmann K, Sperling K, Olins AL, Olins DE. The granulocyte nucleus and lamin B receptor: avoiding the ovoid. *Chromosoma.* 2007;116(3):227-235.

132. Olins AL, Zwerger M, Herrmann H, et al. The human granulocyte nucleus: Unusual nuclear envelope and heterochromatin composition. *Eur J Cell Biol.* 2008;87(5):279-290.

133. Campbell MS, Lovell MA, Gorbsky GJ. Stability of nuclear segments in human neutrophils and evidence against a role for microfilaments or microtubules in their genesis during differentiation of HL60 myelocytes. *J Leukoc Biol.* 1995;58(6):659-666.

134. Aquiles Sanchez J, Karni RJ, Wangh LJ. Fluorescent in situ hybridization (FISH) analysis of the relationship between chromosome location and nuclear morphology in human neutrophils. *Chromosoma.* 1997;106(3):168-177.

135. Biermann H, Pietz B, Dreier R, Schmid KW, Sorg C, Sunderkotter C. Murine leukocytes with ring-shaped nuclei include granulocytes, monocytes, and their precursors. *J Leukoc Biol.* 1999;65(2):217-231.

136.   Shin JW, Spinler KR, Swift J, Chasis JA, Mohandas N, Discher DE. Lamins regulate cell trafficking and lineage maturation of adult human hematopoietic cells. *Proc Natl Acad Sci U S A.* 2013;110(47):18892-18897.

137.   Rowat AC, Jaalouk DE, Zwerger M, et al. Nuclear envelope composition determines the ability of neutrophil-type cells to passage through micron-scale constrictions. *J Biol Chem.* 2013;288(12):8610-8618.

138.   Olins AL, Hoang TV, Zwerger M, et al. The LINC-less granulocyte nucleus. *Eur J Cell Biol.* 2009;88(4):203-214.

139.   Krendel M, Mooseker MS. Myosins: tails (and heads) of functional diversity. *Physiology (Bethesda).* 2005;20:239-251.

140.   Schliwa M, Woehlke G. Molecular motors. *Nature.* 2003;422(6933):759-765.

141.   Bement WM, Mooseker MS. TEDS rule: a molecular rationale for differential regulation of myosins by phosphorylation of the heavy chain head. *Cell Motil Cytoskeleton.* 1995;31(2):87-92.

142.   Foth BJ, Goedecke MC, Soldati D. New insights into myosin evolution and classification. *Proc Natl Acad Sci U S A.* 2006;103(10):3681-3686.

143.   Thompson RF, Langford GM. Myosin superfamily evolutionary history. *Anat Rec.* 2002;268(3):276-289.

144.   De La Cruz EM, Ostap EM. Kinetic and equilibrium analysis of the myosin ATPase. *Methods Enzymol.* 2009;455:157-192.

145.   Schroeder TE. Dynamics of the contractile ring. *Soc Gen Physiol Ser.* 1975;30:305-334.

146.   Maupin P, Phillips CL, Adelstein RS, Pollard TD. Differential localization of myosin-II isozymes in human cultured cells and blood cells. *J Cell Sci.* 1994;107 (Pt 11):3077-3090.

147.   Woolner S, Bement WM. Unconventional myosins acting unconventionally. *Trends Cell Biol.* 2009;19(6):245-252.

148.   McConnell RE, Tyska MJ. Leveraging the membrane - cytoskeleton interface with myosin-1. *Trends Cell Biol.* 2010;20(7):418-426.

149.   Desnos C, Huet S, Darchen F. 'Should I stay or should I go?': myosin V function in organelle trafficking. *Biol Cell.* 2007;99(8):411-423.

150.   Berg JS, Powell BC, Cheney RE. A millennial myosin census. *Mol Biol Cell.* 2001;12(4):780-794.

151.   McIntosh BB, Ostap EM. Myosin-I molecular motors at a glance. *J Cell Sci.* 2016;129(14):2689-2695.

152.   Ruppert C, Kroschewski R, Bahler M. Identification, characterization and cloning of myr 1, a mammalian myosin-I. *J Cell Biol.* 1993;120(6):1393-1403.

153.   Hokanson DE, Ostap EM. Myo1c binds tightly and specifically to phosphatidylinositol 4,5-bisphosphate and inositol 1,4,5-trisphosphate. *Proc Natl Acad Sci U S A.* 2006;103(9):3118-3123.

154.   Adams RJ, Pollard TD. Binding of myosin I to membrane lipids. *Nature.* 1989;340(6234):565-568.

155.   Musacchio A, Noble M, Pauptit R, Wierenga R, Saraste M. Crystal structure of a Src-homology 3 (SH3) domain. *Nature.* 1992;359(6398):851-855.

156.   Kalhammer G, Bahler M. Unconventional myosins. *Essays Biochem.* 2000;35:33-42.

157.   Mermall V, Post PL, Mooseker MS. Unconventional myosins in cell movement, membrane traffic, and signal transduction. *Science.* 1998;279(5350):527-533.

158.   Maravillas-Montero JL, Santos-Argumedo L. The myosin family: unconventional roles of actin-dependent molecular motors in immune cells. *J Leukoc Biol.* 2012;91(1):35-46.

159.   Tyska MJ, Mackey AT, Huang JD, Copeland NG, Jenkins NA, Mooseker MS. Myosin-1a is critical for normal brush border structure and composition. *Mol Biol Cell.* 2005;16(5):2443-2457.

160.   Fath KR, Burgess DR. Golgi-derived vesicles from developing epithelial cells bind actin filaments and possess myosin-I as a cytoplasmically oriented peripheral membrane protein. *J Cell Biol.* 1993;120(1):117-127.

161. Fath KR, Trimbur GM, Burgess DR. Molecular motors are differentially distributed on Golgi membranes from polarized epithelial cells. *J Cell Biol.* 1994;126(3):661-675.

162. Raposo G, Cordonnier MN, Tenza D, et al. Association of myosin I alpha with endosomes and lysosomes in mammalian cells. *Mol Biol Cell.* 1999;10(5):1477-1494.

163. Cordonnier MN, Dauzonne D, Louvard D, Coudrier E. Actin filaments and myosin I alpha cooperate with microtubules for the movement of lysosomes. *Mol Biol Cell.* 2001;12(12):4013-4029.

164. Bose A, Guilherme A, Robida SI, et al. Glucose transporter recycling in response to insulin is facilitated by myosin Myo1c. *Nature.* 2002;420(6917):821-824.

165. Tiwari A, Jung JJ, Inamdar SM, Nihalani D, Choudhury A. The myosin motor Myo1c is required for VEGFR2 delivery to the cell surface and for angiogenic signaling. *Am J Physiol Heart Circ Physiol.* 2013;304(5):H687-696.

166. Huber LA, Fialka I, Paiha K, et al. Both calmodulin and the unconventional myosin Myr4 regulate membrane trafficking along the recycling pathway of MDCK cells. *Traffic.* 2000;1(6):494-503.

167. Gerard A, Patino-Lopez G, Beemiller P, et al. Detection of rare antigen-presenting cells through T cell-intrinsic meandering motility, mediated by Myo1g. *Cell.* 2014;158(3):492-505.

168. Patino-Lopez G, Aravind L, Dong X, Kruhlak MJ, Ostap EM, Shaw S. Myosin 1G is an abundant class I myosin in lymphocytes whose localization at the plasma membrane depends on its ancient divergent pleckstrin homology (PH) domain (Myo1PH). *J Biol Chem.* 2010;285(12):8675-8686.

169. Maravillas-Montero JL, Lopez-Ortega O, Patino-Lopez G, Santos-Argumedo L. Myosin 1g regulates cytoskeleton plasticity, cell migration, exocytosis, and endocytosis in B lymphocytes. *Eur J Immunol.* 2014;44(3):877-886.

170. Dart AE, Tollis S, Bright MD, Frankel G, Endres RG. The motor protein myosin 1G functions in FcgammaR-mediated phagocytosis. *J Cell Sci.* 2012;125(Pt 24):6020-6029.

171. Kim SV, Flavell RA. Myosin I: from yeast to human. *Cell Mol Life Sci.* 2008;65(14):2128-2137.

172. Cheng J, Grassart A, Drubin DG. Myosin 1E coordinates actin assembly and cargo trafficking during clathrin-mediated endocytosis. *Mol Biol Cell.* 2012;23(15):2891-2904.

173. Wenzel J, Ouderkirk JL, Krendel M, Lang R. Class I myosin Myo1e regulates TLR4-triggered macrophage spreading, chemokine release, and antigen presentation via MHC class II. *Eur J Immunol.* 2015;45(1):225-237.

174. Falk DL, Wessels D, Jenkins L, et al. Shared, unique and redundant functions of three members of the class I myosins (MyoA, MyoB and MyoF) in motility and chemotaxis in Dictyostelium. *J Cell Sci.* 2003;116(Pt 19):3985-3999.

175. Wessels D, Murray J, Jung G, Hammer JA, 3rd, Soll DR. Myosin IB null mutants of Dictyostelium exhibit abnormalities in motility. *Cell Motil Cytoskeleton.* 1991;20(4):301-315.

176. Titus MA, Wessels D, Spudich JA, Soll D. The unconventional myosin encoded by the myoA gene plays a role in Dictyostelium motility. *Mol Biol Cell.* 1993;4(2):233-246.

177. Srinivasan S, Wang F, Glavas S, et al. Rac and Cdc42 play distinct roles in regulating PI(3,4,5)P3 and polarity during neutrophil chemotaxis. *J Cell Biol.* 2003;160(3):375-385.

178. Schymeinsky J, Then C, Walzog B. The non-receptor tyrosine kinase Syk regulates lamellipodium formation and site-directed migration of human leukocytes. *J Cell Physiol.* 2005;204(2):614-622.

179. Yan SR, Huang M, Berton G. Signaling by adhesion in human neutrophils: activation of the p72syk tyrosine kinase and formation of protein complexes containing p72syk and Src family kinases in neutrophils spreading over fibrinogen. *J Immunol.* 1997;158(4):1902-1910.

180. Laemmli UK. Cleavage of structural proteins during the assembly of the head of bacteriophage T4. *Nature.* 1970;227(5259):680-685.

181. Schymeinsky J, Sindrilaru A, Frommhold D, et al. The Vav binding site of the non-receptor tyrosine kinase Syk at Tyr 348 is critical for beta2 integrin (CD11/CD18)-mediated neutrophil migration. *Blood.* 2006;108(12):3919-3927.

182. Willeke T, Behrens S, Scharffetter-Kochanek K, Gaehtgens P, Walzog B. Beta2 integrin (CD11/CD18)-mediated signaling involves tyrosine phosphorylation of c-Cbl in human neutrophils. *J Leukoc Biol.* 2000;68(2):284-292.

183. Frommhold D, Mannigel I, Schymeinsky J, et al. Spleen tyrosine kinase Syk is critical for sustained leukocyte adhesion during inflammation in vivo. *BMC Immunol.* 2007;8:31.

184. Zigmond SH. Ability of polymorphonuclear leukocytes to orient in gradients of chemotactic factors. *J Cell Biol.* 1977;75(2 Pt 1):606-616.

185. Pick R, Begandt D, Stocker TJ, et al. Coronin 1A, a novel player in integrin biology, controls neutrophil trafficking in innate immunity. *Blood.* 2017;130(7):847-858.

186. Sperandio M, Pickard J, Unnikrishnan S, Acton ST, Ley K. Analysis of leukocyte rolling in vivo and in vitro. *Methods Enzymol.* 2006;416:346-371.

187. Ley K, Bullard DC, Arbones ML, et al. Sequential contribution of L- and P-selectin to leukocyte rolling in vivo. *J Exp Med.* 1995;181(2):669-675.

188. Forlow SB, Ley K. Selectin-independent leukocyte rolling and adhesion in mice deficient in E-, P-, and L-selectin and ICAM-1. *Am J Physiol Heart Circ Physiol.* 2001;280(2):H634-641.

189. Grommes J, Alard JE, Drechsler M, et al. Disruption of platelet-derived chemokine heteromers prevents neutrophil extravasation in acute lung injury. *Am J Respir Crit Care Med.* 2012;185(6):628-636.

190. Reutershan J, Basit A, Galkina EV, Ley K. Sequential recruitment of neutrophils into lung and bronchoalveolar lavage fluid in LPS-induced acute lung injury. *Am J Physiol Lung Cell Mol Physiol.* 2005;289(5):L807-815.

191. Ortega-Gomez A, Salvermoser M, Rossaint J, et al. Cathepsin G Controls Arterial But Not Venular Myeloid Cell Recruitment. *Circulation.* 2016;134(16):1176-1188.

192. Jung U, Ley K. Regulation of E-selectin, P-selectin, and intercellular adhesion molecule 1 expression in mouse cremaster muscle vasculature. *Microcirculation.* 1997;4(2):311-319.

193. Smith ML, Olson TS, Ley K. CXCR2- and E-selectin-induced neutrophil arrest during inflammation in vivo. *J Exp Med.* 2004;200(7):935-939.

194. Matute-Bello G, Frevert CW, Martin TR. Animal models of acute lung injury. *Am J Physiol Lung Cell Mol Physiol.* 2008;295(3):L379-399.

195. Pick R, Brechtefeld D, Walzog B. Intraluminal crawling versus interstitial neutrophil migration during inflammation. *Mol Immunol.* 2013;55(1):70-75.

196. Nourshargh S, Marelli-Berg FM. Transmigration through venular walls: a key regulator of leukocyte phenotype and function. *Trends Immunol.* 2005;26(3):157-165.

197. Long DS, Smith ML, Pries AR, Ley K, Damiano ER. Microviscometry reveals reduced blood viscosity and altered shear rate and shear stress profiles in microvessels after hemodilution. *Proc Natl Acad Sci U S A.* 2004;101(27):10060-10065.

198. Frommhold D, Kamphues A, Dannenberg S, et al. RAGE and ICAM-1 differentially control leukocyte recruitment during acute inflammation in a stimulus-dependent manner. *BMC Immunol.* 2011;12:56.

199. Kunkel EJ, Jung U, Bullard DC, et al. Absence of trauma-induced leukocyte rolling in mice deficient in both P-selectin and intercellular adhesion molecule 1. *J Exp Med.* 1996;183(1):57-65.

200. Zarbock A, Ley K. Neutrophil adhesion and activation under flow. *Microcirculation.* 2009;16(1):31-42.

201. Green CE, Schaff UY, Sarantos MR, Lum AF, Staunton DE, Simon SI. Dynamic shifts in LFA-1 affinity regulate neutrophil rolling, arrest, and transmigration on inflamed endothelium. *Blood.* 2006;107(5):2101-2111.

202. Zhou X, Gao XP, Fan J, et al. LPS activation of Toll-like receptor 4 signals CD11b/CD18 expression in neutrophils. *Am J Physiol Lung Cell Mol Physiol.* 2005;288(4):L655-662.

203. Thompson RD, Noble KE, Larbi KY, et al. Platelet-endothelial cell adhesion molecule-1 (PECAM-1)-deficient mice demonstrate a transient and cytokine-specific role for PECAM-1 in leukocyte migration through the perivascular basement membrane. *Blood.* 2001;97(6):1854-1860.

204.   Craciun FL, Schuller ER, Remick DG. Early enhanced local neutrophil recruitment in peritonitis-induced sepsis improves bacterial clearance and survival. *J Immunol.* 2010;185(11):6930-6938.

205.   Cash JL, White GE, Greaves DR. Chapter 17. Zymosan-induced peritonitis as a simple experimental system for the study of inflammation. *Methods Enzymol.* 2009;461:379-396.

206.   Walzog B, Scharffetter-Kochanek K, Gaehtgens P. Impairment of neutrophil emigration in CD18-null mice. *Am J Physiol.* 1999;276(5 Pt 1):G1125-1130.

207.   Schmits R, Kundig TM, Baker DM, et al. LFA-1-deficient mice show normal CTL responses to virus but fail to reject immunogenic tumor. *J Exp Med.* 1996;183(4):1415-1426.

208.   Lu H, Smith CW, Perrard J, et al. LFA-1 is sufficient in mediating neutrophil emigration in Mac-1-deficient mice. *J Clin Invest.* 1997;99(6):1340-1350.

209.   Doerschuk CM, Mizgerd JP, Kubo H, Qin L, Kumasaka T. Adhesion molecules and cellular biomechanical changes in acute lung injury: Giles F. Filley Lecture. *Chest.* 1999;116(1 Suppl):37S-43S.

210.   Reutershan J, Ley K. Bench-to-bedside review: acute respiratory distress syndrome - how neutrophils migrate into the lung. *Crit Care.* 2004;8(6):453-461.

211.   Johnson ER, Matthay MA. Acute lung injury: epidemiology, pathogenesis, and treatment. *J Aerosol Med Pulm Drug Deliv.* 2010;23(4):243-252.

212.   Grommes J, Soehnlein O. Contribution of neutrophils to acute lung injury. *Mol Med.* 2011;17(3-4):293-307.

213.   Ware LB. Pathophysiology of acute lung injury and the acute respiratory distress syndrome. *Semin Respir Crit Care Med.* 2006;27(4):337-349.

214.   Manicone AM. Role of the pulmonary epithelium and inflammatory signals in acute lung injury. *Expert Rev Clin Immunol.* 2009;5(1):63-75.

215.   Steinberg KP, Milberg JA, Martin TR, Maunder RJ, Cockrill BA, Hudson LD. Evolution of bronchoalveolar cell populations in the adult respiratory distress syndrome. *Am J Respir Crit Care Med.* 1994;150(1):113-122.

216.   Abraham E, Carmody A, Shenkar R, Arcaroli J. Neutrophils as early immunologic effectors in hemorrhage- or endotoxemia-induced acute lung injury. *Am J Physiol Lung Cell Mol Physiol.* 2000;279(6):L1137-1145.

217.   Ognibene FP, Martin SE, Parker MM, et al. Adult respiratory distress syndrome in patients with severe neutropenia. *N Engl J Med.* 1986;315(9):547-551.

218.   Sivan Y, Mor C, al-Jundi S, Newth CJ. Adult respiratory distress syndrome in severely neutropenic children. *Pediatr Pulmonol.* 1990;8(2):104-108.

219.   Maris NA, de Vos AF, Bresser P, et al. Activation of coagulation and inhibition of fibrinolysis in the lung after inhalation of lipopolysaccharide by healthy volunteers. *Thromb Haemost.* 2005;93(6):1036-1040.

220.   Mackay CR. Moving targets: cell migration inhibitors as new anti-inflammatory therapies. *Nat Immunol.* 2008;9(9):988-998.

221.   Boehncke WH, Schon MP, Girolomoni G, et al. Leukocyte extravasation as a target for anti-inflammatory therapy - Which molecule to choose? *Exp Dermatol.* 2005;14(1):70-80.

222.   Yonekawa K, Harlan JM. Targeting leukocyte integrins in human diseases. *J Leukoc Biol.* 2005;77(2):129-140.

223.   Miller DH, Khan OA, Sheremata WA, et al. A controlled trial of natalizumab for relapsing multiple sclerosis. *N Engl J Med.* 2003;348(1):15-23.

224.   Ghosh S, Goldin E, Gordon FH, et al. Natalizumab for active Crohn's disease. *N Engl J Med.* 2003;348(1):24-32.

225.   Hoepner R, Faissner S, Salmen A, Gold R, Chan A. Efficacy and side effects of natalizumab therapy in patients with multiple sclerosis. *J Cent Nerv Syst Dis.* 2014;6:41-49.

226.   Shulman Z, Shinder V, Klein E, et al. Lymphocyte crawling and transendothelial migration require chemokine triggering of high-affinity LFA-1 integrin. *Immunity.* 2009;30(3):384-396.

227.   Wolf K, Alexander S, Schacht V, et al. Collagen-based cell migration models in vitro and in vivo. *Semin Cell Dev Biol.* 2009;20(8):931-941.

228. Downey GP, Doherty DE, Schwab B, 3rd, Elson EL, Henson PM, Worthen GS. Retention of leukocytes in capillaries: role of cell size and deformability. *J Appl Physiol (1985).* 1990;69(5):1767-1778.

229. Daley WP, Peters SB, Larsen M. Extracellular matrix dynamics in development and regenerative medicine. *J Cell Sci.* 2008;121(Pt 3):255-264.

230. Raub CB, Suresh V, Krasieva T, et al. Noninvasive assessment of collagen gel microstructure and mechanics using multiphoton microscopy. *Biophys J.* 2007;92(6):2212-2222.

231. Gobeaux F, Mosser G, Anglo A, et al. Fibrillogenesis in dense collagen solutions: a physicochemical study. *J Mol Biol.* 2008;376(5):1509-1522.

232. Doyle AD, Petrie RJ, Kutys ML, Yamada KM. Dimensions in cell migration. *Curr Opin Cell Biol.* 2013;25(5):642-649.

233. Skau CT, Fischer RS, Gurel P, et al. FMN2 Makes Perinuclear Actin to Protect Nuclei during Confined Migration and Promote Metastasis. *Cell.* 2016;167(6):1571-1585 e1518.

234. Collins SJ, Gallo RC, Gallagher RE. Continuous growth and differentiation of human myeloid leukaemic cells in suspension culture. *Nature.* 1977;270(5635):347-349.

235. Collins SJ, Ruscetti FW, Gallagher RE, Gallo RC. Terminal differentiation of human promyelocytic leukemia cells induced by dimethyl sulfoxide and other polar compounds. *Proc Natl Acad Sci U S A.* 1978;75(5):2458-2462.

236. Millius A, Weiner OD. Manipulation of neutrophil-like HL-60 cells for the study of directed cell migration. *Methods Mol Biol.* 2010;591:147-158.

237. Fleck RA, Romero-Steiner S, Nahm MH. Use of HL-60 cell line to measure opsonic capacity of pneumococcal antibodies. *Clin Diagn Lab Immunol.* 2005;12(1):19-27.

238. Jacob C, Leport M, Szilagyi C, Allen JM, Bertrand C, Lagente V. DMSO-treated HL60 cells: a model of neutrophil-like cells mainly expressing PDE4B subtype. *Int Immunopharmacol.* 2002;2(12):1647-1656.

239. Hauert AB, Martinelli S, Marone C, Niggli V. Differentiated HL-60 cells are a valid model system for the analysis of human neutrophil migration and chemotaxis. *Int J Biochem Cell Biol.* 2002;34(7):838-854.

240. Collins SJ, Ruscetti FW, Gallagher RE, Gallo RC. Normal functional characteristics of cultured human promyelocytic leukemia cells (HL-60) after induction of differentiation by dimethylsulfoxide. *J Exp Med.* 1979;149(4):969-974.

241. Mark Welch DB, Jauch A, Langowski J, Olins AL, Olins DE. Transcriptomes reflect the phenotypes of undifferentiated, granulocyte and macrophage forms of HL-60/S4 cells. *Nucleus.* 2017;8(2):222-237.

242. Wu J, Kent IA, Shekhar N, et al. Actomyosin pulls to advance the nucleus in a migrating tissue cell. *Biophys J.* 2014;106(1):7-15.

243. Jacobelli J, Estin Matthews M, Chen S, Krummel MF. Activated T cell trans-endothelial migration relies on myosin-IIA contractility for squeezing the cell nucleus through endothelial cell barriers. *PLoS One.* 2013;8(9):e75151.

244. Khatau SB, Bloom RJ, Bajpai S, et al. The distinct roles of the nucleus and nucleus-cytoskeleton connections in three-dimensional cell migration. *Sci Rep.* 2012;2:488.

245. Khatau SB, Hale CM, Stewart-Hutchinson PJ, et al. A perinuclear actin cap regulates nuclear shape. *Proc Natl Acad Sci U S A.* 2009;106(45):19017-19022.

246. Stewart CL, Roux KJ, Burke B. Blurring the boundary: the nuclear envelope extends its reach. *Science.* 2007;318(5855):1408-1412.

247. Fruleux A, Hawkins RJ. Physical role for the nucleus in cell migration. *J Phys Condens Matter.* 2016;28(36):363002.

8.   ACKNOWLEDGMENTS

9.   APPENDIX

9.1   Publications

Major parts of the present work have been published in the journal *Blood*.

Salvermoser M, Pick R, Weckbach LT, Zehrer A, Loehr P, Drechsler M, Sperandio M, Soehnlein O, Walzog B. Myosin 1f is specifically required for neutrophil migration in 3D environments during acute inflammation. *Blood.* 2018;131(17):1887-1898.

Publications

Thome S, Begandt D, Pick R, **Salvermoser M**, Walzog B. β_2 integrin (CD11/CD18) interacting partners in neutrophil trafficking, 2018 submitted.

Rami M, Guillamat-Prats R, Rinne P, **Salvermoser M**, Ring L, Blanchet X, Megens RTA, Döring Y, Walzog B, Soehnlein O, Weber C, Faussner A, Steffens S. Chronic Intake of the Selective Serotonin Reuptake Inhibitor Fluoxetine Enhances Atherosclerosis. *Arterioscler Thromb Vasc Biol.* 2018;38(5):1007-1019.

Salvermoser M, Pick R, Weckbach LT, Loehr P, Drechsler M, Sperandio M, Soehnlein O, Walzog B. Myosin 1f is specifically required for neutrophil migration in 3D environments during acute inflammation. *Blood.* 2018;131(17):1887-1898.

Zehrer A, Begandt D, Pick R, **Salvermoser M**, Weckbach LT, Walzog B. A fundamental role of Myh9 for neutrophil migration in innate immunity, 2018 submitted.

Pick R, Begandt D, Stocker TJ, **Salvermoser M**, Thome S, Boettcher R, Montanez E, Harrison U, Forne I, Khandoga AG, Coletti R, Weckbach LT, Brechtefeld D, Haas R, Imhof A, Massberg S, Sperandio M, Walzog B. Coronin 1A, a novel player in integrin biology, controls neutrophil trafficking in innate immunity. *Blood.* 2017;130(7):847-858.

Roth H, Samereier M, Begandt D, Pick R, **Salvermoser M**, Brechtefeld D, Schleicher M, Walzog B, Mueller-Taubenberger A. Filamin A promotes efficient migration and phagocytosis of neutrophil-like HL-60 cells. *European Journal of Cell Biology.* 2017;96(6):553-566.

Ortega-Gomez A, **Salvermoser M**, Rossaint J, Pick R, Lemnitzer P, Tilgner J, de Jong, RJ, Megens RT, Jamasbi J, Doring Y, Pham CT, Scheiermann C, Siess W, Drechsler M, Weber C, Grommes J, Zarbock A, Walzog B, Soehnlein O. Cathepsin G Controls Arterial But Not Venular Myeloid Cell Recruitment. *Circulation.* 2016;134(16):1176-1188.

Salvermoser M, Chotewutmontri S, Braspenning-Wesch I, Hasche D, Rosl F, Vinzon SE. Transcriptome analysis of Mastomys natalensis papillomavirus in productive lesions after natural infection. *The Journal of General Virology.* 2016;97(7):1658-1669.

Scientific presentations

11/2013	Semmelweis Symposium, Budapest, Hungary (poster presentation)
11/2014	Annual Retreat of the IRTG of the SFB 914, Günzburg, Germany (oral and poster presentation)
06/2015	Joint Meeting of the European Society for Microcirculation (ESM) and the European Vascular Biology Organization (EVBO), Pisa, Italy (poster presentation)
09/2015	37th Annual Meeting of the German Society for Microcirculation and Vascular Biology (GfMVB), Hannover, Germany (oral presentation)
09/2015	Symposium of the SFB 914, Villa Vigoni, Italy (oral and poster presentation)
04/2016	50th Annual Meeting of the European Society for Clinical Investigation (ESCI), Paris, France (poster presentation)
07/2016	Annual Retreat of the IRTG of the SFB 914, Schöntal, Germany (oral presentation)
07/2016	Summer Symposium of the SFB 914, Munich, Germany (oral presentation)
09/2016	Scientific Retreat of the SFB 914, Lochau, Austria (poster presentation)
03/2017	Scientific Retreat of the SFB 914, Obergugl, Austria (oral and poster presentation)
06/2017	Gordon Research Seminar and Conference Phagocytes, Waterville Valley, USA (oral and poster presentation)
10/2017	39th Annual Meeting of the German Society for Microcirculation and Vascular Biology (GfMVB), Grainau/Garmisch, Germany (oral presentation)
03/2018	2nd International Conference on Leukocyte Trafficking, Munich, Germany (oral presentation)

9.2 Affidavit

Salvermoser, Melanie

……

Surname, first name

……

Street

……..

Zip code, town

……

Country

I hereby declare, that the submitted thesis entitled

Myosin 1f plays a fundamental role for neutrophil migration in 3D environments during acute inflammation

is my own work. I have only used the sources indicated and have not made unauthorized use of services of a third party. Where the work of others has been quoted or reproduced, the source is always given.

I further declare that the submitted thesis or parts thereof have not been presented as part of an examination degree to any other university.

Martinsried, 23.05.2018   Melanie Salvermoser

…………………………………………………….   …………………………………………………….

Ort, Datum   Unterschrift, Doktorandin